Perovskite Nanocrystals: Synthesis, Stability, and Optoelectronic Applications

small structures
www.small-structures.com

Perovskite Nanocrystals: Synthesis, Stability, and Optoelectronic Applications

Shizhe Wang, Amir Abbas Yousefi Amin, Linzhong Wu, Muhan Cao, Qiao Zhang,* and Tayebeh Ameri**

Metal halide perovskite (MHP) materials, named as the game changers, have attracted researchers' attention worldwide for over a decade. Among them, nanometer-scale perovskite nanocrystals (PNCs) have exhibited attractive photophysical properties, such as tunable bandgaps, narrow emission, strong light-absorption coefficients, and high defect tolerance, because they combined the excellent optoelectronic properties of bulk perovskite materials with strong quantum confinement effects of the nanoscale. These materials possess a great potential to be applied in the optoelectronic devices. For commercial applications in devices like solar cells (SCs), light-emitting diodes (LEDs), and photodetectors (PDs), the stability of PNCs against ambient atmosphere like oxygen and moisture, as well as light and high temperature is crucial. Herein, the synthetic methods and stability issues of the PNCs are introduced first, followed by the introduction of the strategies for improving their stability by encapsulation. The applications of PNCs in various optoelectronic devices are then briefly presented. Finally, the remained challenges in improving the stability of PNCs toward the PNC-based optoelectronics with high performance and great durability are addressed.

1. Introduction

Perovskite materials have attracted broad attention from different academic circles over a decade. Regarded as the game changer in photovoltaics,[1] these materials achieved a skyrocketing improvement of the power conversion efficiency (PCE), increasing from 3.81%[2] to 23.3%[3] within 10 years, and hitting to 25.5% currently.[4] Except the photovoltaic applications,[5–12] these superstar materials have also been developed for light-emitting diodes (LEDs),[13–16] photodetectors (PDs),[17–19] and as catalysts for photocatalysis,[20–25] to name but a few. The perovskite materials possess great potential to be applied in various commercial products in the future.

"Perovskite", at first, referred to a mineral species with the chemical formula of $CaTiO_3$. In 1839, the German mineralogist, Gustav Rose (1798–1873), first discovered the "perovskite" ($CaTiO_3$) in the Russian Ural Mountains. In honor of L. A. Perovski (a Russian mineralogist, 1792–1856), this type of material is named as "perovskite". Later on, materials with a similar $CaTiO_3$ crystal structure are called "perovskite" in mineralogy, which have a chemical formula of ABX_3 (see **Figure 1**a). The high-temperature superconductivity, catalytic properties, magnetocaloric effect, and ferroelectricity of perovskite consisting of oxygen, named as perovskite oxides, are the previous research center. The B site of perovskite oxides can be bivalent or tetravalent metal cations.[14] Due to the successful application of metal halide perovskite (MHPs) in photovoltaic devices,[2,26] the scholars of different research areas have focused on this type of material and made it one of the most studied research subjects worldwide over the last ten years. MHPs are composed of monovalent organic or inorganic cations (such as $CH_3NH_3^+$ (methylammonium, MA), $CH(NH_2)_2^+$ (formamidinium, FA), Cs^+, Rb^+, etc.) in the A site, divalent metal cations (such as Ge^{2+}, Cu^{2+}, Pb^{2+}, Sn^{2+}, etc.) in the B site, as well as halide anions (Cl^-, Br^-, or I^-) in the X site.

With numerous achievements in bulk perovskite materials, research of MHPs has been extended to nanoscale. Since the first report in 2014,[27] perovskite nanocrystals (PNCs) have also aroused the interest due to their specialties, which possess the excellent optoelectronic properties of bulk perovskite materials and the quantum confinement effects of materials in nanoscale,

S. Wang, Dr. A. A. Yousefi Amin, Dr. T. Ameri
Department of Chemistry and Center for NanoScience (CeNS)
University of Munich (LMU)
Butenandtstrasse 5-13 (E), 81377 Munich, Germany
E-mail: Shizhe.Wang@cup.lmu.de; tayebeh.ameri@lmu.de

L. Wu, Dr. M. Cao, Prof. Q. Zhang
Institute of Functional Nano and Soft Materials (FUNSOM)
Jiangsu Key Laboratory for Carbon-Based Functional Materials and Devices
Soochow University
199 Ren'ai Road, Suzhou 215123, Jiangsu, P. R. China
E-mail: qiaozhang@suda.edu.cn

Dr. T. Ameri
Institute for Materials and Processes, Chemical Engineering
University of Edinburgh
Sanderson Building, Robert Stevenson Road, Edinburgh EH9 3FB, UK

The ORCID identification number(s) for the author(s) of this article can be found under https://doi.org/10.1002/sstr.202000124.

DOI: 10.1002/sstr.202000124

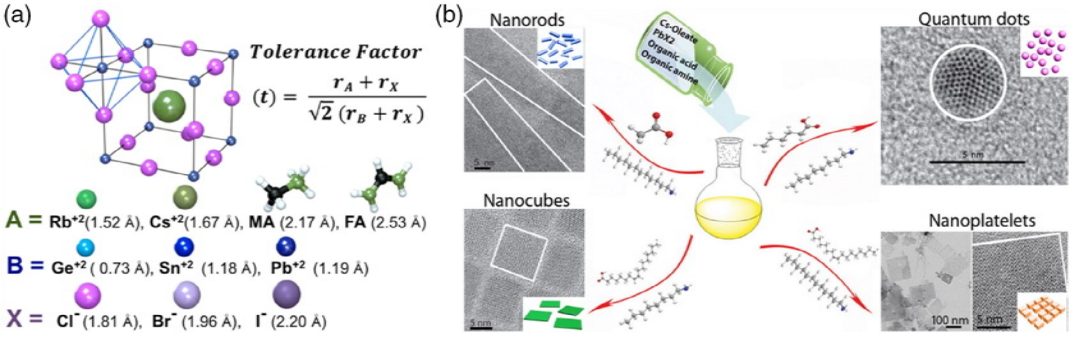

Figure 1. a) Cubic perovskite crystal structure (α-phase) showing the flexibility in the choice of cation (A), metal (B), and anion (X). The ionic radii of different ions are also shown. The tolerance factor (t) for 3D perovskites should be ≈1 to attain an ideal close-packed cubic perovskite phase, where r_A, r_B, and r_X are the effective ionic radii for A, B, and X ions, respectively. Reproduced with permission.[196] Copyright 2019, American Chemical Society. b) Tuning the dimensionality of inorganic $CsPbX_3$ (X = Cl, Br, I) NCs by varying the organic ligands used. Hexanoic acid and octylamine for spherical QDs; oleic acid and dodecylamine for nanocubes; acetate acid and dodecylamine for NRs; oleic acid and octylamine for few-unit-cell-thick NPLs. Reproduced with permission.[48] Copyright 2016, American Chemical Society.

showing the properties of tunable bandgaps, narrow emission, and strong light-absorption coefficients. The notable advantage of PNCs over traditional quantum dots (QDs), like sulfide and selenide QDs, is their high defect tolerance. The dimensions and shapes of PNCs can be facilely adjusted to 0D QDs, 1D nanowires (NWs) and nanorods (NRs), 2D nanosheets (NSs) and nanoplatelets (NPLs), and 3D nanocubes (NCus) by modifying the reaction conditions.[28] Figure 1b shows a good example of adjusting the dimensionality of $CsPbX_3$ (where X = I, Br, Cl) NCs using different organic ligands.

Although PNCs have shown outstanding properties and considerable potential for various applications in the future, the stability issue of these materials is still the main challenge hindering their roads toward commercialization. Researchers have devoted substantial efforts to understand the degradation mechanisms of PNCs[29–32] and develop effective strategies to protect PNCs for highly efficient performance and long-term lifetime.[33–35]

This Review comprehensively summarizes the latest advances of the synthesis methods for both lead-based and lead-free PNCs. Moreover, elements that impact on the stability of the PNCs are introduced. Strategies of encapsulation to protect PNCs are reviewed afterwards. Importantly, various applications of the PNCs in optoelectronics are briefly reviewed. And finally, the challenges remained for improving the stability of PNCs and the outlook to possible directions in developing PNC-based devices with high performance and great operation durability are addressed.

2. Synthesis of PNCs

The facile methods for synthesizing PNCs with different dimensions and shapes have aroused huge research interest in recent years.[36,37] In this section, we discuss the wet synthesis processes, including hot injection method, ligand-assisted reprecipitation (LARP) method, emulsion process, ultrasonic and microwave-based methods, solvothermal method, microfluidic method, template-assisted method, and electrospinning or electrospray method, as well as the dry synthesis processes, chemical vapor deposition (CVD). In addition, the synthesis methods for lead-free PNCs are presented in this section, which is also an important research branch of PNCs in the process of commercialization. Finally, the anion-exchange reaction, an important postsynthetic method, is introduced and discussed.

2.1. Wet Synthesis Processes of PNCs

2.1.1. Hot Injection Method

Hot injection method is a traditional synthesis method for metal chalcogenide or fluoride NCs.[38] **Figure 2**a shows the schematic of hot injection method.[39] Typically, a cation precursor is prepared separately before the injection, for example, Cs-oleate and methylamine are normally chosen for Cs^+ ions and MA^+ ions, respectively. Then, a solution of metal halide salt and organic ligands is dried under vacuum and heated to a certain reaction temperature under nitrogen before injection. Alkyl chain acid and amine are usually chosen as ligands. Upon quick injecting the cation precursor into the mixture of metal halide salt and ligands, the PNCs form immediately due to their fast nucleation and growth kinetics. In 2015, Kovalenko and coworkers first used this method to synthesize PNCs, $CsPbX_3$ (X = Cl, Br, I, or halide mixture).[40] For that, the Cs-oleate precursor was injected into PbX_2 precursor containing organic ligands at a specific high temperature (up to 250 °C) and operated under protective gas, like nitrogen and argon. Then the reaction was instantly quenched by putting the flask into an ice-water bath. The reacting mixture became gel when the temperature suddenly fell, and the growth of PNCs stopped at the same time. By modifying the temperature and time of reaction, PNCs with different sizes and shapes can be obtained.

The as-fabricated $CsPbX_3$ NCus with 4–15 nm lengths of edge exhibited adjustable bandgaps and emission spectra covering the full visible spectral area of 410–700 nm (Figure 2b), as a result of the compositional modulations and quantum confinement. The photoluminescence (PL) of $CsPbX_3$ NCs was characterized by narrow full width at half maximum (FWHM) of 12–42 nm, radiative lifetimes in the range of 1–29 ns, high quantum yields (QYs) of up to 90%, and wide color gamut covering up to 140%

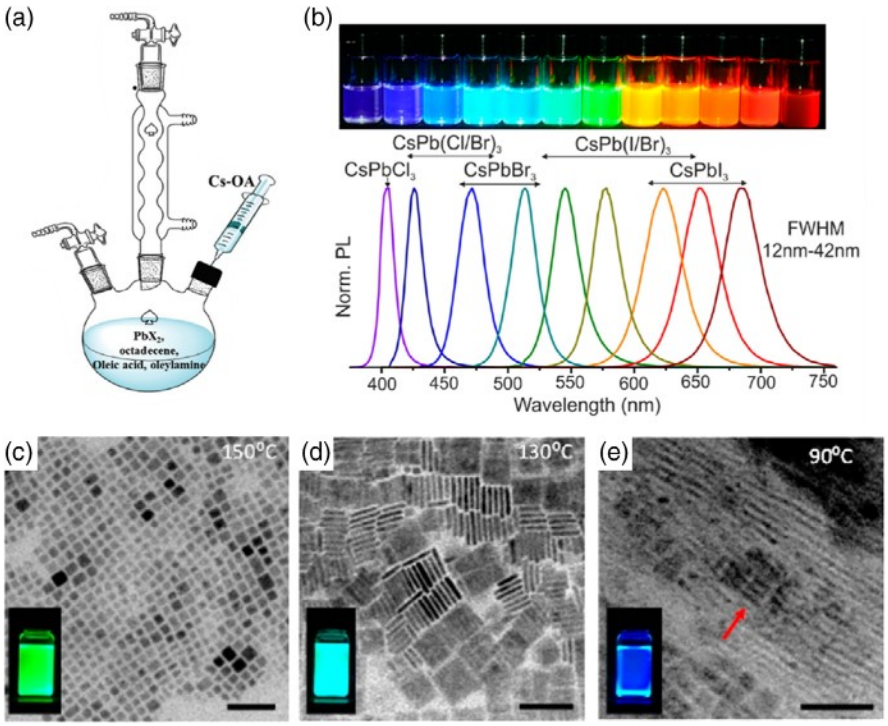

Figure 2. a) Schematic of hot injection method. Reproduced with permission.[39] Copyright 2017, Wiley-VCH. b) $CsPbX_3$ NCs (X = Cl, Br, I) colloidal solutions in toluene under UV lamp ($\lambda = 365$ nm); representative PL spectra ($\lambda_{exc} = 400$ nm for all but 350 nm for $CsPbCl_3$ samples). Reproduced with permission.[40] Copyright 2015, American Chemical Society. Study of the influence of reaction temperature in $CsPbBr_3$ colloidal synthesis: c) At 150 °C, green emitting 8–10 nm NCus are formed; d) At 130 °C, cyan-emitting NPLs with lateral dimensions of 20 nm and thickness of a few unit cells (≈3 nm) are formed; e) At 90 °C, blue-emitting thin NPLs are observed, along with several-hundred nanometers lamellar structures. NPLs growth along the lamellae (red arrow) (c,d, scale bars are 50 nm). c–e) Reproduced with permission.[44] Copyright 2015, American Chemical Society.

of the National Television System Committee (NTSC) color standard.[40]

The reaction temperature can affect the quality of final products. When the temperature is too high, some unwanted variants can be obtained. For example, $CsPb_2Br_5$ and $CsPb_2Cl_5$ would be produced when the synthesis of $CsPbBr_3$ and $CsPbCl_3$ NCs was operated at 260 °C.[41] In addition, some reactants will precipitate when the temperature of solution is too high. For example, the reaction temperature for synthesizing $CsPbBr_3$ is around 190 °C. However, further increasing the temperature to a threshold temperature of 195 °C leads to $PbBr_2$ precipitation.[40] While the precipitation temperature of reactant $PbBr_2$ can rise above 195 °C by adding more ligands into the solution.[42] At low reaction temperature, large $CsPbBr_3$ NPLs form with broad edge length distribution.[43] Alivisatos et al. studied the reaction temperature effect on the morphology of PNCs. They discovered that reactions at lower temperatures between 90 and 130 °C tended to favor asymmetric growth of PNCs, producing quasi 2D materials (Figure 2c,d).[44] The reaction time is another sensitive factor for hot-injection method. Normally, the reaction is completed within 10 s due to the fast nucleation and growth kinetics of PNCs, like $CsPbX_3$ and $MAPbI_3$.

Capping ligands are often used in the hot injection method. They can solvate the metal halide precursors effectively, alter the kinetic pathways to obtain PNCs with various morphologies, and stabilize the final products. The alkyl chain acids and amines play an important role on the crystal growth and surface properties of PNCs. **Figure 3**b shows the dynamic ligands binding on the surface of $CsPbBr_3$ NCs, where oleate or bromide anions bound to the surface cesium or lead ions, and alkyl chain ammonium cations bound to surface bromides with weak hydrogen bonds or electrostatic interactions.[45] To study the surface chemistry, Liu et al. have systematically changed alkyl chain composition of amines and carboxylic acids. They realized that the amine and acid show independent influence on the shape and size of NCs (see Figure 3a). At a relatively higher temperature of 170 °C, larger size $CsPbBr_3$ NCus could be obtained when using a shorter chain acid. However, at the same injecting temperature, a shorter chain amine resulted in a different shape of NPLs comparing with NCus using longer chain amine. At a relatively lower temperature of 140 °C, the length of acid had little impact on the thickness of NPLs, but shorter chain amine led to thinner NPLs. Figure 3c–f shows low- and high-resolution transmission electron microscopy (TEM) images of $CsPbBr_3$ NCs synthesized using different ligands at the temperature of 170 °C (Figure 3c–e) and 140 °C (Figure 3f). Based on ^1H NMR and infrared (IR) spectroscopic results, they indicated that both ammonium and carboxylate bound to the as-fabricated PNCs' surface. However, the final composition of surface ligand was dependent on purification processing. When more polar acetone was used during purification cycles, ammonium ligands tended to leave the surface, but would remain upon the utilization of

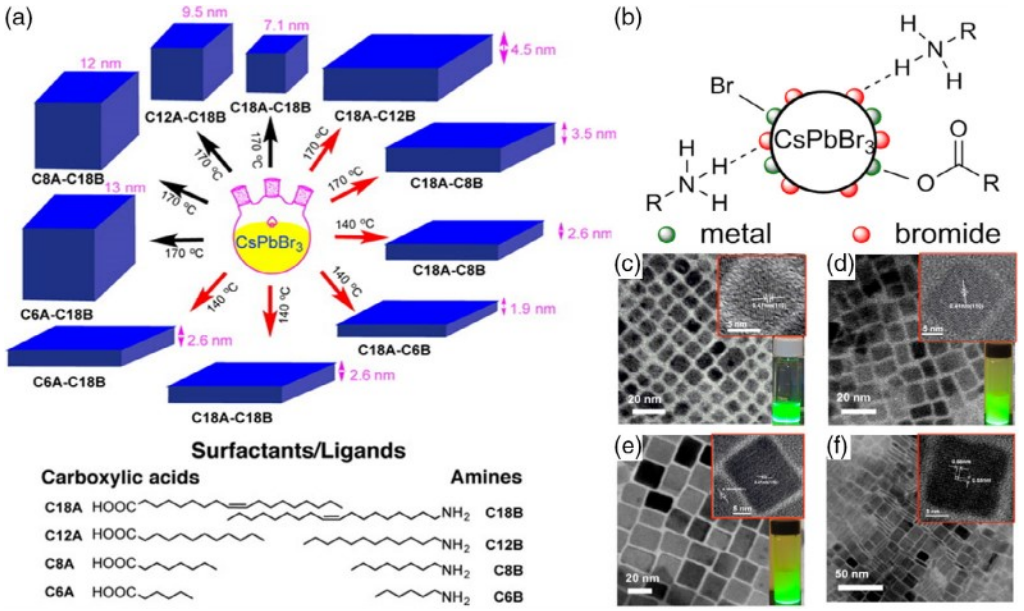

Figure 3. a) Schematic of $CsPbBr_3$ with different sizes and shapes synthesized under temperature of 140 or 170 °C and with different length of ligands. Reproduced with permission.[43] Copyright 2016, American Chemical Society. b) The surface chemical environment of typical $CsPbBr_3$ NCs. Reproduced with permission.[45] Copyright 2016, American Chemical Society. Low- and high-resolution TEM images of $CsPbBr_3$ NCus from 170 °C reactions using c) C12A − C18B, d) C8A − C18B, and e) C6A − C18B, respectively. Insets in (c–e): photographs of $CsPbBr_3$ NCus colloidal solutions in hexane under UV light; f) Low- and high-resolution TEM images of $CsPbBr_3$ NPLs from the 140 °C reaction using C6A−C18B. c–f) Reproduced with permission.[43] Copyright 2016, American Chemical Society.

nonpolar hexane solvent. It confirmed that ammonium ions bound more weakly to the surface than carboxylate ligands did. In addition, the utilization of a more soluble cesium acetate (CsOAc) instead of commonly used Cs_2CO_3 led to smaller particle sizes and improved processability without any detrimental influence on the optoelectronic properties.[43] Recently, Manna et al. reported a novel route for the synthesis of both hybrid organic–inorganic and all-inorganic PNCs by choosing benzoyl halides as halide precursor to be injected into the solution. The halide ions can be released swiftly, following by nucleation and growth of PNCs. The final product synthesized by this method exhibited a good phase stability, uniform particle sizes, and outstanding optical properties.[46]

2.1.2. Ligand-Assisted Reprecipitation Method

Although hot injection method gives the best morphology control on the synthesis of PNCs so far, the high cost of this method is not proper for commercial production. Consequently, other alternative procedures should be developed to address this problem. LARP method is the most common used method to synthesize PNCs at room temperature (RT). **Figure 4**a shows the representative schematic of the LARP method, in which the precursor is a mixture of perovskite reactants and ligands in N-dimethylformamide (DMF). Then, a certain volume of precursor is dropped into toluene or 1-octadecene (ODE), which initiates PNCs formation and aggregation. Apparently, the types of ligands and solvents in precursors are critical factors to control the sizes and shapes of PNCs. The LARP technique is a low-cost and scalable process, which is suitable for fabricating both all-inorganic and hybrid organic-inorganic PNCs.[36]

In 2014, Pérez-Prieto et al. reported the synthesis method of nanometer-sized, organolead halide $MAPbBr_3$ perovskites. Using medium-length alkyl chain ammonium cations (e.g., octadecylammonium) as ligands, they obtained PNCs with an average size of 6 nm. The PNCs were stable for at least 3 months in solution and solid state. This process also allowed to fabricate PNCs thin films via spin-coating. Notably, they obtained luminescent PNCs both in solution and in film, though the photoluminescence quantum yield (PLQY) was only ≈20%.[27] In 2015, Zhong et al. further optimized the LARP technique by changing octadecylammonium bromide and octylammonium bromide ligands to n-octylamine and oleic acid (OA) in the synthesis. The n-octylamine can help to avoid the fast crystallization and aggregation, and the OA can also suppress the QD aggregation effects and make the colloidal solution stable. The colloidal $MAPbBr_3$ QDs showed great enhancement in luminescent with absolute PLQYs up to 70%. They also illustrated that the size reduction and appropriate chemical passivation of Br-rich surface can increase exciton binding energy and PL.[47] Later on, Deng et al. adopted this strategy for the synthesis of all-inorganic $CsPbX_3$ (X = Cl, Br, I) PNCs with controlled shape and achieved PLQY values up to >80%. Using different types of ligands in LARP process, $CsPbX_3$ NCs could be modified into NCus, 1D NRs, and 2D NPLs with precise morphology.[48] Rogach et al. studied the size-tunability of the bandgap of $MAPbBr_3$ perovskite quantum dots (PQDs) by adjusting temperature to control over the LARP synthesis. The PL peaks of as-synthesized PQDs can be tuned between 475 and 520 nm (see Figure 4b).[49]

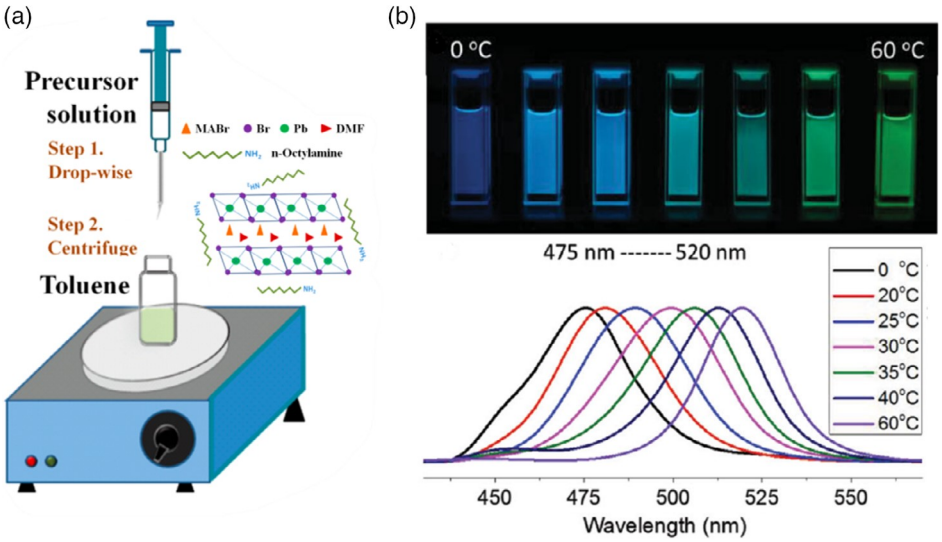

Figure 4. a) Schematic of LARP method (inset: starting materials in the precursor solution). Reproduced with permission.[47] Copyright 2015, American Chemical Society. b) Photograph of colloidal $MAPbBr_3$ PQDs solutions in toluene under UV lamp excitation ($\lambda = 365$ nm) and size-tunable PL spectra over the range of wavelengths. Reproduced under the terms of the CC-BY license.[49] Copyright 2015, The Authors. Published by Wiley-VCH.

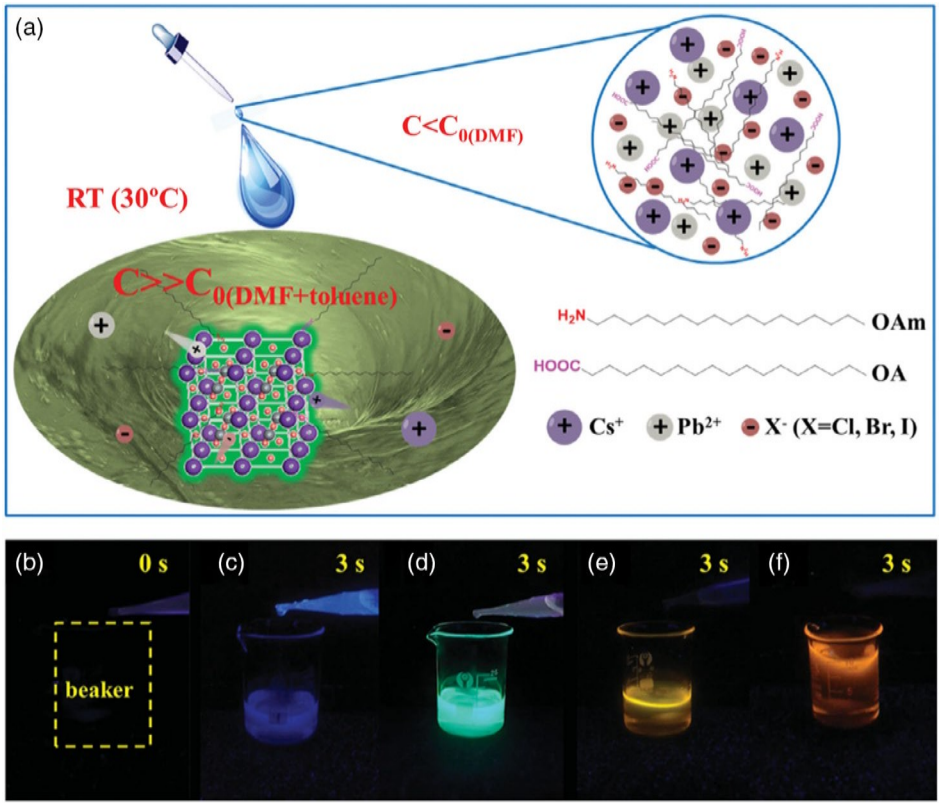

Figure 5. a) The SR can be finished within 10 s through transferring the Cs^+, Pb^{2+}, and X^- ions from the soluble to insoluble solvents at RT without any protecting atmosphere and heating (C: ion concentration in different solvents. C_0: saturated solubilities in DMF, toluene, or mixed solvents [DMF + toluene]). b) Clear toluene under a UV light. Snapshots of four typical samples after the addition of precursor ion solutions for 3 s, c) blue (Cl:Br = 1), d) green (pure Br), e) yellow (I:Br = 1), and f) red (I:Br = 1.5), respectively. Reproduced with permission.[50] Copyright 2016, Wiley-VCH.

Inspired by Zhong's work, Zeng et al. created a RT supersaturated recrystallization (SR) procedure to fabricate $CsPbX_3$ (X = Cl, Br, I) NCs (see **Figure 5**). The process does not require heating, inert gas, and injection operation, thus can be completed very fast. They dissolved PbX_2 and CsX (X = Cl, Br, I, or their mixture) in dimethyl sulfoxide (DMSO) or DMF, and added

OA and oleylamine (OAm) as surface ligands. Toluene was chosen as an antisolvent due to the poor solubility for these ions ($<10^{-7}$ g mL^{-1}). Then, the precursor was dropped into toluene. Due to the huge solubility difference, a highly supersaturated state was produced at once and, consequently, fast recrystallization occurred under stirring condition. OAm and OA worked as dispersants for these PNCs and also helped to control the particle size.[50]

However, polar solvents, like DMF, as reaction medium can severely degrade or form defective PNCs and, therefore, decrease the production yield. For example, $CsPbX_3$ NCs often lose colloidal stability and brightness of PL when polar solvents are added to separate them.[45] To address this issue, Pan et al. reported a room temperature and gram-scale synthetic strategy, based on a homogeneous reaction in various nonpolar organic solvents using precursors containing long alkyl chain acid salts of cesium and lead and quaternary ammonium bromides. The as-prepared PNCs exhibited a tunable PL in the region from 440 to 682 nm and PLQYs of 50–85%.[51] Recently, Macdonald et al. reported an oleic and amine-acid-free RT synthesis of $CsPbBr_3$ and $FAPbBr_3$ NCs using a mixture of diisooctylphosphinic acid and trioctylphosphine oxide. This mixture of ligands provided a stable platform for the polar-solvent-free synthesis of fully inorganic $CsPbBr_3$ (FWHM $\approx$ 14 nm, emission = 519 nm) and hybrid organic–inorganic $FAPbBr_3$ (FWHM $\approx$ 19 nm, emission = 532 nm) NCs in the air. In addition, it was shown that compared with a traditionally used ligand combination, phosphine ligands could be washed off easily, which would benefit the future development of optoelectronic devices.[52]

2.1.3. Emulsion Method

As shown in **Figure 6**a,b, Zhong et al. developed a facile nonaqueous emulsion synthesis of PNCs by mixing a demulsifier with an emulsion of precursors. First, they created an emulsion system by mixing DMF and n-hexane, which were immiscible to each other. Then, they subsequently added *tert*-butanol into the initialized solvent mixture, which worked as the demulsifier and induced the crystallization process. By using this method, they could control the crystallization process and the size of PNCs by varying the amount of demulsifier, and they succeeded in obtaining monodisperse $MAPbBr_3$ QDs with size between 2 and 8 nm (Figure 6c–f) and PLQYs of 80–92%, which were higher than samples fabricated by LARP methods.[47] They also used the same method to synthesize inorganic $CsPbBr_3$ PNCs and obtained $CsPbBr_3$ NCus with the size between 9 and 20 nm.[53]

2.1.4. Ultrasonic and Microwave-Based Method

The ultrasonic and microwave-assisted methods show potential for large-scale production due to the polar solvent-free fabrication. Song et al. first reported ultrasound-assisted synthesis of colloidal $APbX_3$ NCs, where A represents Cs^+, MA, or FA, and X represents I^-, Br^-, or Cl^-. **Figure 7**a shows $CsPbBr_3$ NCs with the size of 10 nm. They added PbX_2, MAX (or FAX, CsX), and OAm to toluene to make a precursor. The reaction vessel of precursor was placed in a high-density probe-type ultrasonicator. The reaction temperature was kept at 20 °C by immersing it in a water jacket connected to a circulator with a temperature controller. Furthermore, they used the same method to produce a series of mixed halides PNCs.[54] Bals, Urban, Polavarapu and their colleagues developed a polar-solvent-free synthesis method of $CsPbX_3$ ($X = Cl^-$, Br^-, and I^-) PNCs (Figure 7b–d) with high quality, which was based on direct tip sonication of the combination of capping ligands (OAm and OA) and precursor salts (Cs_2CO_3 and PbX_2) in a nonpolar solvent under ambient atmospheric conditions. The average crystal sizes were between 10 and 15 nm for $CsPbBr_3$ and between 8 and

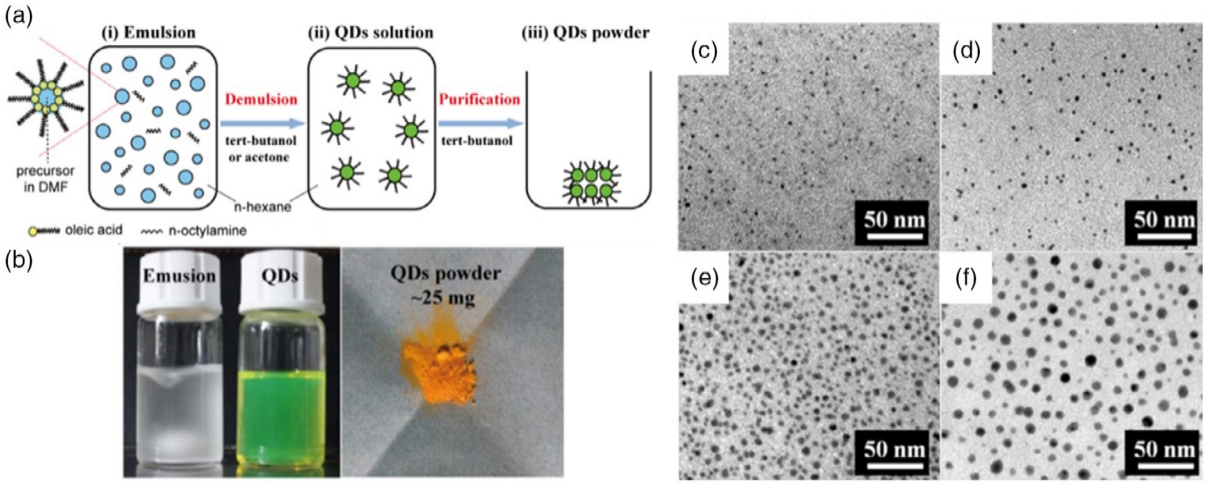

Figure 6. a) Schematical illustration of the QD emulsion synthesis, (i) formation of the emulsion, (ii) demulsion by adding demulsifier, and redisperse into colloidal solution, (iii) purification into solid-state powder. b) Optical photographs of typical $MAPbBr_3$ emulsion, resultant colloidal solution, and solid-state powder of $MAPbBr_3$ QDs. c–f) Low-resolution TEM image of $MAPbBr_3$ QDs with diameter of 2.6 ± 0.6, 3.3 ± 0.7, 4.6 ± 1.1, and 7.2 ± 1.7 nm. The amounts of *tert*-butanol used were 1.5, 2, 4, 6, and 8 mL, respectively. Reproduced with permission.[53] Copyright 2015, American Chemical Society.

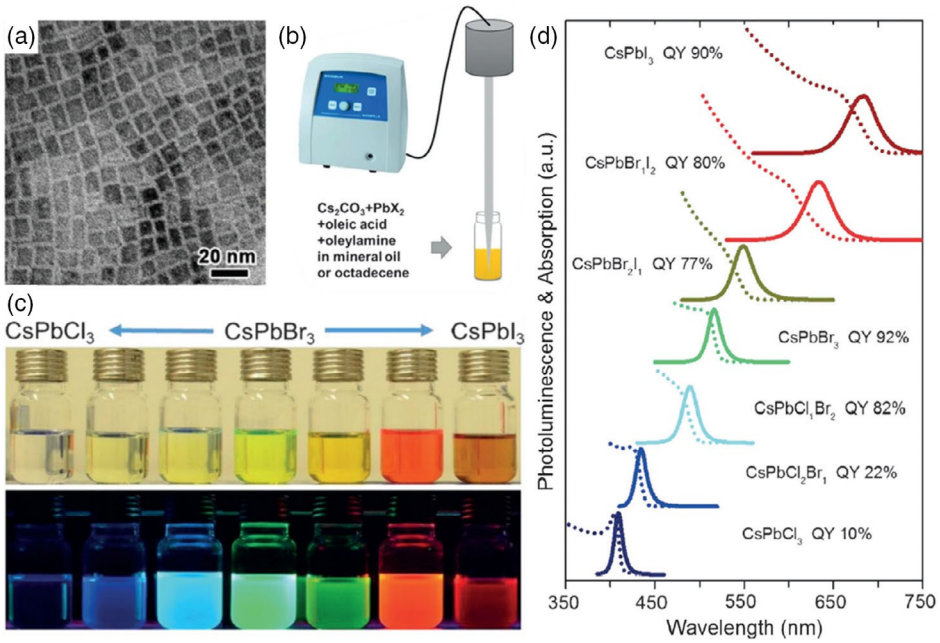

Figure 7. a) High-resolution transmission electron microscopy (HRTEM) image of monodisperse 10 nm $CsPbBr_3$ NCs. Reproduced with permission.[54] Copyright 2016, Royal Society of Chemistry. b) Synthesis of $CsPbX_3$ NCs through single-step tip sonication. c) Photograph of colloidal dispersions of $CsPbX_3$ NCs with different halides (X = Cl, Br, and I) compositions in hexane under room light (top) and 367 nm UV light (bottom). d) Corresponding UV–vis and PL spectra and PLQYs of the samples shown in c). b–d) Reproduced with permission.[55] Copyright 2016, Wiley-VCH.

12 nm for $CsPbI_3$. It was interesting that lower cesium content reduced reaction rate and strongly support 2D growth, thereby synthesizing NPLs.[55]

Zhang et al. reported a rapid and efficient microwave-assisted process to produce $CsPbX_3$ NCs with controllable morphology and high quality. The microwave heating has some advantages like low energy cost and high heating rate, which are favored by industrial communities. In addition, the as-obtained materials possessed superior photophysical properties. The emission peak could be adjusted in the region of 410 to 694 nm by altering the anion composition. The FWHM were very narrow (9–34 nm), which showed their potential in lighting and display application.[56] Nearly at the same time, Na et al. used a simple microwave irradiation to synthesize $CsPbX_3$ PNCs with adjustable properties and morphology (NCus, NRs, NWs, quadrate NPLs, and hexagonal NPLs). The precursor was a solid–liquid mixture containing PbX_2 (X = Cl, Br, I), Cs_2CO_3, ODE, OA, and OAm, which was placed into a glass vessel and positioned in the microwave oven. Finally, $CsPbX_3$ PNCs were produced via static microwave irradiation for ≈4 min.[57] Zhang et al. modified the previous method by using cesium acetate (CsOAc) and bis(2,4,4-trimethylpentyl) phosphinic acid (TMPPA) as Cs precursor and capping ligand, rather than commonly used Cs_2CO_3 and OA. The mixture of OA and TMPPA could solvate CsOAc completely at RT, whereas Cs_2CO_3 precursor was insoluble. The reason was that carbonic acid was less acidic than acetic acid, correspondingly, it was harder for Cs_2CO_3 than CsOAc to coordinate and form soluble Cs−ligand complex monomers. Consequently, more soluble monomers could be released by CsOAc, resulting in supersaturation, nucleation, and growth of NCs.[58]

2.1.5. Solvothermal Method

Solvothermal methods are one of the most used techniques to obtain well-defined NCs under increased pressure and modest temperature. This method shows a relatively slow reaction, comparing with the traditional hot-injection and LARP. Therefore, it can control the kinetics of nucleation and growth process during the PNCs' synthesis. In addition, this method has the feature of high crystallinity and uniformity, controllable size and shape, as well as simple, low-cost and scalable synthesis. Typically, the precursor solution is added into a Teflon liner, which is held by a stainless-steel autoclave. Then, the sealed tank is put into an oven and heated at a specific temperature. The reaction is normally conducted at high temperature and pressure.

Zhang et al. first reported the successful production of high-quality all-inorganic $CsPbX_3$ NCs through a simple solvothermal approach. The as-prepared PNCs are shown in **Figure 8**a–e. $CsPbX_3$ NCs were cube-like shape with an average edge length of around 10 nm. They also found that the growth of $CsPbI_3$ NCs was faster than the other halides perovskite, leading to the relatively larger size (≈12.5 nm). The optimized $CsPbX_3$ NCus showed a high PLQYs of over 80%. More importantly, $CsPb(Br/I)_3$ ultrathin NWs could also be prepared through this approach with a high yield (Figure 8f,g). The concentration and aging effect of precursors determined the morphology of PNCs. As shown in Figure 8i, the concentration of precursor ions was relatively low when precursor was directly heated without predissolving. Then, precursors were gradually dissolved when the temperature increased and little amount of PNCs nucleated at specific concentration. Under this condition, the nuclei grew into NCus finally. In opposite, when precursors were predissolved,

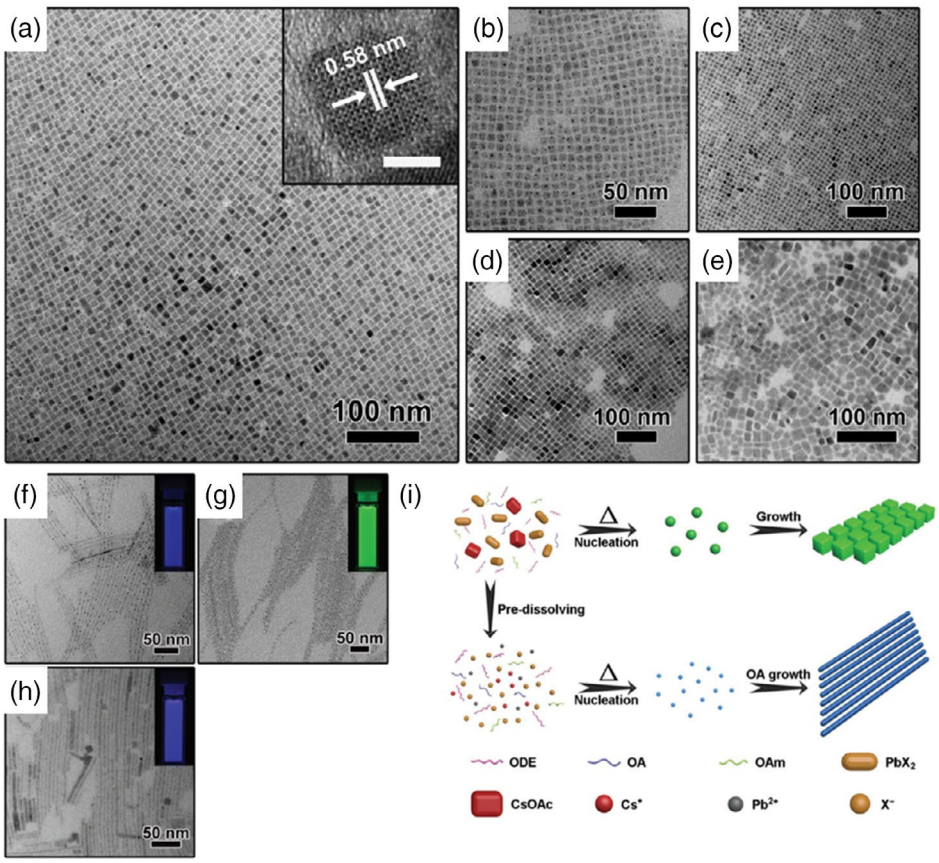

Figure 8. TEM images of a) $CsPbBr_3$, b) $CsPbCl_3$, c) $CsPb(Cl/Br)_3$, d) $CsPb(Br/I)_3$, and e) $CsPbI_3$ NCs. (The inset in (a) is the HRTEM image of $CsPbBr_3$ nanocrystals. The scale bar in the inset is 5 nm.) TEM images of ultrathin f) $CsPbBr_3$, g) $CsPb(Br/I)_3$, and h) $CsPb(Cl/Br)_3$ NWs. Insets show the bright emission color of colloidal $CsPbX_3$ solution in hexane under UV illumination ($\lambda = 365$ nm). i) the proposed growth process of $CsPbBr_3$ NCs without and with predissolving step. Reproduced with permission.[59] Copyright 2017, Wiley-VCH.

and the concentration of ions was high at the beginning, more nuclei were formed, resulting in smaller nuclei. Here, by increasing the reaction time, the morphology of NCs could change from NCus to NWs.[59]

Zheng and coworkers[60] and Chen and coworkers[61] also reported a solvothermal synthesis process of Mn-doped $CsPbCl_3$ PNCs nearly at the same time. Zheng et al. reported 2D Mn-doped $CsPbCl_3$ NPLs accompanied with the phenomenon of a gradual phase segregation of pure $CsMnCl_3$ from Mn:$CsPbCl_3$ NPLs by spinodal decomposition.[60] Chen et al. systematically studied the effect of Cs/Pb ratio on crystal structure of Mn-doped $CsPbCl_3$ product. When the Cs/Pb ratio was low (0.3:1 or 0.6:1), rhombohedral Cs_4PbCl_6 phase coexisted with cubic $CsPbCl_3$ phase. When the ratio increased (0.9:1 and 1.2:1), the as-synthesized products were pure cubic $CsPbCl_3$ phase without any obvious impurities. PNCs still remained as the cubic $CsPbCl_3$ phase when further increasing the ratio (1.5:1 and 1.8:1). When the Cs/Pb ratio was fixed at 1.2:1, undoped sample showed tetragonal $CsPbCl_3$ phase while all the Mn-doped PNCs were pure cubic $CsPbCl_3$ phase, which indicated that Mn^{2+} dopants could modify crystal structure. In addition, Mn-doped $CsPbCl_3$ NCs synthesized by this method showed better stability than those synthesized by hot-injection method.[62] Except lead-based PNCs, the solvothermal method could also be applied to synthesize lead-free PNCs, like $CsSnX_3$,[63,64] $CsGeX_3$,[65] etc.

2.1.6. Microfluidic Method

Microfluidic method is suitable for rapid mass and energy transfer, which allows to create or homogenize both temperature and reagent on ultrashort time scales. This method can provide researchers with the fabrication of NCs with diverse and complex composition, and a fast, accurate, and economical testing of parameters via varying volumetric flow rates of the precursor and controlling sequentially addition of the reagents.[66,67]

In 2015, just after the first successful synthesis of PNCs by hot injection method, Kovalenko et al. used microfluidic reaction systems to study the kinetics and factors on the formation of $CsPbX_3$ NCs. As shown in **Figure 9**a, the setup was relatively simple for studying the formation of PNCs. The precursors, which were put into precision syringe pumps, were mixed rapidly via a cross-mixing junction and formed droplets that can be heated to a certain reaction temperature rapidly. The obtained materials showed tunable PL and narrow FWHM

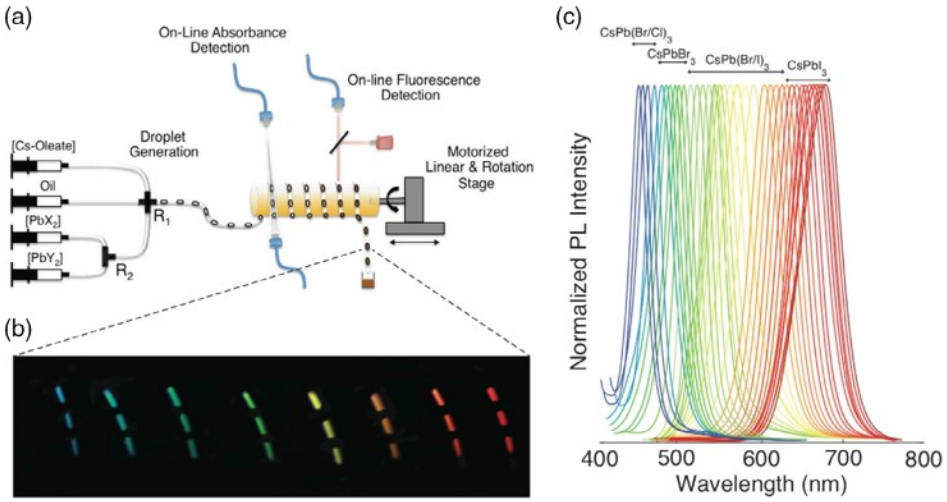

Figure 9. a) Illustration of the droplet-based microfluidic platform integrated with online absorbance and fluorescence detection for the synthesis and real-time characterization of $CsPbX_3$ PNCs. b) Image of the generated droplets after exiting the heating zone taken under UV excitation ($\lambda_{ex} = 405$ nm), showing bright PL of $CsPbX_3$ NCs. c) Online fluorescence spectra of $CsPbX_3$ NCs (X: Cl, Br, I, and Cl/Br and Br/I mixed halide systems) spanning the whole visible spectral region with narrow emission linewidths. Reproduced with permission.[68] Copyright 2016, American Chemical Society.

(Figure 9b,c). Benefiting from this simple and economic synthesis method, months-to-years of time and between 10 and 100 kg of reagents cost were saved compared with standard batch-by-batch screening routes. Depending on the synthesis methods, they studied the rapid reaction kinetics and formation mechanism for mixed-halide PNCs. Only a really short time (within 5 s) was needed to complete the nucleation and growth of $CsPbX_3$ NCs, so the time could not be used to control the size of NCs in traditional batch syntheses. In addition, the temperature used in hot injection method was between 1 and 10 °C lower than that in microfluidic method.[68]

2.1.7. Template-Assisted Synthesis

Template-assisted approach is a versatile and straightforward method to grow monodisperse PNCs. The crystallization kinetics and NCs formation are conducted on a particular template instead of using capping ligands. Yamauchi et al. used mesoporous silica templates to synthesize $MAPbBr_xI_{x-3}$ NCs. The particle size was controlled by the pore sizes of the templates, which showed quantum confinement effect as the samples' color changed by adjusting particle size.[69] Kaltenbrunner et al. used nanoporous alumina and silicon thin films as templates to synthesize PNCs directly without the utilization of stabilizers.[70] Recently, Li et al. used mesoporous Al_2O_3 as the template and developed a high temperature solid-state confined growth strategy to prepare highly emissive $CsPbBr_3$ NCs. The obtained $CsPbBr_3$ NCs possessed excellent optical properties comparable with colloidal $CsPbBr_3$ NCs, such as high PLQY (70%), narrow emission line width (FWHM = 25 nm), and much better thermal stability. It is worth noting that large amounts of expensive and toxic organic solvents can be avoided using this method, which paves a new route for economical synthesis of high-quality PNCs.[71]

2.1.8. Electrospinning or Electrospray Method

Ogale et al. used electrospinning or electrospray method to synthesize $MAPbX_3$ NCs successfully, where instead of a solid substrate a bath of the antisolvent (without or with a capping agent) in a metal-electrode container was used as the substrate. It was quite like LARP method but applying the high electric field to the droplets of precursor solution, which broke them into a jet of nanodroplets. The nanodroplets fell into antisolvent (toluene) bath, resulting in rapid crystallization of the perovskite leading to uncapped 0D NCs. Interestingly, the capping agent, OAm, also contributed to the formation of 2D sheet-like layered perovskites by intercalation via host–guest chemistry.[72]

2.1.9. Other Wet Synthesis Methods

Except the methods mentioned earlier, some novel wet synthesis methods have been also reported recently. Kovalenko et al. developed wet ball milling method to synthesis $APbBr_3$ NCs (A = Cs, FA). In detail, bulk $CsPbBr_3$ or $FAPbBr_3$ was added into a zirconia bowl with zirconia balls. The diameters of the balls are 4 and 5 mm. Then, OAmBr (ligand) and mesitylene (solvent) were added into the mixture. After milling at a certain speed for certain time, $CsPbBr_3$ or $FAPbBr_3$ NCs could be obtained. The optoelectronic quality of the products was as good as that synthesized by hot-injection method. However, this method was not applicable to iodide systems like $CsPbI_3$ and $MAPbI_3$.[73] To form heterostructures, Xing et al. reported an in situ solution growth method to decorate $MAPbBr_3$ NCs on the surface of MXene ($Ti_3C_2T_x$) NSs, which was achieved by an optimal mixed solvent ratio. The surface terminations of MXene NSs, such as fluorine, oxygen, and hydroxyl groups, are prone to interact with OA and OAm, which would form kinetically favorable nucleation points. Then, $MAPbBr_3$ NCs can grow on these points.[74]

2.2. Dry Synthesis Processes of PNCs

2.2.1. Chemical Vapor Deposition

CVD is an effective method for fabricating traditional semiconductor nanocrystals. In 2014, Xiong et al. first used this method to synthesize PNCs ($MAPbX_3$, X = I, Br, Cl, or halide mixture) in shape of NPLs, which possessed lateral dimensions from 5 to 30 μm and thicknesses from some atomic layers to hundred nanometers. The NPLs were fabricated via a two-step CVD process. First, they grew PbX_2 NPLs on muscovite mica utilizing van der Waals epitaxy in a vapor transport chemical deposition system. Next, the as-fabricated platelets were turned into perovskites by a gas–solid heterophase reaction with MAX. In addition, $MAPbCl_3$ NWs were also fabricated as by-products during this process.[75] To obtain perovskite NWs, Xiong et al. used silicon oxide rather than mica as substrates and succeeded in synthesizing the single-crystalline $MAPbI_xCl_{3-x}$, $MAPbBr_3$, $MAPbI_3$, and NWs via a two-step vapor-phase synthesis process.[76] Song et al. reported that the inorganic perovskite NWs of $CsPbCl_3$, $CsPbBr_3$, and $CsPbI_3$ were synthesized by vapor transport method. The NWs consisted of a single-crystalline cubic or pseudocubic phase with a uniform [100] growth direction and straight surfaces. The bandgap of perovskite NW was successfully adjusted covering a broad range using three different compositions of halides.[77] Pan's group used vapor-phase deposition method to grow all-inorganic halide alloy perovskite NRs. They placed an alumina boat with a combination of CsX and PbX_2 at the heating area of the vapor deposition system and placed some SiO_2/Si substrates at the downstream of the quartz tube to synthesize the $CsPbX_3$ products. The as-grown $CsPbX_3$ NRs had a single crystalline structure with super smooth surface and precise triangular facets.[77] Yan and coworkers synthesized composition-graded $CsPbBr_xI_{3-x}$ NWs via desynchronized deposition of PbX_2 and temperature controlled halide exchange reaction.[78]

2.3. Synthesis Methods of Lead-Free PNCs

Despite the excellent optoelectronic properties of lead-based perovskite materials, the toxicity of lead element remains a serious issue in the view of commercialization. The lead-based perovskites can degrade to water-soluble lead ions, which bind strongly to sulfhydryl groups on proteins and damage the central nervous system.[79] Thus, great effort has been also devoted to synthesize lead-free PNCs. Here, we briefly introduce the synthesis method for lead-free PNCs.

Same as Pb, Sn and Ge belong to Group 14 and can fulfill the coordination and balance the charge to form a conventional perovskite structure. The tin-based PNCs ($CsSnX_3$, X = Cl, $Cl_{0.5}Br_{0.5}$, Br, $Br_{0.5}I_{0.5}$, I) are also the first reported lead-free PNCs (**Figure 10**a).[80] The absorbance and emission of the as-fabricated PNCs showed that bandgaps could be extended from visible to near-IR area by adjusting the amount of different halides (Figure 10b). Here, the hot injection method was a little different with lead-based PNCs. The tin precursor was dissolved in tri-*n*-octylphosphine, a mildly reducing and coordinating solvent, to avoid the precipitation of CsX during its injection into the Cs_2CO_3 precursor solution.[80] However, the easy oxidation of Sn^{2+} to Sn^{4+} makes tin-based material hard to be directly used in the environment. The tin(IV)-based PNCs, like Cs_2SnX_6 PNCs, are attractive as the substitutions to tin(II)-based PNCs due to their stability in the air. The first Cs_2SnI_6 NWs were synthesized by anodized aluminum oxide (AAO) templates (Figure 10c). So that, the perovskite precursor solution was added and allowed to penetrate the pores of AAO. Then, the excess liquid was removed from the surface followed by annealing to evaporate the solvent and obtain the final perovskite NWs.[81] Deng et al. obtained Cs_2SnX_6 NCs with various morphologies via a simple hot-injection method without using phosphine (Figure 10d–i). The Cs-oleate precursor was swiftly injected into tin precursor containing OA and OAm in ODE at 220 °C. At the initial stage, the shapes of the samples were QDs. Then NRs were obtained after 5 min of reaction. The NRs grew into NWs and the length extended after 10 min reaction time. After 30 min reaction period, NWs assembled side by side and nanobelts were formed, which could also be transformed into NPLs.[82] The germanium-based perovskite is another candidate to substitute lead in MHP. As far as we know, there is only one report about Ge-based NCs, $CsGeX_3$, which was synthesized by the hot-injection approach.[83]

Due to the easy oxidation of lead-substitution from 14 group, $A_3B_2X_9$ PNCs, where B represents trivalent oxidation state of Bi or Sb, have been considered as another choice for replacing lead-based PNCs. $MA_3Bi_2X_9$ (X = Cl, Br, I) QDs were first reported by Tang's group synthesized by LARP method (**Figure 11**a–d). Ethyl acetate and DMF were used as good solvents to solvate $BiBr_3$ and MABr and octane as poor solvent to precipitate $MA_3Bi_2X_9$ QDs. In addition, *n*-octylamine was used to control the rate of crystallization and OA was used to stabilize the colloidal solution.[84] Based on this achievement, further study was carried out on the Cl-passivation of $MA_3Bi_2Br_9$ QDs, which led to a bright blue emission with PLQY up to 54.1% at the wavelength of 422 nm. Unlike the lead-based PNCs, the halide exchange in $MA_3Bi_2Br_9$ is not so fast that the core−shell or locally concentrated Cl^- onto $MA_3Bi_2Br_9$ QDs can be achieved.[85] Gamelin et al. systematically studied the Cs–Bi–X compositions using a combination of hot-injection and postsynthetic anion exchange methods. $Cs_3Bi_2X_9$ (X = Cl, Br) NPs, Cs_3BiX_6 (X = Cl, Br) NCs, and $Cs_3Bi_2I_9$ (dimer modification) NCs were obtained by injecting trimethylsilyl halide (TMSX) reagents into the hot precursors of Cs and Bi acetate salts. The $Cs_3Bi_2X_9$ (X = Cl, Br) NPs could be formed when a high Bi/Cs ratio and a large excess of OA were used. However, higher Cs/Bi ratios and less OA favored the formation of Cs_3BiCl_6 over $Cs_3Bi_2Cl_9$. Interestingly, Cs_3BiBr_6 NCs synthesized by hot injection method suffered from a persistent CsBr impurity comparing with the one obtained by anion exchange using TMSBr.[86] The $Cs_3Sb_2X_9$ and $Rb_3Sb_2X_9$ PNCs were synthesized by hot-injection for the first time in 2017 (Figure 11e–g).[87] Nag et al. reported that the NPLs and NRs morphology of the $Cs_3Sb_2I_9$ NCs could be obtained by varying the reaction temperature, which was also reported for $CsPbBr_3$ NCs. Using the same synthesis method, the 2D layered structure of $Rb_3Sb_2I_9$ NCs were obtained. All these samples showed emissions in the yellow–red region.[87]

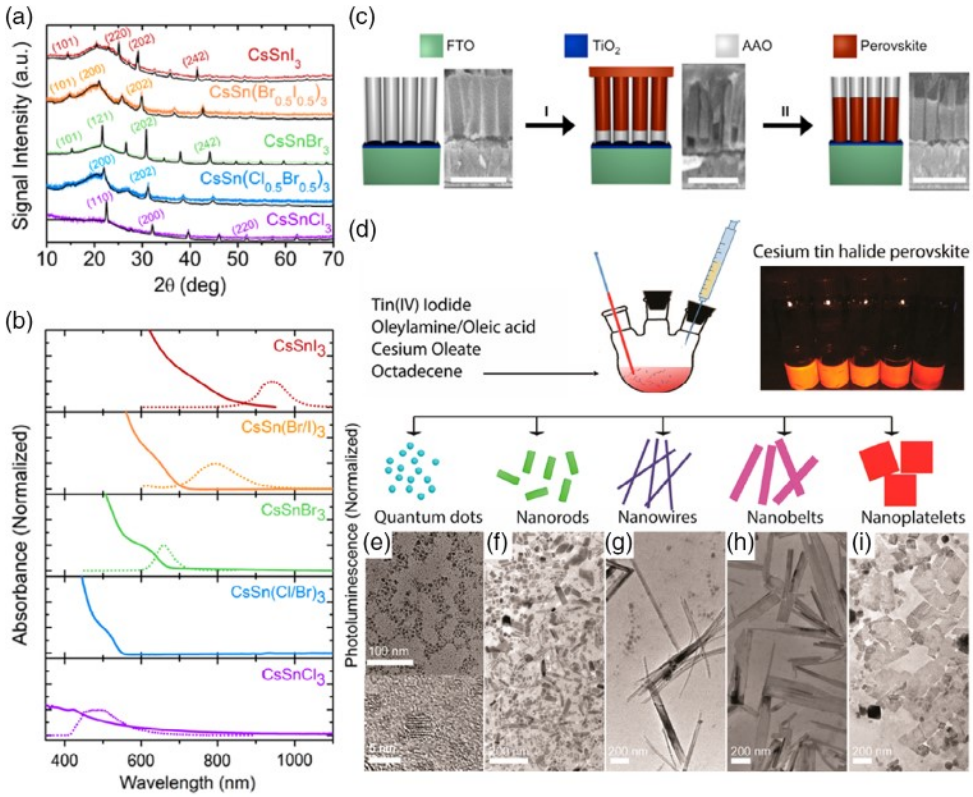

Figure 10. a) PXRD spectra of $CsSnX_3$ (X = Cl, $Cl_{0.5}Br_{0.5}$, Br, $Br_{0.5}I_{0.5}$, I) PNCs. b) Absorbance and steady-state PL of nanocrystals containing pure and mixed halides. The PL spectrum of $CsSn(Cl_{0.5}Br_{0.5})_3$ particles was identical to the pure chloride-containing nanocrystals. a,b) Reproduced with permission.[80] Copyright 2016, American Chemical Society. c) Synthesis of perovskite NW arrays in AAO. perovskite precursor solution penetrates the AAO pores, followed by spin coating and annealing (I). Sample is exposed to a DMSO/chlorobenzene solution followed by a short annealing step (II). Reproduced with permission.[81] Copyright 2016, American Chemical Society. d) Schematic of procedures for the controlled synthesis of perovskite Cs_2SnI_6 nanocrystals (left panel) and photograph of the as-prepared Cs_2SnI_6 samples under UV light (right panel). e–i) TEM images of Cs_2SnI_6 nanocrystals with different shapes (the inset of (e) gives an HRTEM image of Cs_2SnI_6 spherical QDs). d–i) Reproduced with permission.[82] Copyright 2016, American Chemical Society.

2.4. Anion-Exchange Reaction

By virtue of ionic property and structural instability of PNCs, the anion-exchange reaction is a simple and effective method to adjust the optical properties of PNCs. For example, the bandgap and the absorption spectra of PNCs can be adjusted easily for different applications in SCs, LEDs, and PDs.[36] Park et al. first reported the finding of reversible anion-exchange reaction of $MAPbX_3$ (where X = Cl, Br, and I). The mixed halide $MAPbBr_{3-x}Cl_x$ or $MAPbBr_{3-x}I_x$ NCs can be synthesized by adding a starting material ($MAPbBr_3$) into MACl or MAI solution, respectively. The composition of the final products can be controlled easily by adjusting the molar ratio of starting material and MAX, enabling the absorption and PL spectra of PNCs to cover a wide range.[88]

The anion-exchange reaction for all-inorganic $CsPbX_3$ was also demonstrated by Manna et al, where different halide precursors, such as oleylammonium halides (OLAM-X), octadecylammonium halides (ODA-X), tetrabutylammonium halides (TBA-X), and lead halide salts (PbX_2), were tested in the exchange reactions. Interestingly, when TBA-X was chosen as halide precursor, anion-exchange reactions did not work from Cl to Br or from Br to I, but worked from Br to Cl or from I to Br. For other halide precursor tested in this work, the reversible anion-exchange reaction could be achieved. The hard/soft acid/base interaction can explain this phenomenon. TBA cation prefers binding to softer halide ions because it is a soft acid. The Br^- (or I^-) ions are softer than Cl^- (or Br^-) ions, thereby remaining associated with TBA.[89]

Previous anion-exchange reactions were commonly carried out using OAm-halide precursors, which needed to prepare in a Schlenk line at high temperature. In addition, the optical performance was prone to be damaged due to unstable crystal structures of PNCs. Wang et al. reported a novel precursor, which was consisted of OAm–copper halide complexes. The reaction could be operated at RT and the final products showed good structural stability and crystallinity improvement. The PLQY and stability of PNCs treated with CuX_2 showed an obvious improvement.[90] Chen et al. first used MgX_2 as a halide precursor to study the anion-exchange reaction in $CsPbBr_3$ NCs. The morphology and crystal phase of the original $CsPbBr_3$ NCs retained after the reaction. Also, the final products showed good stability and tunable bandgap. Furthermore, they selected a series of metal halide salts MX_2 (M = Cd, Pb, Sn, Zn, Sr, Ca, Cu, Ba,

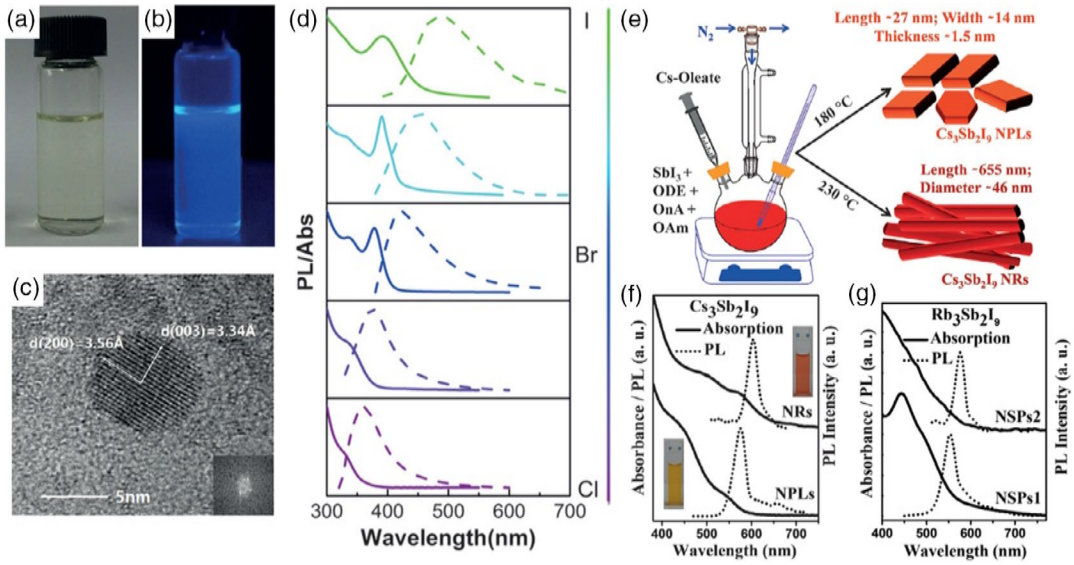

Figure 11. Optical image of a colloidal $MA_3Bi_2Br_9$ solution under a) visible light and b) 365 nm UV light. c) HRTEM image of a typical QD. The inset in the bottom right corner is the corresponding fast Fourier transform (FFT) image. d) Composition-tunable absorption and PL spectra of perovskite $MA_3Bi_2X_9$ QDs by halide substitution. a–d) Reproduced with permission.[84] Copyright 2016, Wiley-VCH. e) Schematic representation of the synthesis of $Cs_3Sb_2I_9$ NPLs and $Cs_3Sb_2I_9$ NRs. ODE = 1-octadecene, OnA = octanoic acid, OAm = oleylamine. f) UV–vis absorption and PL spectra of $Cs_3Sb_2I_9$ NPLs and $Cs_3Sb_2I_9$ NRs. Insets: photographs of colloidal $Cs_3Sb_2I_9$ NPLs (yellow) and $Cs_3Sb_2I_9$ NRs (red) under visible light. g) UV–vis and PL spectrum of $Rb_3Sb_2I_9$ NSPs1 (reaction temperature 180 °C) with the diameter of around 7.5 nm and $Rb_3Sb_2I_9$ NSPs2 (reaction temperature 230 °C) with the diameter of around 17 nm. e–g) Reproduced with permission.[87] Copyright 2017, Wiley-VCH.

Mn, Ba) as precursors for halide-exchange reaction to find a predication rule of precursors. After comprehensive study, they concluded that the similar bonding dissociation energy (BDE) values within the precursor and host lattice can make the halide exchange proceed easily.[91]

3. Stability of PNCs

Stability is one of the critical issues for commercialization of PNCs. To solve the instability problem of PNCs, we should have a deep understanding of the origin of degradation mechanisms. This section reviews crystal structural stability, interface-induced stability, and environmental stability such as oxygen, moisture, light, and thermal stability.

3.1. Crystal Structural Stability

As shown in Figure 1a, the typical structure of halide perovskite is a cube, where the divalent metal cation is placed in the center, and monovalent cations and halide anions occupy the vertexes and face centers, respectively. The center B-site cation coordinates with six halides and forms a BX_6 octahedral configuration. By sharing the corner halides, a continuous array can be obtained. And A-site cations, which are bigger than B-site cations, occupy the vacancy between BX_6 octahedra. That is the ideal 3D framework perovskite structure. However, under normal conditions, perovskites tend to distort away from a highly symmetric cubic structure, thereby forming an orthorhombic phase. Some reason can cause this transformation (vide infra). Obviously, this distortion leads to different electronic and optical properties and we will discuss them in the following paragraphs.

To evaluate structural stability of perovskite materials comprising different cations and anions, we can use the well-known Goldschmidt's tolerance factor, t, which is defined as[92]

$$t = \frac{r_A + r_X}{\sqrt{2}(r_B + r_X)} \quad (1)$$

where r_A, r_B, and r_X correspond to the radius of components A, B, and X, respectively. In an ideal condition, the value of t equals to 1, that is to say, the crystal structure is a cube. Generally, the t value is in the range of around $0.813 \leq t \leq 1.107$ for 3D perovskites. Zeng et al. consider that the range of $0.9 \leq t \leq 1.0$ is ideal for cubic perovskite structure in general. The range of $0.71 \leq t \leq 0.9$ is considered as likely formation of orthorhombic or rhombohedral structure due to distortion of BX_6 octahedrons. In other cases, that is $t \leq 0.71$ or $t \geq 1$, nonperovskite structures such as NH_4CdCl_3-type (1D orthorhombic structures formed by the edge sharing of octahedra) or $CsNiBr_3$-type structures (1D hexagonal structures formed by the face-sharing of octahedra) are formed.[93] These nonperovskite materials normally have large bandgaps and low electronic conductivity. The other semi-empirical geometric parameter to assess the structural stability of the BX_6 octahedra is octahedral factor, μ, which can be defined as

$$\mu = r_B/r_X \quad (2)$$

The stable BX_6 octahedral structure has μ value between 0.442 and 0.895. These two empirical indicators can effectively describe and predict the putative perovskite's structural stability, leading

to the conclusion that ionic radii of components play a crucial role in the crystal structural stability.

Both $MAPbCl_3$ and $MAPbBr_3$ have cubic structures, and $MAPbI_3$ has a tetragonal structure at RT. As for $CsPbI_3$, the cubic perovskite phase can be obtained at high temperature (315 °C), however, this material changes to the nonperovskite phase at the temperature below 315 °C, which accompanies with bandgap changed from direct to indirect with value from 1.73 to 2.82 eV, respectively.[94–96] $CsPbBr_3$ is one of the most studied PNCs which also shows superior stability to $CsPbI_3$. However, the binding energy and the effective Bohr diameter of Wannier–Mott exciton of $CsPbBr_3$ are 40 meV and 7 nm, respectively, which are inferior to $CsPbI_3$ (20 meV, 12 nm). In addition, the bandgap of $CsPbBr_3$ is 2.0 eV which is also inferior to $CsPbI_3$ (1.44 eV) in terms of photovoltaic applications. For FA-based PNCs, they have been synthesized by hot injection method and LARP method. Indeed, a tolerance factor closer to 1 can be achieved with FA cation than MA and Cs ones,[97] although the sizes of MA ($R_A = 2.17$ Å) and FA ($R_A = 2.53$ Å) are similar. The fact is that the crystal structures of $MAPbI_3$ is tetragonal but $FAPbI_3$ is trigonal or pseudocubic. It is because that FA^+ is more prone to form hydrogen bonds than MA^+, thus more stable pseudocubic structure can be obtained.[98] However, it has been reported that $FAPbI_3$ exists in two kinds of polymorphs: one is a perovskite-type material with trigonal symmetry ($P3m1$); the other is a yellow hexagonal nonperovskite material ($P6_3mc$).[99]

Currently, using a mixture of different cations, like Cs/MA,[100,101] Cs/FA,[102–105] MA/FA,[106] Cs/Rb,[107–109] etc., as the monovalent cations in A-site of perovskite structure is widely adopted by researchers, which can adjust the value of tolerance factor close to 1 to make PNCs stable. In addition to stability, optoelectronic properties and shapes of PNCs can also be modified. A great review published recently has comprehensively summarized the effect of doping and substitution in metal halide PNCs.[97] Therefore, we do not unfold this topic here.

Low-dimensional perovskites, like 2D perovskites arranged in the Ruddlesden–Popper phase, have become the research hotspot recently due to their excellent environmental stability. 2D perovskites have a general formula $R_2A_{n-1}B_nX_{3n+1}$, where R is an additional bulky organic cation (such as an aliphatic or aromatic alkylammonium) as a spacer between the inorganic sheets and n defines the number of inorganic layers held together. These 2D perovskites are much more stable than 3D perovskites due to the van der Waals interactions exited among organic molecules and consequently, increased formation energy. In addition, unlike 3D perovskites which limit the radius of the A-site cations to around 2.6 Å,[110] a wide choice of organic cations is available for 2D perovskites, which can also benefit the designing of new types of perovskite with desired properties for various optoelectronic applications.

Importantly, structural stability of PNCs is slightly different from bulk perovskite. On the one hand, the large specific surface area could speed up decomposition.[111] On the other hand, the large surface energy can stabilize the cubic phase.[112] For instance, as mentioned before, bulk $CsPbI_3$ with a cubic phase is only sable at high temperature, and it tends to transform into a nonperovskite phase with a larger bandgap by reducing the temperature. However, $CsPbI_3$ NCs can maintain cubic crystal structure for some months in air.[112]

Pressure can significantly induce a structural phase transition, thereby changing the optoelectronic properties of the corresponding perovskite materials, such as bandgap, carrier lifetime, photocurrent, electrical resistance, etc.[113–116] For example, 0D Cs_4PbBr_6 NCs which show initially nonfluorescent property can obtain a distinct emission at high pressure (above 3.01 GPa). The reason is the large distortion of $[PbBr_6]^{4-}$ octahedra due to the structural phase transition from rhombohedral to monoclinic. Moreover, the excited-state structural reorganization, which is required to trap an exciton, is considered to be smaller than the one of the ambient pressure. Thus, Cs_4PbBr_6 NCs with high-pressure monoclinic structural phase exhibit PL.[113]

3.2. Interface-Induced Instability

Perovskite interface is crucial for stability and performance of devices like solar cells (SCs), PDs, and LEDs. Here, we only focus on the interface between PNCs and their environments. The PNCs show high ionicity and structural instability. So, the interaction between the surfaces of PNCs and the capping ligands is ionic and labile, which is crucial to the stability of structure. First, we want to introduce the Covalent Bond Classification (CBC) to classify metal–ligand interactions, which was developed by Green and coworkers.[117,118] According to CBC, ligands are classified as L-type, X-type, or Z-type, which depend on the amount of electrons that the neutral ligand contributes to the metal–ligand bond (2, 1, or 0, respectively).

Hens and coworkers first studied the surface chemistry of $CsPbX_3$.[45] They used ^1H solution nuclear magnetic resonance (NMR) spectroscopy to characterize the purity of sample, clarify the surface chemistry, and estimate the influence of purification process on the surface composition. In short, they found that surface ligands binding to the $CsPbBr_3$ NC surface are highly dynamic, that is to say, ligands are lost during isolation and purification in an easy way. Both carboxylic acids and long-chain amines were required to stabilize the surface during purification, as well as sustaining optical and material integrity. They also measured the diffusion coefficient D of a molecule in NC suspension to further study the dynamic surface by using Diffusion Ordered NMR Spectroscopy (DOSY), because the diffusion coefficient of a bound ligand can be considered as the same as that of the whole object (PNC core with ligand shell). The diffusion coefficient D is associated with molecule size via the Stokes–Einstein equation with k_B the Boltzmann constant, T the absolute temperature, and f the friction coefficient

$$D = \frac{k_B T}{f} \tag{3}$$

The value of D for oleylammonium bromide without $CsPbBr_3$ NCs and in the suspension was measured to be 361 and $166 \pm 18\ \mu m^2\ s^{-1}$, respectively. This indicated that surface ligands in the PNCs' solutions were not tightly attached on the surface but undergo a rapid exchange between free state and bound. This dynamic stabilization mechanism with oleylammonium bromide can well elucidate the fast halide exchange reaction during device fabrication.

3.3. Environmental Stability

The environmental stability of PNCs has become a primary concern for their applications in the real world. A comprehensive understanding of the degradation mechanism of PNCs including the degradation under moisture, oxygen, and light exposure, allows for a rational design of stable PNCs implemented in quantum dot solar cells (QDSCs), quantum dot light-emitting diodes (QLEDs), etc.

3.3.1. Moisture

Moisture, which exists everywhere in our life, is considered to be harmful to the stability of PNCs. Although some groups have reported that water can be valuable for perovskite device fabrication,[119–121] it is considered as a "toxicant" to PNCs, regardless of the duration of exposure and amount of water.[122–124] The large perovskite crystals can be obtained with the assistant of moisture, because it can be absorbed within grain boundaries and then induce grain boundary creep and merge the adjacent grains together, as well as enhance the ion diffusion length by providing the aqueous environment.[125] However, when exposed to the moisture atmosphere, the perovskite structure showed a fast degradation, characterized by color change from black to yellow for perovskite structure like $MAPbI_{3-x}Cl_x$. Snaith et al. attributed the color change to the transformation of perovskite crystal structure to 0D system, where compounds are present as isolated octahedral. When water molecules are introduced into the crystal structure, they form weak hydrogen bonds to hydroscopic MA^+, which lead to a bond dissociation between the crystal constituents.[124] Although there are some discrepancies, an evident conclusion is that water worked as a catalysis in the process of degradation. Therefore, water only speeds up the decomposition of PNCs by carrying the proton of MA^+ to I^- and liberating CH_3NH_2. Alberti et al. found that $MAPbI_3$ undergo a comparable degradation dynamics pathway, where the crystal structure of $MAPbI_3$ changed from tetragonal to cubic without hydration taking place.[126] For all-inorganic perovskite materials like $CsPbI_3$, water also catalyzed the conversion of γ-$CsPbI_3$ to δ-$CsPbI_3$ illustrated by in situ powder X-ray diffraction (PXRD) measurement.[127]

3.3.2. Oxygen

The ground-state lead-based perovskites show good stability in oxygen atmospheres. Li et al. reported that PL of $CsPbBr_3$ NCs showed no obvious decrease when exposed to the relative humidity (RH) levels of 60% and 80% for 8 h.[125] However, PL intensity increased under oxygen atmospheres, which was called the "oxygen boost" effects.[14] It was revealed by density functional theory (DFT) modeling that oxygen molecules effectively inactivated deep hole traps related to iodide interstitials by forming reasonably stable oxidized products in $MAPbI_3$. Upon illumination in an inert atmosphere, some sub-bandgap states are formed in $MAPbI_3$.[128] Then, the oxygen molecules could attenuate the trap density. Thus, suppression of traps led to brighter PL emission under oxidizing conditions.

However, the temporal "oxygen boost" effects only occurred at the beginning of illumination. Upon continuous illumination, the green film of $CsPbBr_3$ NCs would change to yellow soon (within 1 h).[125] Haque et al. combined experimental and computational methods and proposed the probable degradation mechanism as (see **Figure 12**a): a) oxygen diffusion and incorporation into the lattice, b) photoexcitation of $MAPbI_3$ to create holes and electrons c) superoxide formation from oxygen, and d) reaction and degradation to layered PbI_2, H_2O, I_2, and CH_3NH_2.[129]

3.3.3. Light

The stability issues against moisture and oxygen can be avoided using encapsulation strategies, but the light stability of perovskite materials is still a serious topic.[130] For the application as absorber in SCs to capture solar energy and as convertor in LEDs to change the blue/UV light into various visible light, PNCs need a long-term stability under continue illumination. Thus, a deep understanding of the original reason for the photodegradation of PNCs is of great importance to enhance the performance and lifetime of the PNCs-based optoelectronic devices.

The phenomenon of photoinduced "brightening" of the perovskite PL, called the light soaking effect, is widely reported in perovskite-based SCs and LEDs. For bulk perovskite, PL intensity of $MAPbI_3$ film would increase up to three orders of magnitude and PL lifetime would increase from several nanoseconds to several hundred nanoseconds upon light irradiation with an excitation power density of 0.01–1 $W\,cm^{-2}$. In addition, light-induced PL enhancement is reversibly enabled by switching off excitation light. The most interesting discovery is that switching the atmosphere between nitrogen and oxygen would also reverse the photo-induced "brightening" (Figure 12b).[131] However, Mohite et al. have observed that the oxygen had minor effects on photoinduced "brightening" due to the large-grain perovskite structures, preventing direct exposition to the external atmosphere.[130] McGehee et al. has reported a similar phenomenon in $MAPbI_{3-x}Br_x$ films. They also observed the X-ray diffraction (XRD) peaks split with light soaking, which means the crystal segregated into two crystalline phases (Figure 12c). After leaving for a few minutes in the dark, the XRD pattern reverted to their original shape.[30]

The photo-induced "brightening" of emission can be associated with an order-of magnitude decrease in density of trap state, which was caused by ion migration under illumination. Stranks et al. used confocal PL microscopy and time-of-flight secondary ion-mass spectrometry to study this phenomenon. From time-of-flight secondary ion mass spectrometry (ToF-SIMS) image of iodide distribution mapping and line scan (Figure 12d,e), the areas exposed to high radiation showed depleted levels of iodide (lower than the background iodide levels), while the adjacent areas showed iodide-rich levels compared with the background iodide levels. This work provides obvious evidence for photoinduced halide migration in $MAPbI_3$. Thus, field-induced both vertical and lateral migration allowed a large number of iodide to occupy the vacancies and yield a decrease in density of vacancies,

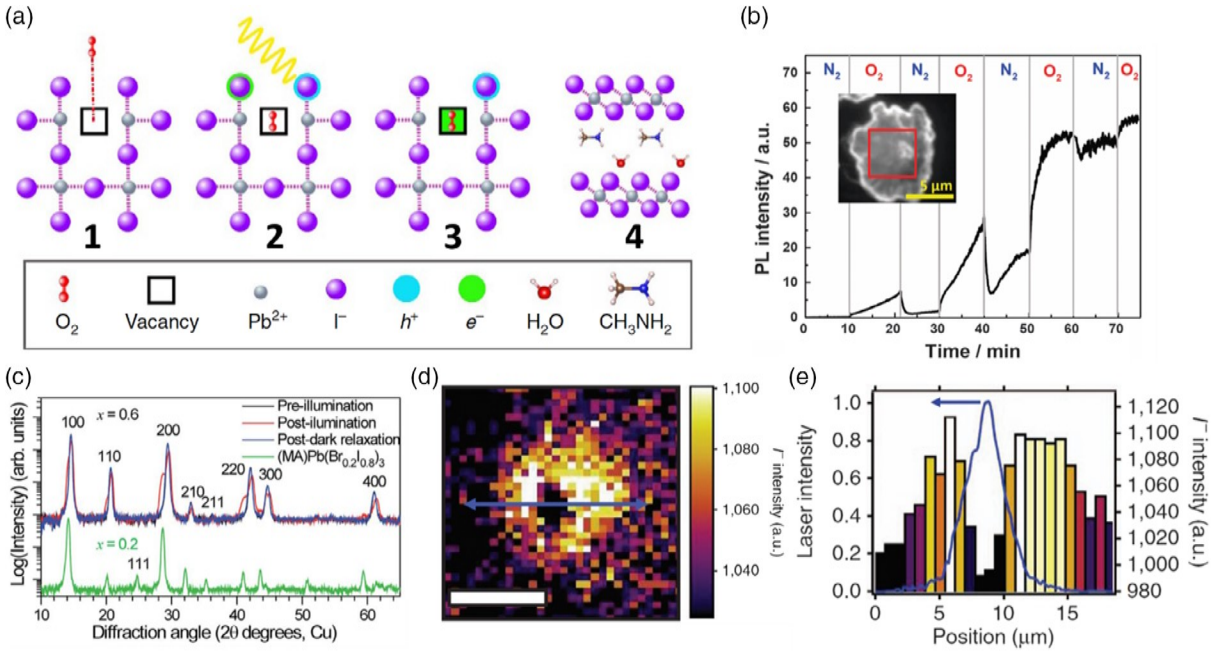

Figure 12. a) Oxygen-induced photodegradation. Schematic representation of the reaction steps of O_2 with $MAPbI_3$. Reproduced under the terms of the CC-BY license.[129] Copyright 2017, Springer Nature. b) The atmosphere effect on the PL enhancement of $MAPbI_3$. The atmosphere was switched between N_2 and O_2 at the time moments indicated by the gray vertical lines. The sample was continuously irradiated by 0.2 W cm^{-2}. Inset shows the PL micrograph of the sample and the selected region (red square) taken for the analysis. The sample was kept in N_2 for 5 min before the experiment. Reproduced with permission.[131] Copyright 2015, Royal Society of Chemistry. c) XRD pattern of an $x = 0.6$ film before (black) and after (red) white-light soaking for 5 min at ≈50 mW cm^{-2}, and after 2 h in the dark (blue). The XRD pattern of an $x = 0.2$ film (green) is offset for comparison. Reproduced under the terms of the CC-BY license.[30] Copyright 2014, Royal Society of Chemistry. d) ToF-SIMS image of the iodide (I^-) distribution summed through the film depth (the image has been adjusted to show maximum contrast), scale bar, 10 mm. e) Line scan of the blue arrow in (c) to show the iodide distribution (right axis). The measured spatial profile of the illumination laser (blue) is shown on the left axis. d,e) Reproduced under the terms of the CC-BY license.[31] Copyright 2016, Springer Nature.

which can suppress the nonradiative recombination and enhance the intensity of PL.[31]

3.3.4. Temperature

Temperature is another factor that causes the degradation of PNCs. The all-inorganic PNCs have shown better thermal stability than organic–inorganic hybrid PNCs. For example, according to thermogravimetric analysis (TGA) measurements, the sublimation of HX and CH_3NH_2 for $MAPbBr_3$ and $MAPbI_3$ is around 220 °C[132] and 250 °C,[133] respectively. But for $CsPbX_3$, the decomposition temperature is over 500 °C because of the collapse of crystal structures.[133] In addition, high temperature can even accelerate the degradation caused by oxygen and moisture.[124] Interestingly, Schaller et al. studied the reversibility of PL intensity of $CsPbBr_3$ QDs under the operations of multiple heating and cooling steps. The sample lost ≈5% of original PL intensity at 300 K when heated to 400 K and lost ≈20% for 450 K. However, when the sample was heated to a higher temperature, the PL quenching was irreversible. The reason might be the desorption and decomposition of organic ligands above 450 K.[134] The reversible PL feature is favored by LED application, in which the operation of devices always caused a certain amount of temperature increase.

4. Encapsulation for Improving the Stability

Encapsulation is one of the most potential strategies to enhance the stability of PNCs. Recently, some great articles about encapsulation of PNCs have been published, introducing different methods and materials. Chen and coworkers have reviewed these works and present a nice summary, as shown in **Figure 13**.[34] In this section, we focus on the most used materials for encapsulation.

4.1. Organics Protection

The mixture of NPs and polymers as composite material has been practiced for decades.[135] In the early 1990s, Kamigaito et al. reported that the addition of mica to nylon can produce a fivefold increase in the tensile strength and yield of the material.[136,137] Actually, polymers can also work as surface coating to enhance the stability of PNCs.

Kovalenko et al. embedded $CsPbX_3$ NCs into poly(methyl methacrylate) (PMMA) polymer by a RT photoinduced polymerization and fabricated multishapes of PNCs-PMMA composite material (**Figure 14**a). They also reported that $CsPbX_3$ NCs accelerated the rate of photopolymerization when comparing to the experiment with pure MMA.[40] Zhong et al. reported

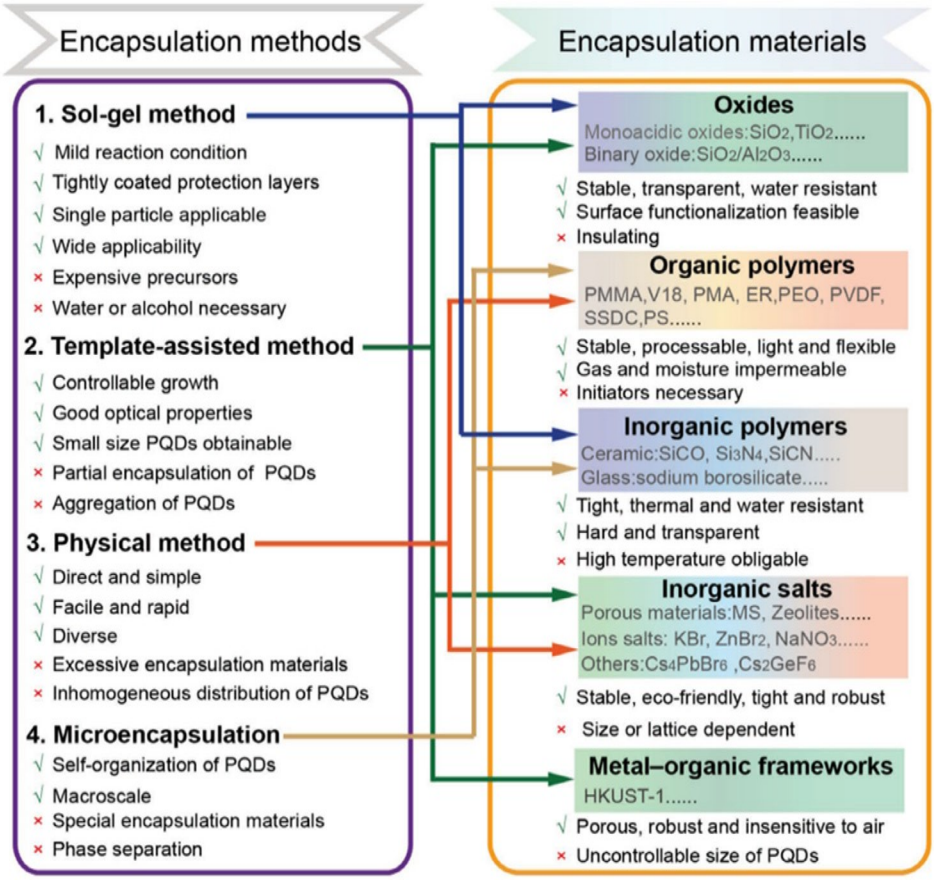

Figure 13. Relations between encapsulation methods and materials as well as their advantages and disadvantages. Reproduced with permission.[34] Copyright 2019, Wiley-VCH.

an in-situ synthesis method of $MAPbX_3$ NCs, which were embedded in polyvinylidene fluoride (PVDF) matrix. They dissolved MAX, PbX_2, and PVDF in DMF. Subsequently, DMF solvent was dried under low pressure and $MAPbX_3$ NCs crystallized in PVDF film. A variety of composite films with colorful emissions on glass substrates were successfully fabricated (Figure 14b). Figure 14c,d shows the transmittance and PL emission spectra of these $MAPbX_3$/PVDF composite films.[138] Polyvinyl pyrrolidone (PVP) was also used as capping ligand to protect PNCs, which was physically adsorbed and wrapped on the surface of PNCs.[139,140] Fu et al. synthesized $CsPbBr_3$ NCs via a simple one-step solution self-assembly process and used biocompatible PVP as ligand to control the coprecipitation of Cs^+, Pb^{2+}, and X^- species.[139] Recently, He et al. used 100 nm cellulose nanocrystal (CNC) instead of traditional ligands to synthesize $MAPbBr_3$ PQDs paper using a vacuum filtration growth method. The cellulose has a large amount of —HSO_3^- and —O^-, which can work as ligands to control the formation of PNCs. After the solvent was removed, $MAPbBr_3$ PQDs were crystallized with the assistance of surface ligands. In addition, the $MAPbBr_3$ PQDs were also protected by CNC and their relative PL intensity remained at around 80% after exposure to an environment of 60% RH and 20 °C for 8 months.[141]

4.2. Inorganics Protection

4.2.1. Silica

Among inorganic materials, silica is one of the best choices to cover the PNCs. Silica is widely distributed in nature and also possess excellent stability in the environment. It can work as a template and serve via a facile, complementary, noncolloidal, and ligand-free preparation route.[142] In addition, silica with an excellent compatibility is accepted as "Generally Recognized As Safe" (GRAS) by the Food and Drug Administration (FDA). This material has been broadly utilized in cosmetics and also as food additives approved by FDA, which can make application of PNCs in bio-applications possible.

Liu et al. first used silica to protect PNCs. They mixed $CsPbBr_3$ QDs solution with the commercial mesoporous silica particles in hexane to synthesize $CsPbBr_3$-mesoporous silica composites (**Figure 15**a). The pore sizes of mesoporous silica are ≈12–15 nm. This treatment can avoid halide exchange and increase the stability of QDs, which is of great importance for LED packaging.[143] Kovalenko et al. used a related approach to introduce perovskite precursor into the pores of mesoporous silica, where PNCs can crystallize there (Figure 15b). In addition, the sizes of PNCs could be adjusted by mesoporous silica's pore

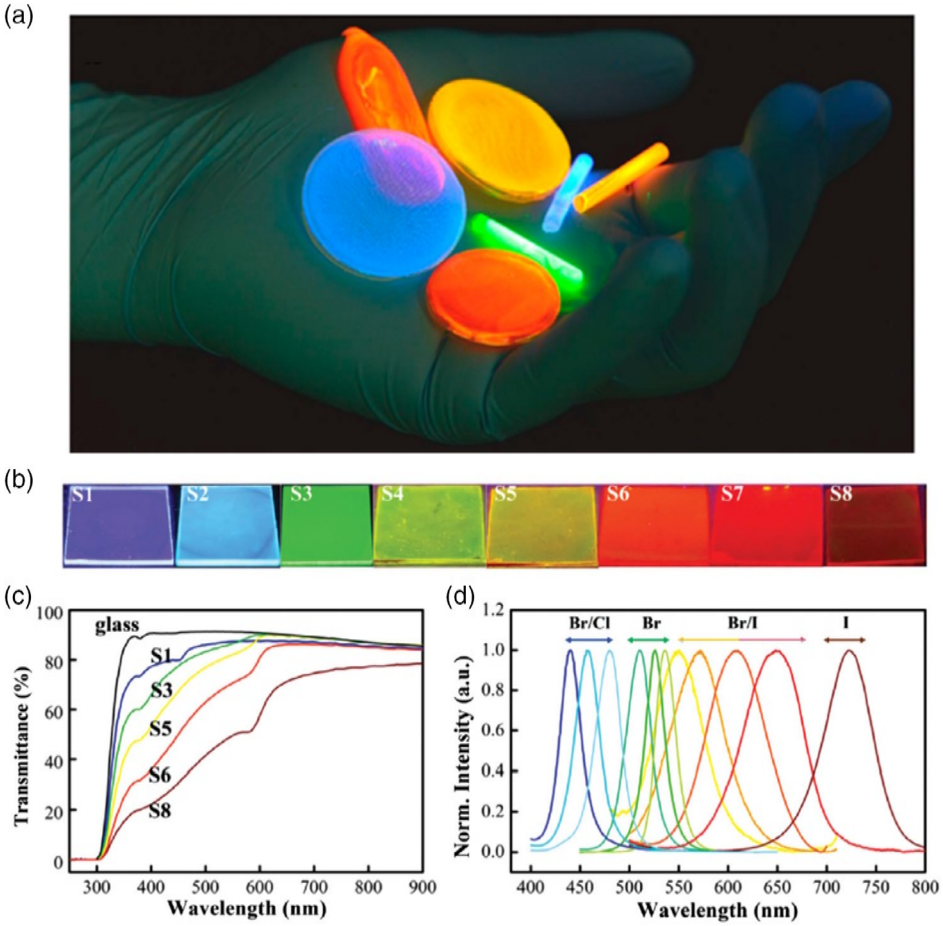

Figure 14. a) Photograph ($\lambda_{exc} = 365$ nm) of highly luminescent $CsPbX_3$ NCs-PMMA polymer monoliths obtained with Irgacure 819 as photoinitiator for polymerization. Reproduced with permission.[40] Copyright 2015, American Chemical Society. b) Optical images under a UV lamp (365 nm) of color-tunable $MAPbX_3$/PVDF composite films with different halogen constitutions on glass substrates (S1: $MAPbClBr_2$, S2: $MAPbCl_{0.5}Br_{2.5}$, S3: $MAPbBr_3$, S4: $MAPbBr_{2.7}I_{0.3}$, S5: $MAPbBr_{2.5}I_{0.5}$, S6: $MAPbBr_2I$, S7: $MAPbBr_{1.5}I_{1.5}$, S8: $MAPbI_3$). c) Transmittance spectra of the correlated composite films on glass substrate. d) PL spectra of the composite films. b–d) Reproduced with permission.[138] Copyright 2016, Wiley-VCH.

sizes, which also improved the uniformity of PNCs.[142] Li et al. developed a novel SiO_2 encapsulation method by choosing tetramethyl orthosilicate (TMOS) as precursor to synthesize silica cover on the $MAPbX_3$ PNCs. TMOS was used as the precursor, and its hydrolysis rate is much quicker than that of tetraethyl orthosilicate (TEOS). Thus, it can avoid a higher water consumption rate, which can damage perovskite's phase structure. After 4 days, the green light emission of the pure PQDs solution totally disappeared, but the PQDs solutions with TEOS and TMOS still emitted green light, in which TMOS-modified sample showed better stability (Figure 15c).[35] Yu et al. chose (3-aminopropyl) triethoxysilane (APTES) as both capping agent for inorganic PQDs and precursor for silica matrix. They mixed APTES with PbX_2 precursor in a water-free system to synthesize PNCs. But after crystallization of PNCs, the system was opened to air and stirred for 3 h for the hydrolytic reaction (Figure 15d,e). The stability of the PNCs improved that the luminescence of PNC with silica showed no obvious reduction after exposure to air for 90 days.[144]

Zhang et al. developed an interfacial synthesis of $CsPbX_3/SiO_2$ Janus NCs by treating a mixture of Cs_4PbX_6 NCs and alkoxide with water. The as-obtained material exhibited significantly enhanced PL stability against damages by air, water, and light treatment. However, the $CsPbX_3$ NCs were partially covered with oxides, the long-term stability of product remained as an issue.[145] Zhang's group focused on the PNCs/Silica combination strategies and designed a facile one-pot synthesis of $CsPbBr_3@SiO_2$ core–shell NPs. They injected a mixture of CsBr, $PbBr_2$, OA, OAm, DMF, and ammonia solution into toluene containing TMOS and successfully obtained monodisperse $CsPbBr_3@SiO_2$ core–shell NPs, which showed excellent stability in humid air or even under ultrasonication in water.[146]

4.2.2. Salts

Except for silica, Zhong et al. used $NaNO_3$ as the matrix to protect $MAPbBr_3$ PNCs due to the virtue of its transparency, low refractive index, and nontoxicity. The $NaNO_3$ could also be dissolved in DMF, which made the one-step reprecipitation procedure achievable for fabrication of $MAPbBr_3/NaNO_3$ nanocomposites (**Figure 16**a). This strategy was extremely fast, facile, and efficient

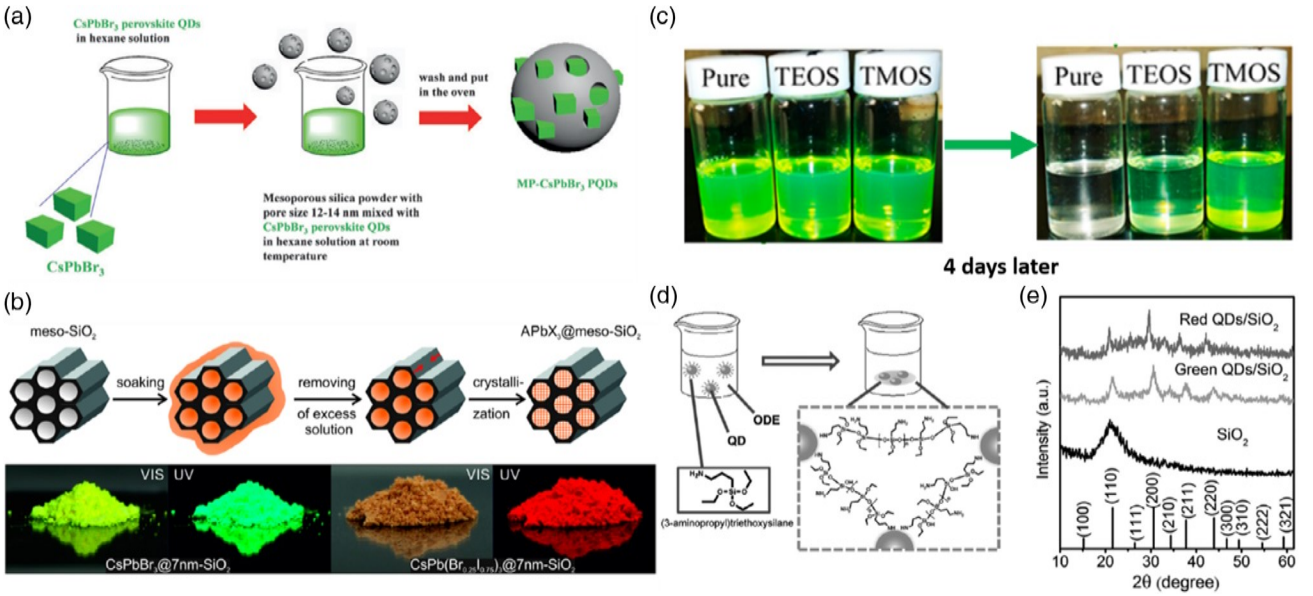

Figure 15. a) The synthesis process of mesoporous silica green PQD nanocomposite (MP-PQDs). Reproduced with permission.[143] Copyright 2016, Wiley-VCH. b) Schematic of the template-assisted synthesis of $APbX_3$ NCs ($A = Cs^+$, MA^+ or FA^+; $X = Br^-$ or I^-) in the pores of mesoporous silica (up) and the photographs of mesoporous silica impregnated with $CsPbBr_3$ (left) and $CsPb(Br_{0.25}I_{0.75})_3$ NCs (right) under daylight and under UV illumination (down). Reproduced with permission.[142] Copyright 2016, American Chemical Society. c) Optical images of the colloidal $MAPbBr_3$-QD solutions with TEOS and TMOS before and after 4 days. Reproduced with permission.[35] Copyright 2016, American Chemical Society. d) Schematic illustration of formation of QD/silica composites. e) XRD patterns of SiO_2, Red QDs/SiO_2, and Green QDs/SiO_2. Reproduced with permission.[144] Copyright 2016, American Chemical Society.

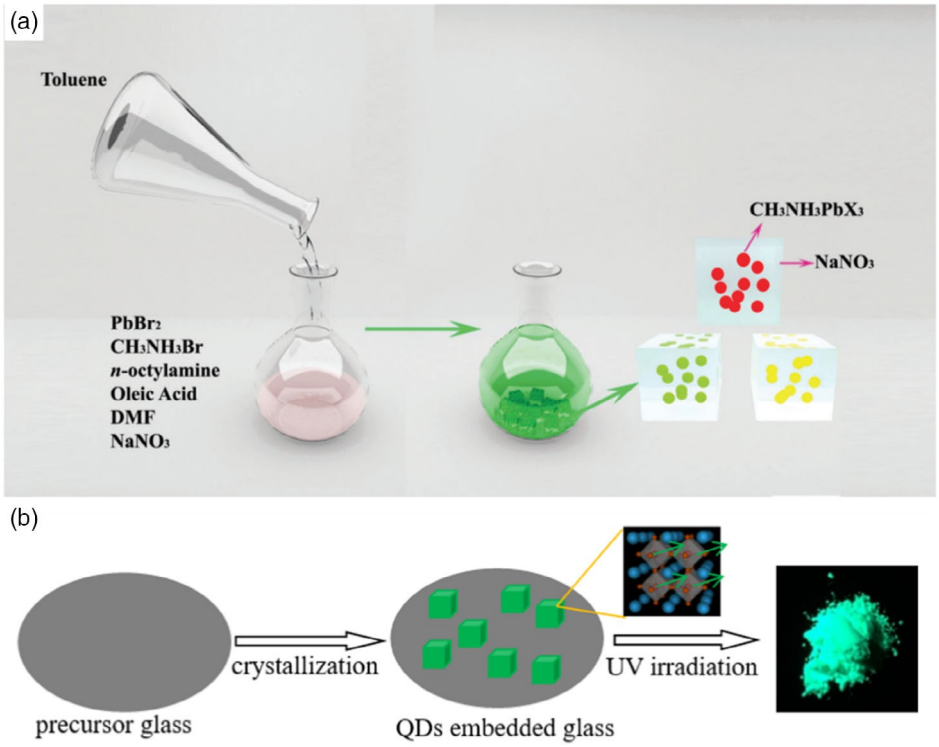

Figure 16. a) Scheme of a one-step reprecipitation procedure for synthesis of $MAPbBr_3/NaNO_3$ nanocomposites. Reproduced with permission.[147] Copyright 2016, Royal Society of Chemistry. b) Glass crystallization strategy to fabricate QD-embedded glass: $CsPbX_3$ crystal structure and luminescent photograph of QDs@glass powder under irradiation of UV lamp (365 nm) are also provided. Reproduced with permission.[148] Copyright 2018, American Chemical Society.

that the $MAPbBr_3/NaNO_3$ composites could be formed immediately after pouring the poor solvent toluene into the precursor. The sizes of $MAPbBr_3$ NCs were 30–50 nm and they were homogenously distributed in the matrix. The $NaNO_3$ matrix made PNCs highly resistant to heat, light, and polar solvent, like chloroform.[147] Chen et al. realized the in situ crystallization of $CsPbBr_3$ QDs among a particularly designed TeO_2-based glass matrix (Figure 16b). In addition, the melting temperature of TeO_2-based glass could be lowered down to 650 °C, comparing with high melting temperature (up to 1100 °C) of other commonly used glass hosts, which could avoid the volatilization of Br sources and increase the amount of crystallized $CsPbBr_3$ QDs in the glass. The $CsPbBr_3$ QD-embedded glasses (QDs@glass) showed a high PLQY of ≈70%, superior photo/thermal stability and excellent water resistance.[148]

Hou et al. chose magnesium silicate as the protector for $MAPbX_3$ PQDs because this material is a transparent and ecofriendly inorganic material, with a unique structure and good thermal stability. They developed a simple strategy that incorporated $MAPbX_3$ PQDs into magnesium silicate hollow spheres (MSHSs) in toluene via a modified LARP method at ambient condition. These nanocomposites ($MAPbX_3$ QDs-MSHSs) showed outstanding PL that the emission peaks were broadly tunable in the blue-to-red region and the quantum yields (QYs) was above 50%, which also had surprisingly high thermal stability and high photostability (**Figure 17**).[149]

4.2.3. Perovskite

Some stable perovskite materials can also serve as protectors for PNCs. Sun and Zeng et al. reported a ligand-free low-temperature solution-growth $CsPbBr_3/Cs_4PbBr_6$ perovskite nanocomposites (**Figure 18**). They incorporated $CsPbBr_3$ QDs into matrix of Cs_4PbBr_6 PNCs by low temperature solution-phase synthesis, which could significantly improve the thermal stability and photostability of PQDs. $CsPbBr_3/Cs_4PbBr_6$ nanocomposites showed high PLQY of up to ≈55% and $CsPbBr_3$ QDs exhibited a steady stimulated emission profile irrespective of temperature change, which was beneficial to long-term stable operating optoelectronic devices.[150] Zhong et al. also used a slow-cooling method to grow Cs_4PbBr_6 assisted by HBr. They found the non-stoichiometry of original Cs_4PbBr_6 crystals led to the formation

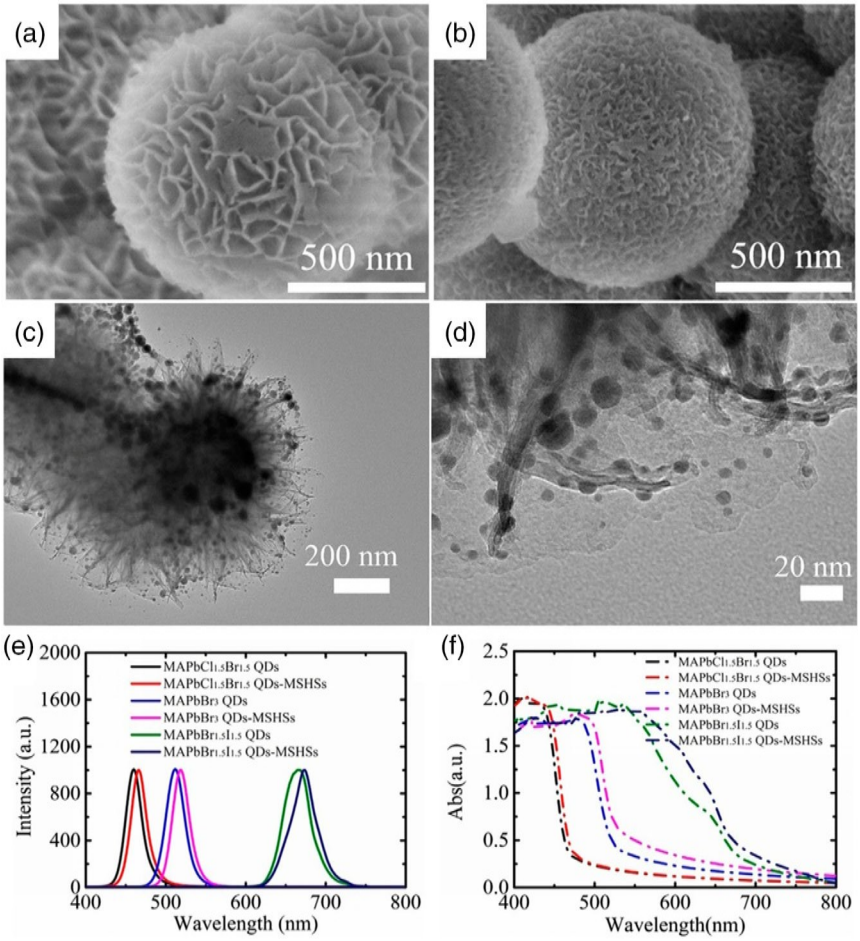

Figure 17. a) Scanning electron microscope (SEM) photograph of magnesium silicate hollow spheres (MSHSs). b) SEM photograph of $MAPbBr_3$ QDs-MSHSs nanocomposites. c) TEM and d) HRTEM photographs of $MAPbBr_3$ QDs-MSHSs nanocomposites. e) PL spectra and f) optical absorption of $MAPbX_3$ QDs and $MAPbX_3$ QDs-MSHSs nanocomposites with different halide components. Reproduced with permission.[149] Copyright 2018, American Chemical Society.

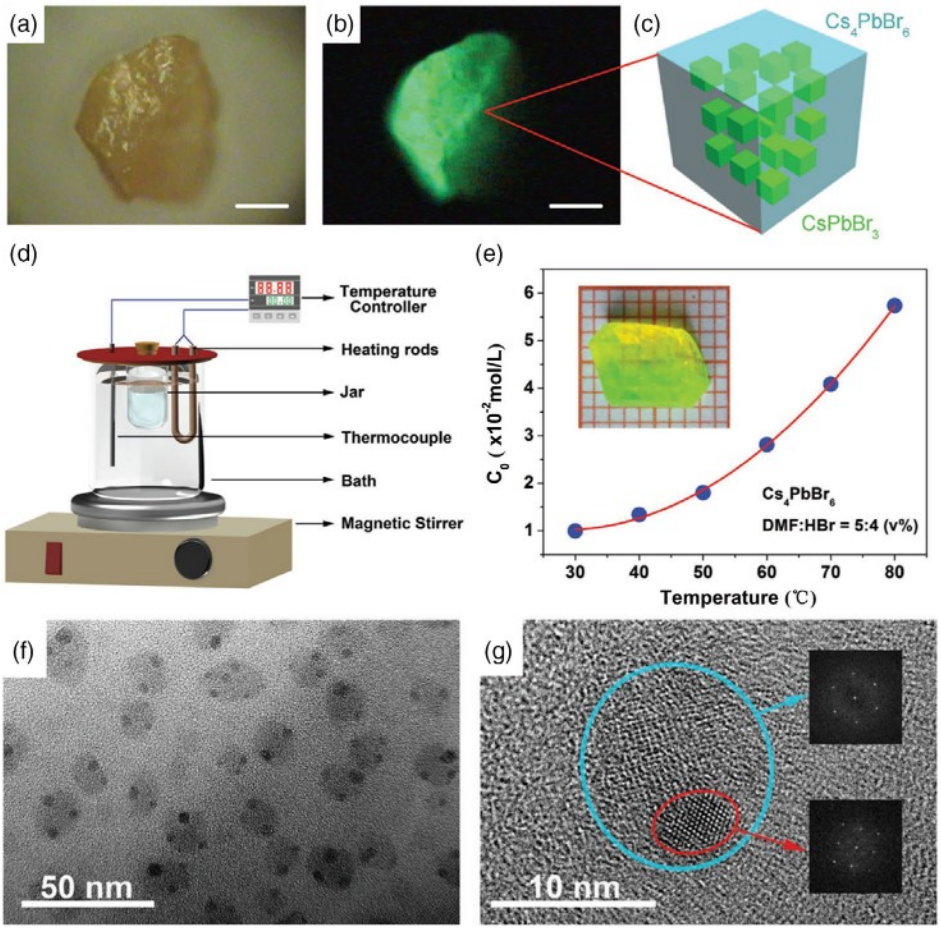

Figure 18. a) The optical image of a representative $CsPbBr_3/Cs_4PbBr_6$ nanocomposite microcrystal. Scale bar: 50 μm. b) The PL image of the $CsPbBr_3/Cs_4PbBr_6$ nanocomposite microcrystal. Scale bar: 50 μm. c) The schematic structure of $CsPbBr_3$ nanocrystals embedded in Cs_4PbBr_6 host matrix for $CsPbBr_3/Cs_4PbBr_6$ perovskite nanocomposites. a–c) Reproduced with permission.[150] Copyright 2017, Wiley-VCH. d) Schematic illustration of the setup for crystal growth. e) Solubility curves of Cs_4PbBr_6 in mixed HBr-DMF solution, inset: the as-fabricated green emissive crystal. The grid in the inset is 1 mm. f) Typical TEM images of the particles processed from green emissive Cs_4PbBr_6 crystals with embedded $CsPbBr_3$ NCs. g) HRTEM image of a typical particle. The inset in the bottom right corner is the corresponding FFT image of $CsPbBr_3$ and the top right corner is the corresponding FFT image of Cs_4PbBr_6 crystals with embedded $CsPbBr_3$ NCs. d–g) Reproduced with permission.[151] Copyright 2018, Wiley-VCH.

of $CsPbBr_3$ NCs in Cs_4PbBr_6 matrix, which was supported by evolution process and structural characterizations. They combined highly luminescent Cs_4PbBr_6 crystals with embedded $CsPbBr_3$ NCs as green emitters, $K_2SiF_6:Mn^{4+}$ (KSF) phosphor as red emitters, and GaN chips as blue emitters to fabricate White LED devices, which generated white lights of high quality with luminous efficiency of $\approx 151\,lm\,W^{-1}$ and color gamut of 90.6% Rec. 2020 at 20 mA. These devices had improved efficiency and stability than LEDs based on traditional PNCs with comparable color quality.[151]

5. Application

PNCs possess excellent optoelectronic properties, i.e., tunable bandgaps, narrow emission, strong light-absorption coefficients, high PLQYs, and high defect tolerance, which pave the way for designing highly efficient PNC-based optoelectronic devices, for example, laser[152,153], field-effect transistor (FET),[154–157] SCs, LEDs, and PDs. The promising progress and recently reported achievements in the application fields of SCs, LEDs, and PDs are briefly reviewed in the following sections.

5.1. Solar Cells

Perovskite photovoltaic technology achieved a rapid and breakthrough development since 2006 that the first application of these materials in SCs was reported.[26] The power conversion efficiency (PCE) of single-junction perovskite solar cells (PSCs) has hit 25.5%,[4] which is comparable with the performance of other photovoltaic technologies (23.35% for copper indium gallium selenide, 26.7% for crystalline silicon, and 29.1% for GaAs SCs[158]). Significantly, the low-cost solution-processed fabrication of PSCs shows priority to those traditional photovoltaic devices, which appeals to both academic communities and industrial corporations. However, different issues such

as, most importantly, the stability needs to be addressed toward PSCs commercialization. As already discussed in Section 3, the main problem of instability is the perovskite structure, originating from their low lattice energies and intrinsic ionic bond properties. In this regard, applying the PNCs instead of bulk perovskite as light-absorber in SCs can be a potential route toward increasing stability. For example, $CsPbI_3$ QDs with a high specific surface area have more stable cubic structure at RT comparing with bulk $CsPbI_3$, due to the large surface energy.[40] The performance of PNC-based SCs reported in recent years is shown in **Table 1**.

Luther et al. led the research on substituting bulk perovskite materials with PNCs as light-absorber in PSCs. They used the

Table 1. Performance of representative PNC-based SCs.

PNCs	Synthesis Method	Nanocrystal size [nm]	Device Structure	Scan direction	V_{OC} [eV]	J_{SC} [mA cm^{-2}]	FF [%]	PCE [%]	SPO [%]	Area [cm^2]	Refs.
$CsPbI_3$	Hot injection	10	FTO/TiO_2/$CsPbI_3$/Spiro-OMeTAD/MoO_x/Al	R	1.23	13.47	65	10.77	8.16	0.1	[112]
$CsPbI_3$	Hot injection	30	FTO/TiO_2/FAI-coated $CsPbI_3$/Spiro-OMeTAD/MoO_x/Al	R	1.16	15.25	76.6	13.58	13.43	0.058	[159]
$CsPbI_3$	Hot injection	≈ 20	FTO/TiO_2/$CsPbI_3$/Spiro-OMeTAD/Au	R	1.18	15.5	73.0	13.47	12.37	0.058	[164]
				F	1.17	15.2	66.0	11.75			
$CsPbI_3$	Hot injection	10	FTO/TiO_2/$CsPbI_3$-μGR/PTAA/Au	–	1.18	13.59	72.6	11.64	–	0.09	[161]
$CsPbI_3$	Hot injection	≈ 8	FTO/TiO_2/$CsPbI_3$/PTB7/MoO_3/Ag	–	1.27	12.39	80.0	12.55	12.35	0.0725	[197]
$CsPbI_3$	Hot injection	9.86	FTO/c-TiO_2/α-$CsPbI_3$/Spiro-OMeTAD/Au	R	1.04	16.98	67.2	11.87	11.00	–	[198]
				F	1.03	16.64	62.2	10.70			
$CsPbI_3$	Hot injection	–	FTO/TiO_2/$CsPbI_3$/PTAA/MoO_3/Ag	R	1.25	14.96	75.6	14.10	13.90	0.0725	[199]
				F	1.25	14.89	75.3	14.00			
$CsPbI_3$	Hot injection	10	FTO/TiO_2/Yb-doped $CsPbI_3$/PTB7/MoO_3/Ag	–	1.25	14.18	74.0	13.12	–	0.0725	[200]
$CsPbI_3$	Hot injection	12	FTO/TiO_2/$CsPbI_3$/Spiro-OMeTAD/Au	–	1.11	14.80	74.0	12.15	–	0.16	[201]
$CsPbI_3$	Hot injection	9.3	FTO/c-TiO_2/$CsPbI_3$/Spiro-OMeTAD/Au	–	1.10	11.30	66.0	8.10	–	0.11	[202]
$CsPbI_3$	Hot injection	10	FTO/TiO_2/$CsPbI_3$/Spiro-OMeTAD/Au	–	1.11	14.40	70.0	11.20	10.60	0.12	[203]
$CsPbI_3$	Hot injection	9	ITO/PTAA/$CsPbI_3$/C60/BCP/Ag	R	1.11	11.80	73.5	9.60	9.20	0.054	[204]
				F	1.10	11.62	73.9	9.42			
			ITO/PTAA/$CsPbI_3$/C60/BCP/Graphene	R	1.09	10.90	57.5	6.80	6.40		
				F	1.08	10.79	57.7	6.73			
$CsPbI_3$	Hot injection	10	FTO/c-TiO_2/$CsPbI_3$/Spiro-OMeTAD/MoO_x/Au	–	1.18	15.21	74.2	13.3	–	0.096	[205]
$CsPbI_3$	Hot injection	9.1	FTO/c-TiO_2/s-m-TiO_2/$CsPbI_3$/Spiro-OMeTAD/Au	R	1.06	17.77	75.8	14.32	13.87	–	[206]
				F	1.06	17.73	74.0	13.89			
$CsPbI_3$	Hot injection	9.5	FTO/NiO_x/$CsPbI_3$/C60/ZnO/Ag	–	1.19	14.25	77.6	13.10	–	0.056	[207]
$CsPbI_2Br$	Hot injection	13	FTO/TiO_2/$CsPbI_2Br$/Spiro-OMETAD/Au	–	1.30	5.32	77.0	5.34	–	0.0314	[165]
$CsPbI_2Br$	Hot injection	10.3	ITO/TiO_2/$CsPbI_2Br$/P3HT/Au	R	1.20	14.22	71.3	12.2	10.20	–	[208]
				F	1.13	13.07	58.0	8.5			
$CsPbBr_3$	One-step injection	15 – 20	FTO/c-TiO_2/$CsPbBr_3$/Spiro-OMeTAD/Au	R	1.54	5.65	62.4	5.42	≈3.60	0.0935	[209]
				F	1.31	4.77	38.1	2.37			
$CsPbBr_3$	Hot injection	10	FTO/c-TiO_2/$CsPbBr_3$/Spiro-OMeTAD/MoO_3/Au	–	0.90	7.38	40.0	2.65	–	0.06	[210]
$FAPbI_3$	Hot injection	≈20	FTO/TiO_2/$FAPbI_3$/Spiro-OMeTAD/Au	R	1.12	11.81	64.0	8.52	8.83	0.058	[164]
				F	1.12	11.85	68.0	9.01			
$FAPbI_3$	Hot injection	12.8 – 17.7	ITO/SnO_2/$FAPbI_3$/Spiro-OMeTAD/Au	–	1.10	11.83	64.4	8.38	8.05	–	[162]
$FAPbI_3$	Hot injection	14	ITO/SnO_2/$FAPbI_3$ (ITIC mixed)/Spiro-OMeTAD/Ag	–	1.10	15.40	74.8	12.7	12.70	–	[163]
$Cs_{0.75}FA_{0.25}PbI_3$	Hot injection	≈ 20	FTO/TiO_2/$Cs_{0.75}FA_{0.25}PbI_3$/Spiro-OMeTAD/Au	R	1.15	14.36	68.0	11.14	10.93	0.058	[164]
				F	1.14	14.23	66.0	10.77			
$CsPbI_3$/$FAPbI_3$	Hot injection	–	FTO/TiO_2/$CsPbI_3$/$FAPbI_3$/PTAA/MoO_3/Ag	R	1.22	17.26	74.0	15.60	15.10	0.0725	[211]
				F	1.20	17.21	72.0	14.90			
$Cs_{0.25}FA_{0.75}PbI_3$/$CsPbI_3$	Hot injection	–	ITO/TiO_2/$Cs_{0.25}FA_{0.75}PbI_3$/$CsPbI_3$/Spiro-OMeTAD/MoO_x/Al	–	1.20	18.91	76.0	17.39	15.52	0.059	[166]
$Cs_{1-x}FA_xPbI_3$	Hot injection	14	ITO/SnO_2/$Cs_{1-x}FA_xPbI_3$/Spiro-OMeTAD/Au	–	1.17	18.30	78.3	16.60	–	0.058	[167]

hot-injection method, which was developed by Kovalenko and coworkers[40] to synthesize cubic-phase $CsPbI_3$ NCs and improve the purification method via the utilization of methyl acetate (MeOAc) as antisolvent to wash off excess unreacted precursors without causing agglomeration. The purified $CsPbI_3$ QDs retained the cubic structure in air and even at low temperatures for some months, and also showed efficient dot-to-dot electronic transport. First, the $CsPbI_3$ QDs dispersed in octane were spin coated to deposit the photoactive-layer films. Then, films were dipped in a saturated MeOAc solution of $Pb(NO_3)_2$ or $Pb(OAc)_2$ to enhance the surface passivation. The champion SC possessed an open-circuit voltage (V_{OC}) of 1.23 V and a PCE of 10.77% with an active area of 0.10 cm^2 cell characterized in ambient conditions.[112] The same group further optimized the quality of QDs-based photoactive layers via A-site cation halide salt (AX) treatments, where A represents FA^+, MA^+, or Cs^+ and X represents I^- or Br^-. This post-treatment tuned and greatly enhanced electronic coupling among QDs. Consequently, the carrier mobility and therefore the short-circuit current density (J_{SC}) of device were enhanced. The FAI-treated device obtained the highest PCE of 13.4%, which was a record-efficiency for QDSCs at that time. A notably reduced hysteresis between reverse and forward scans and a better agreement between the stabilized power output (SPO) and reverse *J*–*V* scan were obtained after the FAI post-treatment.[159] To better understand the surface chemistry of PQDs in this system, they used various spectroscopic techniques to present a molecular picture of QD surface according to the results. Interestingly, they found that controlling the atmospheric moisture was paramount for fabricating high-efficiency QDSCs because water assisted the process by hydrolysis of MeOAc to make methanol and acetic acid. Then, oleate ligands on the surface of QDs were replaced by acetic acid, while the native oleylammonium ligands remain until exchanged with smaller FA^+ during the final treatment. They also realized that the time for the final treatment should be controlled because the treatment led to a tighter coupled QD regime, which would turn into a perovskite film after longer treatment.[160]

Using a different strategy, Liu et al. used high mobility micrometer-sized graphene (μGR) sheets to crosslink $CsPbI_3$ QDs. The conductivity was enhanced by designing an effective channel for carrier transport. Meanwhile, the stability against moisture and high temperature was also improved by keeping QDs from agglomeration. Consequently, the performance of the $CsPbI_3$ QDs-μGR was improved by over 12%, reaching an 11.4% PCE compared with 10.17% PCE for control device. In regard to stability, over 98% of the initial efficiency of optimized device remained after one-month storage in N_2 atmosphere. For moisture stability, when exposed to RH of 60%, PCE of control devices decreased by 90% of initial PCE while the μGR/$CsPbI_3$ device decreased by 10% only. For thermal stability, optimized μGR/$CsPbI_3$ SCs maintained 85% of its initial PCE after they were heated at 100 °C for 3 h while the reference cell performance decreased to only 20% of the initial value after the same treatment.[161]

However, the Cs-based PNCs have a relatively larger bandgap and short carrier lifetime compared with the organic-inorganic hybrid ones. For photovoltaic application, the $FAPbI_3$ has a more desirable bandgap of around 1.5 eV.[162–164] Yang et al. developed the $FAPbI_3$ QDSCs for the first time. The absorption edge of $FAPbI_3$ QDs is 1.55 eV, which is superior to $CsPbI_3$ QDs (1.80 eV). Furthermore, the time-resolved photoluminescence (TRPL) decay showed the $FAPbI_3$ QDs has a longer carrier lifetime. By solvent treatment to control ligands of $FAPbI_3$ QDs, the best device yielded a PCE of 8.38% with the SPO of 8.05%. Surprisingly, $FAPbI_3$ QDs and devices showed better stability than bulk $FAPbI_3$ film and devices, which can turn to yellow phase easily under ambient atmospheres.[162] In another work published by Yang et al., the PCE of $FAPbI_3$ QDSCs was boosted to 12.7% by adding a conjugated small molecule 2,2′-[[6,6,12,12-tetrakis(4-hexylphenyl)-6,12-dihydrodithieno[2,3-d:2′,3′-d′]-s-indaceno[1,2-b:5,6-b′]dithiophene-2,8-diyl]bis[methylidyne(3-oxo-1H-indene-2,1(3H)-diylidene)]]bis[propanedinitrile] (ITIC) into QDs film, which can effectively enhance charge separation.[163]

Perovskite materials are tunable in A, B, or X sites, which gives them exceptional optoelectronic versatility. For the X-site, Konstantatos et al. synthesized mixed-halide ($CsPbBrI_2$) NCs using halide exchange reactions of concentrated $CsPbBr_3$ NCs solutions with I^-. To study their photovoltaic performance, SCs were fabricated by coating $CsPbBr_xI_{3-x}$ NCs layer through either a single-step method or layer-by-layer coating method. The best device showed the PCE of 5.3% along with a V_{OC} of 1.31 V via the single-step deposition of $CsPbBrI_2$ NCs. However, the devices were current-limited confirmed by the external quantum efficiency (EQE) spectrum, and also showed an obvious hysteresis in both types of devices.[165]

Luther et al. reported the tunable A-site alloys of $Cs_{1-x}FA_xPbI_3$ NCs by the cation-exchange approach. The $Cs_{1-x}FA_xPbI_3$ NCs showed adjustable emission in the red and near-IR region from 650 and 800 nm as the value of X increases from 0 to 1. They estimated the activation energy related to the alloying process to be ~0.65 eV, which is higher than that associated with halide exchange.[164] A controllable synthesis of $Cs_{1-x}FA_xPbI_3$ QDs film with the whole composition range, even in the form of spatial heterostructure, was achieved using $Cs_{1-x}FA_xPbI_3$ QDs solution. In this regard, Luther et al. used a layer-by-layer deposition method to fabricate PQSCs. They demonstrated SCs with abrupt compositional changes throughout the perovskite film, by which they can control the composition of the photoactive layer to form an internal heterojunction. By optimizing composition of each heterostructure-component, more efficient charge separation at interface was achieved, resulting in enhanced photocarrier harvesting. As a result, they obtained a record PCE of 17.39% with a SPO of 15.52%.[166] Wang et al. reported an OA ligand-assisted cation-exchange strategy to synthesize $Cs_{1-x}FA_xPbI_3$ QDs with high quality. They found that cross-exchange of cations is facilitated in an OA-rich environment, enabling a fast formation of $Cs_{1-x}FA_xPbI_3$ QDs with decreased defect density. The best $Cs_{1-x}FA_xPbI_3$ QDSCs achieved a certified PCE of 16.6% without obvious hysteresis.[167] Finally, it is worthwhile to mention that the PNCs are also used in dye-sensitized SCs as an absorber.[168–170]

In addition to directly serving as the absorber in a photovoltaic device, PNCs are also used as raw materials to fabricate bulk films.[160,171–175] Kamat et al. deposited $CsPbBr_3$ QDs layer by layer, followed by annealing to cast stable films of desired thickness, which solve the problem of $CsPbBr_3$ deposition via solution processing due to the poor solubility of CsBr.[174] In addition, PNCs have been used as the interface modifier to engineer the

band alignment.[176–178] Liu et al. developed a bulk–NS–QDs or 3D–2D–0D dimension profiled interface, which promoted carrier extraction by introducing an electric field in the device, leading to increased current and a PCE as high as 12.39% for bulk $CsPbBrI_2$ PSCs.[177]

5.2. Light-Emitting Diodes

In the past few years, wurtzite or zinc blende Cd-based QDs, for example, CdS, CdSe, CdTe, Cu-doped ZnInS, and InP@ZnSeS, have been the dominant materials for quantum dot-based light-emitting diodes (QLEDs), which cost lots of time and efforts to synthesize.[179] PNCs have the merit of facile synthesis procedure and superior optical performance, like adjustable emission wavelength, high brightness and color purity, and high defect tolerance. These advantages make PNCs a promising alternative to conventional materials. Comparing with the bulk perovskite LEDs, where the excitons formed by injected carriers (in electrical excitation) are able to dissociate back to free charge carriers easily, the charge carriers are confined in a small domain by the grain boundary and surface ligands in PNCs with particle size from several to tens of nanometers. This importance can significantly increase the luminescence efficiency.

The initial attempts to fabricate perovskite-based light-emitting diodes (PeLEDs) should date back to over 20 years ago; however, electroluminescence could only be obtained at liquid nitrogen temperature[180] and at very high applied voltage.[181] The massive research on PSCs triggered a huge progress also in the field of PeLED, started from 2009. In 2014, Friend et al. highlighted the truth that an efficient photovoltaic material can also be a good light emitter. They reported high-brightness LEDs based on solution-processed perovskites and demonstrated electroluminescence in the near-IR, red, and green by adjusting the anion compositions of perovskite.[13] This work started intensive research on PeLEDs. **Table 2** shows the performance of PNC-based LEDs in recent publications. In the following, just a few examples of important strategies and achievements are reviewed.

In 2015, for the first time, Zeng et al. reported the QLED based on all-inorganic perovskite cesium lead halide ($CsPbX_3$, X = Cl, Br, I) nanocrystals. The typical QLED device composed of ITO/PEDOT:PSS/poly(9-vinlycarbazole)(PVK)/QDs/TPBi/LiF/Al exhibited blue, green, and yellow electroluminescence, which was achieved by controlling the particle sizes and varying the anion element composition. In more details, PL peak shifted to shorter or longer wavelength sides when the size of QDs was decreased or increased, respectively, and the PL peak shifted to longer or shorter wavelength sides when the I anions or Cl anions were introduced into the $CsPbBr_3$ PNCs. These devices showed the luminance of 742, 946, and 528 cd m^{-2}, with EQE of 0.07%, 0.12%, and 0.09% for the blue, green, and red LEDs, respectively.[182]

The surface ligands of PNCs play a crucial role in the performance of QLEDs. Normally, surface ligands of PNCs have double-side effects on QLEDs, for instance, a certain amount of ligands are required to provide sufficient surface passivation but excessive ligands will lead to low conductivity. Bakr et al. introduced a halide ion pair (e.g., di-dodecyl dimethyl ammonium bromide [DDAB]) to cap $CsPbX_3$ QDs by ligand-exchange strategy. DDAB is a relatively short ligand, thereby facilitating carrier transport in the QD film to obtain high-performance PeLEDs. As a result, the device based on these halide-ion-pair-capped $CsPbBr_3$ QDs achieved a maximum EQE of 3.0% and luminance of 330 cd m^{-2}, which is much better comparing with all-inorganic PQD LEDs without ligand exchange.[183] Except for replacing longer ligand with shorter ligand, Zeng et al. succeeded in controlling the ligand density of QDs film to balance surface passivation and carrier injection by a highly efficient solution-processed treatment. After screening various solvents, they chose the combination of hexane and ethyl acetate as solvent for QDs treatment to control surface ligand density. With proper treatment, the QDs solution stability, PLQYs, film uniformity, and microstructure were all improved. At the same time, the EQE and current efficiency were also increased from 0.12% to 6.27% and from 0.43 to 13.3 cd A^{-1}, respectively, comparing with the QDs using one cycle of acetone treatment.[184]

On the other hand, PNCs are believed to be potential alternative down-conversion materials in phosphor-converted light-emitting diodes (pc-LEDs) for lighting and next-generation display technology. The advantageous properties such as narrow emission bandwidth and high PLQYs, enable PNCs to work as color converters in pc-LEDs. In 2015, Dong et al. used the LARP method to synthesize brightly luminescent and color-adjustable $MAPbX_3$ (X = Br, I, Cl) QDs with absolute QY up to 70% at RT and low excitation fluencies. The as-fabricated $MAPbBr_3$ QDs with the particle size of 3.3 nm had a Br-rich surface with the Br/Pb molar ratio of 3.5. Through analyzing the temperature-dependent emission spectra, they reported that the $MAPbBr_3$ QDs possess an exciton binding energy of ≈375 meV and an optical phonon energy of ≈42 meV. They also fabricated the wide-color gamut prototype pc-WLED devices via the combination of green emissive $MAPbBr_3$ QDs, red emissive rare-earth phosphor $K_2SiF_6:Mn^{4+}$ (KSF), and blue emissive GaN chips.[47] Zeng's group developed a facile method to synthesize $CsPbX_3$ (X = Cl, Br, I) inorganic PQDs, which based on SR could be carried out at RT in a fast and simple way, without inert gas and injection operation. The synthesized PQDs had the QYs of 80%, 95%, 70%, and FWHM of 35, 20, and 18 nm for the red, green, and blue emissions, respectively. They also measured the exciton binding energy of $CsPbBr_3$ QDs as 40 meV, which was found to be much higher than those of GaN (25 meV) and RT thermal disturbance energy (26 meV). This means that excitons in $CsPbBr_3$ QDs can have a rapid recombination at RT, inducing excellent PL properties.[50]

5.3. Photodetectors

The PDs have the functions of capturing optical signals and converting them into electrical signals, which are crucial for various industrial and scientific applications, including biomedical sensing, imaging, defense, and optical communications.[185–187] Perovskite material has the merits of excellent optoelectronic properties, such as highly efficient absorption, ambipolar charge-transport characteristics, long carrier diffusion length, high dielectric constant, and ferroelectric polarization, making

Table 2. Performance of representative PNC-based LEDs.

PNCs	Synthesis Method	Device Structure	Morphology	EL/FWHM [nm]	V_T [V]	EQE_{max} [%]	Current efficiency [cd A^{-1}]	Peak luminance [cd m^{-2}]	Refs.
$(FA)_{1-x}(MA)_xPbBr_3$	LARP	ITO/PEDOT:PSS/$(FA)_{1-x}(MA)_xPbBr_3$ NPs without electrolyte matrix and with electrolyte matrix/Al	NPs	550/≈20	≈17	–	0.013	2	[212]
$MAPbBr_3$	Emulsion Synthesis	ITO/PEDOT/$MAPbBr_3$/TPBi/CsF/Al	QDs	524/≈26	2.9	1.1	4.5	2503	[53]
$MAPbBr_3$	–	SOCP/$MAPbBr_3$/TPBi/LiF/Al	NPs	≈547/20	≈3.6	8.53	42.9	–	[213]
$CsPbX_3$	Hot injection	ITO/PEDOT:PSS/PVK/$CsPbX_3$/TPBi/LiF/Al	QDs	455/23	5.1	0.07	14	742	[182]
				516/29	4.2	0.12	0.43	946	
				586/21	4.6	0.09	0.08	528	
$MAPbBr_{3-x}I_x$	RT solution growth	ITO/PEDOT:PSS/$MAPbBr_{3-x}I_x$/F8/Ca/Ag	NRs	533/26	–	–	–	–	[214]
$MAPbBr_3$	LARP	ITO/PEDOT:PSS/$MAPbBr_3$/TPBi/LiF/Al	NPLs	436/≈30	3.5	2.31	8.1	8.5	[215]
$MAPbX_3$	LARP	ITO/PEDOT:PSS/PVK/$MAPbBr_3$/TPBi/LiF/Al	QDs	520/21	7.8	1.06	3.72	2398	[216]
$CsPbBr_3$	Hot injection	ITO/PEDOT:PSS/Poly-TPD/PFI/$CsPbBr_3$/TPBi/LiF/Al	NCus	516/18	2.5	0.06	0.19	1377	[217]
$CsPbBr_3$–$CsPb_2Br_5$	Hot injection	ITO/PEDOT:PSS/$CsPbBr_3$–$CsPb_2Br_5$/TPBi/LiF/Al	NPs	527/24	4.6	2.21	8.98	3853	[218]
$CsPbX_3$	Hot injection	ITO/ZnO/PEI/$CsPbX_3$/CBP/TCTA/MoOx/Au	QDs	688/36	1.9	7.25	0.49	435	[219]
				648/33	1.9	6.3	3.42	2216	
				516/20	2.4	0.4	1.32	3019	
				404/14	3.4	0.61	0.0049	11	
$CsPbBr_xCl_{3-x}$	Hot injection	ITO/PEDOT:PSS/PVK/DDAB – OA – $CsPbX_3$/TPBi/LiF/Al	NCus	515/19	3	3	–	330	[183]
				490/19	3	1.9	–	35	
$CsPbX_3$	Hot injection	ITO/ZnO/$CsPbX_3$-TMA/TFB/MoO_3/Ag	NCus	698/31	–	5.7	–	206	[220]
				619/29	–	1.4	–	1559	
				523/19	–	0.19	–	2335	
				480/17	–	0.0074	–	8.7	
$CsPb_{1-x}Sn_xBr_3$	Hot injection	ITO/PEDOT:PSS/poly-TPD/$CsPb_{1-x}Sn_xBr_3$/TPBi/LiF/Al	QDs	508/–	5	–	3.6	5495	[221]
$CsPbX_3$	Hot injection	ITO/TiO_2/$CsPbX_3$/F8/MoO_3/Au	QDs	650/35	2.6	0.05	–	90–930	[222]
				510/25	2.8	0.325	–	–	
				495/21	4.1	0.075	–	–	
$CsPbBr_3$	Hot injection	ITO/PEDOT:PSS/poly-TPD/$CsPbBr_3$/TPBi/LiF/Al	QDs	512/20	3.4	6.27	13.3	15 185	[184]
$CsPbX_3$	Hot injection	ITO/PEDOT:PSS/NPB/$CsPbX_3$/BCP/LiF/Al	QDs	445/–	4	–	0.025	15.2	[223]
				510/–	5	–	0.308	51.7	
				640/–	4	–	0.027	21.7	
$CsPbBr_3$	–	ITO/PEDOT:PSS/Ag rods/NPB/$CsPbBr_3$/TPBi/LiF/Al	QDs	Green	3.8	0.43	1.42	8911	[224]
$CsPbBr_3$	LARP	ITO/ZnO/$CsPbBr_3$/TFB/MoO_x/Au	QDs	510/20	3	0.06	–	–	[225]
$CsPbBr_3$	Hot injection	ITO/NiO/$CsPbBr_3$/ZnO/Al	QDs	516/21	2.4	0.11	0.57	3091	[226]
$CsPbBr_3$	Hot injection	ITO/PEDOT:PSS/PVK/$CsPbBr_3$-PMMA/TPBi/LiF/Al	QDs	Green	–	0.25	0.96	637	[227]
$CsPbBr_3$	Hot injection	ITO/PEDOT:PSS/poly-TPD/$CsPbBr_3$/TPBi/Liq/Al	QDs	512/17	2.6	8.73	26.2	1660	[228]
$CsPbBr_3$	Hot injection	ITO/PEDOT:PSS/poly-TPD/$CsPbBr_3$/TPBi/LiF/Al	QDs	515/18	4.6	1.194	3.1	12 090	[229]
$CsPbX_3$	Hot injection	ITO/PEDOT:PSS/poly-TPD/$CsPbX_3$:Mn/TPBi/LiF/Al	QDs	511/20	4.2	1.49	6.4	9971	[230]
				685/42	4.1	1.04	0.15	132	
$CsPbBr_3$	Hot injection	ITO/ZnO/MZO/$CsPbBr_3$/CBP/TCTA/MoO_x/Au	QDs	Green	2.9	1.1	3.66	3059	[231]
$CsPbBr_3$	Microwave	ITO/PEDOT:PSS/PTPD/$CsPbBr_3$/PVK/ZnO/Al	NBs	520/17	2.2	1.1	–	590	[232]

Table 2. Continued.

PNCs	Synthesis Method	Device Structure	Morphology	EL/FWHM [nm]	V_T [V]	EQE_{max} [%]	Current efficiency [cd A^{-1}]	Peak luminance [cd m^{-2}]	Refs.
$CsPb_{0.67}Sn_{0.33}Br_3$	Hot-injection	ITO/PEDOT:PSS/TFB/ $CsPb_{0.67}Sn_{0.33}Br_3$/ TPBi/LiF/Al	QDs	517/–	3.6	4.13	11.63	12 500	[233]
PEABr:$CsPbBr_3$	–	ITO/PEDOT:PSS/PEABr:$CsPbBr_3$/TPBi/Ca/Al	quasi-2D	514/20	3	1.97	6.16	9957	[234]
$CsPbI_3$	Hot-injection	ITO/PEDOT:PSS/$CsPbI_3$/TPBi/LiF/Al	QDs	693/32	3	0.21	0.012	7.2	[235]
$CsPb_2X_5$	–	ITO/PEDOT:PSS/TFB/$CsPb_2X_5$/TPBi/LiF/Al	quasi-2D	520/20	3.8	1.1	–	7317	[236]
				693/30	4	0.14	–	–	
IDA-$CsPbI_3$	Hot-injection	ITO/PEDOT:PSS/poly-TPD/IDA-$CsPbI_3$/TPBi/LiF/Al	NCs	688/33	4.1	5.02	–	748	[237]
OPA-$CsPbBr_3$	Hot-injection	ITO/PEDOT:PSS/poly-TPD/OPA-$CsPbBr_3$/ TPBi/LiF/Al	QDs	516/19	2.8	6.5	18.13	7085	[238]
$CsPbBr_3$	Hot-injection	ITO/NiO/$CsPbBr_3$/$Zn_{1-x}Mg_xO$/Al	QDs	519/19	2.8	3.79	7.96	6093.2	[239]
Ce^{3+}-Doped $CsPbBr_3$	Hot-injection	ITO/PEDOT:PSS/poly-TPD/Ce-doped $CsPbBr_3$/ TPBi/LiF/Al	NCs	515/19	2.5	4.4	14.2	>3000	[240]
$CsPbBr_3$	LARP	ITO/ZnO/$CsPbBr_3$/TCTA/MoO_3/Au	NCs	460/–	–	1.7	5.8	4428	[241]
$CsPbBr_3$	Self-assembly	ITO/PEDOT:PSS/PVK/$CsPbBr_3$/TPBi/Liq/Al	core/shell QDs	510/21	3.9	15.17	40	18 600	[242]
$CsPbBr_3$	Hot-injection	ITO/Li:TiO_2/$CsPbBr_3$/TiO_2/Au	QDs	530/25	2.3	2.38	3	2210	[243]
$CsPbBr_3$	LARP	ITO/PEDOT:PSS/PTAA/$CsPbBr_3$/TPBi/LiF/Al	QDs	515/18	2.75	11.6	45.4	55 800	[244]
$FAPbBr_3$	Self-assembly	ITO/PEDOT:PSS/$FAPbBr_3$/PO-TOT/Ca/Al	NCs	528–532/25–26	2.2	13.4	57.6	56 000	[245]
$CsPbBr_3$	Hot-injection	ITO/PEDOT:PSS/Poly-TPD/$CsPbBr_3$/TPBi/Liq/Al	QDs	508/18	5.6	0.17	–	–	[246]
		ITO/PEDOT:PSS/Poly-TPD/$CsPbBr_3$ + OAM-I/ TPBi/Liq/Al		649/31	2.8	21.3	10.6	500	
		ITO/PEDOT:PSS/Poly-TPD/$CsPbBr_3$ + An-HI/ TPBi/Liq/Al		644/29	2.7	14.1	11.6	794	
$Cs_xFA_{1-x}PbBr_3$	–	ITO/NiO/TFB/PVK/$Cs_xFA_{1-x}PbBr_3$/TPBi/LiF/Al	NPs	483/–	3.3	9.5	12	700	[247]
$(PEA)_2PbBr_4$	LARP	ITO/PEDOT:PSS/PVK:TAPC/$(PEA)_2PbBr_4$/ TPBi/Ca/Ag	NPLs	408.8/18	4.2	0.31	0.19	147.6	[248]
$CsPbBr_xCl_{x-3}$	Directly mixing	ITO/PEDOT:PSS/Poly-TPD/$CsPbBr_xCl_{3-x}$/TPBi/Ca/Ag	NCs	469	3.8	0.65	0.47	30	[249]
				479	3.2	1	0.94	119	
				489	3.4	1.8	2.4	182	
				496	3.2	2.6	4.5	603	

it a potential candidate for PDs application. In addition, the low-cost solution-processed fabrication methods benefit the large-scale production and commercialization, to some extent, which makes it more competitive comparing with the most widespread inorganic semiconductors such as Si and GaN.[19]

The PDs can be classified into three types: photodiodes, photoconductors, and phototransistors. **Figure 19** shows the two-terminal devices including photodiodes and photoconductors, and the three-terminal devices including phototransistors, which have the source, drain, and gate electrodes. Regarding the spatial layout, the PDs can also be classified as vertical and lateral types. For photodiodes and phototransistors, they only show vertical and lateral types, respectively. However, photoconductors have two kinds of types.[188] Depending on the width of the spectral response window, the PDs can also be classified as spectrally broadband or narrowband PDs. Broadband PDs can sense a broad spectrum of light, for instance, X-rays, UV light, and visible light, whereas narrowband PDs can only sense a narrow range of light, for instance, red, green, blue, etc. PNCs have a narrow spectrum, which is really suitable for narrowband PDs. The spectrally selective PDs are favored by the market, where only a small spectral range of light can be detected.

The photodiodes show similar device structures as SCs, but work under reverse applied field with low dark currents. Both electrons and holes can be extracted through a built-in potential, inducing a high responsivity and a rapid response speed. In contrast, the photoconductors only transfer a single carrier. A long response time is one of the most critical restrictions of photoconductors. In photoconductors, potentially, if the opposite photogenerated carriers get trapped by inner defects or material surface, transporting photogenerated carriers recirculate multiple times during the lifetime of the trapped ones, inducing a high photoconductive gain. Unfortunately, a photoconductive gain is beneficial for achieving a high responsivity but also drives to a slow response.[17] In this case, the high responsivity of the photoconductors may result from the generation of a secondary

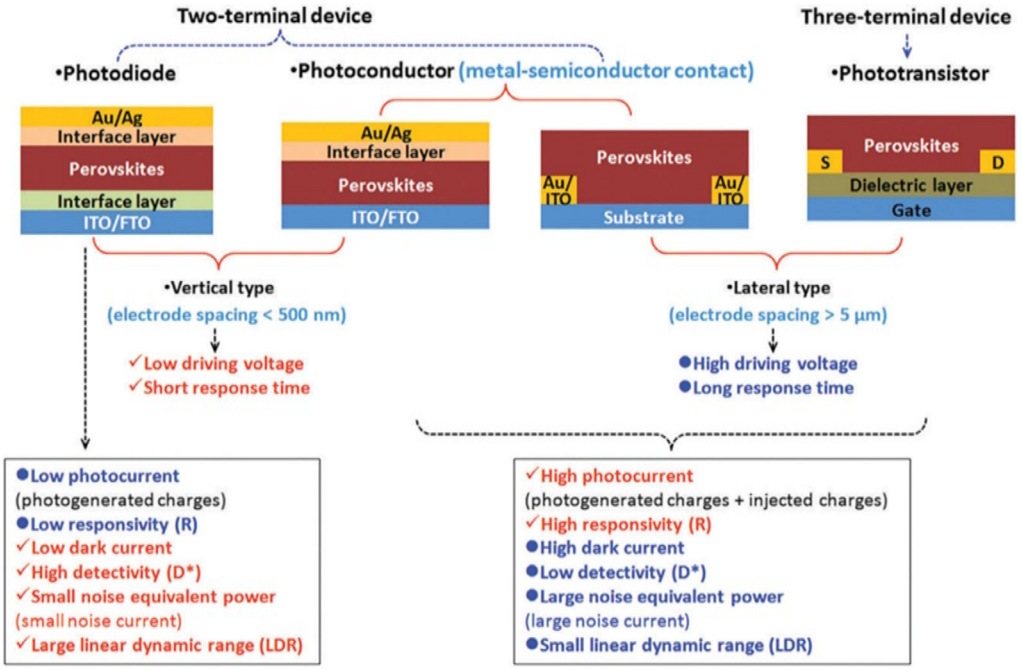

Figure 19. Schematic of architectures for perovskite-based PDs and the characteristics of photodetection performance for different devices. Reproduced with permission.[18] Copyright 2017, Royal Society of Chemistry.

photocurrent and photoconductive gain. Furthermore, the detectivity in photoconductors is usually small due to their high dark currents and noises. As mentioned earlier, photoconductors have vertical and lateral device structures. It could be challenging to implement the PNCs in the vertical type devices because of the high requirement of film uniformity to perfectly cover the surface of active layer. In contrast, the lateral structure devices can be simply fabricated using 1D NWs and 2D NS perovskite. **Table 3** shows a summary of the performance of recent PNC-based PDs.

Table 3. Performance of representative PNC-based PDs.

PNCs	Synthesis Method	Morphology	Devices Structure	Input light intensity and wavelength [mW cm^{-2} nm^{-1}]	Bias voltage [V]	Responsivity [A W^{-1}]	On/off ratio	Rise/decay time [ms]	Detectivity [Jones]	Refs.
$CsPbI_3$	Hot injection	NCs	Au/$CsPbI_3$/Au	1.98, 405	1	–	10^5	24/29	–	[191]
$MAPbI_3$	One-step self-assembly	NWs	Au/$MAPbI_3$/Au	2.36, 530	1	4.95	250	< 0.1	2×10^{13}	[190]
$CsPbBr_3$	Hot injection	NSs	ITO/$CsPbBr_3$/ITO	10, 442	5	0.64	$>10^4$	0.019/0.024	–	[192]
$CsPbBr_3$	Dissolution–recyrstallization	NCs	Au/$CsPbBr_3$/Au	1.01, 442	3	0.18	8×10^3	1.8/1.0	6.1×10^{10}	[194]
$MAPbI_3$	Solution process and vapor-phase conversion	NSs	Ti and Au/$MAPbI_3$/Ti and Au	–, 405	1	22	10^2	< 20/< 40	–	[250]
				–, 532		12				
$MAPbI_3$	Vapor-phase deposition	NPLs	Cr and Au/$MAPbI_3$/Cr and Au	60, 633	1	23.3	–	150	–	[193]
$MAPbI_3$	Dissolution–recyrstallization	NWs	Ag/$MAPbI_3$/Ag	1, 532	3	–	13	120/210	–	[251]
$CsPb(Br/I)_3$	Hot injection	NRs	Au/$CsPb(Br/I)_3$/Au	20, 532	1	–	2000	680/660	–	[252]
$CsPbBr_3$	LARP	micro	$CsPbBr_3$/CNTs	–, 400	10	31.1	10^5	0.016/0.38	–	[253]
$MAPbI_3$	Saturated vapor-assisted crystallization	NWs	Au/MoO_3/$MAPbI_3$/MoO_3/Au	–	–	460	–	0.18/0.33	2.6×10^{13}	[254]
$CsPbI_{3-x}Br_x$	Oxygen-assisted chemical vapor deposition	QDs	Au/$CsPbI_{3-x}Br_x$/MoS_2/Au	–, 532	0.1	7.7×10^4	10^4	590/320	5.6×10^{11}	[255]
$CsPbCl_3$-graphene	Hot injection	NCs	Au/$CsPbCl_3$-graphen/Au	8.17×10^{-3}, 400	0.5	10^6	–	0.3×10^3/ 1.35×10^3	2×10^{13}	[155]

The 1D architecture of perovskite NWs has provided a well-confined carrier transport channel for application as PDs due to their less grain boundary, morphological anisotropy, and good mechanical flexibility.[189] However, the large surface area of $MAPbI_3$ NWs could cause much easier carrier recombination and material decomposition, which would be detrimental to the performance and stability of the device. Tang et al. used OA soaking to passivate $MAPbI_3$ NWs' surface defects to enhance the stability and sensitivity of the perovskite NW-based PDs. By this treatment, the carrier lifetime was improved from 28.1 to 51.3 ns. As a result, a high responsivity of 4.95 A W^{-1}, detectivity of 2×10^{13} Jones, and response time of less than 0.1 ms were achieved.[190]

In 2016, Lee et al. first demonstrated the all-inorganic PNCs-based PDs. They chose $CsPbI_3$ NCs as active material for PDs, which is a red emitter. The as-obtained PNC solution was drop-casted on a doped Si substrate with prepatterned gold electrodes. The device showed good photosensitivity with an on/off photocurrent ratio of 10^5 and relatively fast rise ($t_{rise} = 24$ ms) and decay times ($t_{decay} = 29$ ms).[191] Zeng et al. applied the 2D $CsPbBr_3$ NSs for solution-processed flexible PDs for the first time. These $CsPbBr_3$ NSs with a thickness of ≈3.3 nm and edge length of ≈1 μm are proper to be assembled into high-quality, large-area films via a solution process. The flexible, 2D $CsPbBr_3$ visible-light PDs showed excellent charge transport properties, a high photosensitivity with an on/off ratio higher than 10^3.[192] Liu et al. used a simple two-step vapor transport chemical deposition method to grow $MAPbI_3$ NPLs with lateral dimension of about 5–20 μm on SiO_2/Si substrates. The thickness of these 2D materials was distributed in the region of 5–300 nm, which depended on the controlled growing time. They further studied the thickness-dependent photoresponse of the devices and concluded that the sample with a thickness of around 30 nm exhibits the best performance due to the dominant longest lifetime of perovskite excitons (≈ 4.5 ns).[193]

And finally, to obtain compact and smooth carrier channels for the PD devices, Zeng et al. reported a recyclable dissolution-recrystallization method for $CsPbBr_3$ PNCs. Specifically, the large particles could be gradually dissolved from the surface, and the PNCs could be obtained by adjusting the ratio of the dissolved part. In addition to the size decreasing behavior, the PNCs would aggregate after washing off the highly dynamic surface species. The as-fabricated films exhibited large numbers of holes and gaps. Then, they used a combination of toluene and ethanol as washing solvent to form a liquid circumstance in films. The surface and sharp parts dissolved, and the liquid matters filled the holes and gaps. After solvent evaporation, the dissolved species between isolated particles would be attached on the surfaces of particle and recrystallized. The film treated by this micro-self-healing method showed decreased hole size and smooth morphologies, which benefited the performance of PD devices.[194]

6. Conclusions

MHP nanocrystals possess excellent optoelectronic properties, which make them a competitive candidate for the next-generation optoelectronics and photonics. This article briefly reviewed the synthesis methods, stability issues, encapsulation strategies, and few photoelectronic applications of PNCs. Although great contributions from worldwide multidisciplinary researchers have made this field more and more mature, there are still different critical issues to be addressed in further research, which will be briefly discussed here.

Various processes for the synthesis of PNCs are described here, among which the ligands are always necessary to form nanoscale structures. However, it is not still well-understood how surface passivation and stability of PNCs are affected by different types of ligands. Comparing with conventional nanoscale semiconductors, the precise control of the size and shape of PNCs needs further effort. In addition, the mechanisms of how ligands control the size and shape of the PNCs are needed to be elaborated. A systematic exploration of the novel ligands for the sake of stable surface termination in PNCs and a deep understanding of their functionality are highly demanded. In addition, it is also of great interest to study the impact of ligands on the electronic band structure of PNCs.

Lead-based PNCs are the most studied due to their better optoelectronic properties comparing to other MHPs; however, the ever-growing concerns about the toxicity of these materials has encouraged many research groups to develop lead-free PNCs substitutes. Unfortunately, replacing the lead by other single metal elements has limited choices. Most of the "single metal" lead-free perovskite materials show inferior properties when comparing with lead-based one. Despite tin(II)-based perovskites have a suitable bandgap, their easy oxidation from Sn(II) to Sn(VI) impedes the application of these materials. In recent years, the so-called double perovskite materials appear on the scene, represented by Cs_2AgBiX_6 perovskite. Supported by computational studies on the elements screening for a possible combination of A^+, B^+, B^{3+}, and X^- ions, 11 optimal materials were screened out and three of them showed the appropriate direct bandgaps of 1.68, 1.77, and 1.83 eV (for Cs_2AgSbI_6, Cs_2AgBiI_6, and $Cs_2AuBiBr_6$, respectively).[195] To date, just a few new double perovskite materials have been reported, but not in the nanosized form. This is also an exciting direction for future research.

One of the most significant challenges for the commercialization of PNCs is their stability. The interior and exterior factors that may cause the degradation of PNCs are summarized in this Review. For the interior factors like perovskite structural stability, doping a small amount of other metal cations into perovskite structure is an effective way to improve stability. However, the structure–property relationship needs further investigation both in theoretical and experimental fields, especially for the lead-free PNCs. The function of ligands working as the surface passivators, on the other hand, needs to be systematically studied to achieve stable surface passivation with least effect on the optoelectronic properties of PNCs.

Numerous studies on coating and encapsulation of PNCs with various materials have been discussed in this Review. However, these protectors are mostly chemical and environment stable but insulated. That means even if the stability can be improved dramatically, these materials act as barriers for charges at the same time and could be detrimental to the optoelectronic properties of PNCs. To address this issue, novel strategies should be explored, for instance, reducing the protector's amount and doping the insulated protectors might improve the carriers transport.

Although they are still in the development phase, PNCs have shown high potential in various optoelectronic and photonic applications. However, a much longer lifetime and durable performance are required to ensure a bright industrial future for PNC-based technologies. In addition, the toxicity issue of the lead-based PNCs should be ideally resolved no matter what fields these materials are used for. Exploring the novel PNCs with nontoxic properties and soluble in water will extend their application to further fields such as bio-application and water-splitting. With numerous efforts from the researchers and global cooperation among the chemists, physicists, materials scientists, and engineers, this field has shown great progress with the skyrocketing numbers of research works in recent years and the breaking record presented in every few days. We believe that the PNCs have very high potential to be implemented as one of the most-used materials in different technologies in the near future.

Acknowledgements

The authors gratefully acknowledge funding by the Deutsche Forschungsgemeinschaft (DFG, German Research Foundation) under Germany's Excellence Strategy—EXC 2089/1—390776260 (e-conversion) and funding by the Bavarian Ministry of Science (Solar Technologies go Hybrid—SolTech). T. A. acknowledges the financial support of the German Research Foundation (DFG project with grant number of AM 519/1-1). S. W. and L. W. acknowledge the financial support of China Scholarship Council (CSC).

Conflict of Interest

The authors declare no conflict of interest.

Keywords

encapsulation of perovskite nanocrystals, light-emitting diodes, perovskite nanocrystals, perovskite solar cells, photodetectors, stabilities

Received: October 27, 2020
Revised: January 7, 2021
Published online:

[1] S. Kazim, M. K. Nazeeruddin, M. Gratzel, S. Ahmad, *Angew. Chem. Int. Ed.* **2014**, *53*, 2812.
[2] A. Kojima, K. Teshima, Y. Shirai, T. Miyasaka, *J. Am. Chem. Soc.* **2009**, *131*, 6050.
[3] Q. Jiang, Y. Zhao, X. Zhang, X. Yang, Y. Chen, Z. Chu, Q. Ye, X. Li, Z. Yin, J. You, *Nat. Photonics* **2019**, *13*, 460.
[4] National Renewable Energy Laboratory, Best research-cell efficiencies chart. https://www.nrel.gov/pv/cell-efficiency.html (accessed: January 2021).
[5] J. You, L. Meng, T.-B. Song, T.-F. Guo, Y. Yang, W.-H. Chang, Z. Hong, H. Chen, H. Zhou, Q. Chen, Y. Liu, N. De Marco, Y. Yang, *Nat. Nanotechnol.* **2016**, *11*, 75.
[6] H. S. Kim, C. R. Lee, J. H. Im, K. B. Lee, T. Moehl, A. Marchioro, S. J. Moon, R. Humphry-Baker, J. H. Yum, J. E. Moser, M. Gratzel, N. G. Park, *Sci. Rep.* **2012**, *2*, 591.
[7] M. Liu, M. B. Johnston, H. J. Snaith, *Nature* **2013**, *501*, 395.
[8] Y. Hu, J. Schlipf, M. Wussler, M. L. Petrus, W. Jaegermann, T. Bein, P. Müller-Buschbaum, P. Docampo, *ACS Nano* **2016**, *10*, 5999.
[9] J. You, L. Meng, T.-B. Song, T.-F. Guo, Y. Yang, W.-H. Chang, Z. Hong, H. Chen, H. Zhou, Q. Chen, Y. Liu, N. De Marco, Y. Yang, *Nat. Nanotechnol.* **2015**, *11*, 75.
[10] P. Wang, X. Zhang, Y. Zhou, Q. Jiang, Q. Ye, Z. Chu, X. Li, X. Yang, Z. Yin, J. You, *Nat. Commun.* **2018**, *9*, 2225.
[11] C. Zuo, L. Ding, *Nanoscale* **2014**, *6*, 9935.
[12] Y. Gao, Y. Dong, K. Huang, C. Zhang, B. Liu, S. Wang, J. Shi, H. Xie, H. Huang, S. Xiao, J. He, Y. Gao, R. A. Hatton, J. Yang, *ACS Photonics* **2018**, *5*, 4104.
[13] Z.-K. Tan, R. S. Moghaddam, M. L. Lai, P. Docampo, R. Higler, F. Deschler, M. Price, A. Sadhanala, L. M. Pazos, D. Credgington, F. Hanusch, T. Bein, H. J. Snaith, R. H. Friend, *Nat. Nanotechnol.* **2014**, *9*, 687.
[14] Y. Wei, Z. Y. Cheng, J. Lin, *Chem. Soc. Rev.* **2019**, *48*, 310.
[15] Q. Van Le, H. W. Jang, S. Y. Kim, *Small Methods* **2018**, *2*, 1700419.
[16] P. Docampo, T. Bein, *ACC. Chem. Res.* **2016**, *49*, 339.
[17] J. P. Deng, J. L. Li, Z. Yang, M. Q. Wang, *J. Mater. Chem. C* **2019**, *7*, 12415.
[18] H. Wang, D. H. Kim, *Chem. Soc. Rev.* **2017**, *46*, 5204.
[19] M. Ahmadi, T. Wu, B. Hu, *Adv. Mater.* **2017**, *29*, 1605242.
[20] S. Park, W. J. Chang, C. W. Lee, S. Park, H.-Y. Ahn, K. T. Nam, *Nat. Energy* **2016**, *2*, 16185.
[21] X. L. Zhu, Y. X. Lin, Y. Sun, M. C. Beard, Y. Yan, *J. Am. Chem. Soc.* **2019**, *141*, 733.
[22] W. Wang, M. O. Tade, Z. P. Shao, *Chem. Soc. Rev.* **2015**, *44*, 5371.
[23] S. Shyamal, N. Pradhan, *J. Phys. Chem. Lett.* **2020**, *11*, 6921.
[24] S. Shyamal, S. K. Dutta, T. Das, S. Sen, S. Chakraborty, N. Pradhan, *J. Phys. Chem. Lett.* **2020**, *11*, 3608.
[25] S. Shyamal, S. K. Dutta, N. Pradhan, *J. Phys. Chem. Lett.* **2019**, *10*, 7965.
[26] A. Kojima, K. Teshima, T. Miyasaka, Y. Shirai, *210th ECS Meeting*, IOP Publishing, USA **2006**, *MA2006-02*, p. 397.
[27] L. C. Schmidt, A. Pertegás, S. González-Carrero, O. Malinkiewicz, S. Agouram, G. M. Espallargas, H. J. Bolink, R. E. Galian, J. Pérez-Prieto, *J. Am. Chem. Soc.* **2014**, *136*, 850.
[28] A. B. Yusoff, M. K. Nazeeruddin, *Adv. Energy Mater.* **2018**, *8*, 1702073.
[29] F. Lang, O. Shargaieva, V. V. Brus, H. C. Neitzert, J. Rappich, N. H. Nickel, *Adv. Mater.* **2018**, *30*, 1702905.
[30] E. T. Hoke, D. J. Slotcavage, E. R. Dohner, A. R. Bowring, H. I. Karunadasa, M. D. McGehee, *Chem. Sci.* **2015**, *6*, 613.
[31] D. W. deQuilettes, W. Zhang, V. M. Burlakov, D. J. Graham, T. Leijtens, A. Osherov, V. Bulović, H. J. Snaith, D. S. Ginger, S. D. Stranks, *Nat. Commun.* **2016**, *7*, 11683.
[32] S. Draguta, O. Sharia, S. J. Yoon, M. C. Brennan, Y. V. Morozov, J. S. Manser, P. V. Kamat, W. F. Schneider, M. Kuno, *Nat. Commun.* **2017**, *8*, 200.
[33] D. D. Yang, X. M. Li, H. B. Zeng, *Adv. Mater. Interfaces* **2018**, *5*, 1701662.
[34] W. Z. Lv, L. Li, M. C. Xu, J. X. Hong, X. X. Tang, L. G. Xu, Y. H. Wu, R. Zhu, R. F. Chen, W. Huang, *Adv. Mater.* **2019**, *31*, 1900682.
[35] S. Huang, Z. Li, L. Kong, N. Zhu, A. Shan, L. Li, *J. Am. Chem. Soc.* **2016**, *138*, 5749.
[36] M. N. Liu, H. C. Zhang, D. Gedamu, P. Fourmont, H. Rekola, A. Hiltunen, S. G. Cloutier, R. Nechache, A. Priimagi, P. Vivo, *Small* **2019**, *15*, 29.
[37] H. Y. Fu, *J. Mater. Chem. A* **2019**, *7*, 14357.
[38] C. D. Donega, P. Liljeroth, D. Vanmaekelbergh, *Small* **2005**, *1*, 1152.
[39] X. Li, F. Cao, D. Yu, J. Chen, Z. Sun, Y. Shen, Y. Zhu, L. Wang, Y. Wei, Y. Wu, H. Zeng, *Small* **2017**, *13*, 1603996.

[40] L. Protesescu, S. Yakunin, M. I. Bodnarchuk, F. Krieg, R. Caputo, C. H. Hendon, R. X. Yang, A. Walsh, M. V. Kovalenko, *Nano Lett.* **2015**, *15*, 3692.
[41] A. Dutta, R. K. Behera, S. K. Dutta, S. Das Adhikari, N. Pradhan, *J. Phys. Chem. Lett.* **2018**, *9*, 6599.
[42] G. Almeida, L. Goldoni, Q. Akkerman, Z. Y. Dang, A. H. Khan, S. Marras, I. Moreels, L. Manna, *ACS Nano* **2018**, *12*, 1704.
[43] A. Pan, B. He, X. Fan, Z. Liu, J. J. Urban, A. P. Alivisatos, L. He, Y. Liu, *ACS Nano* **2016**, *10*, 7943.
[44] Y. Bekenstein, B. A. Koscher, S. W. Eaton, P. Yang, A. P. Alivisatos, *J. Am. Chem. Soc.* **2015**, *137*, 16008.
[45] J. De Roo, M. Ibáñez, P. Geiregat, G. Nedelcu, W. Walravens, J. Maes, J. C. Martins, I. Van Driessche, M. V. Kovalenko, Z. Hens, *ACS Nano* **2016**, *10*, 2071.
[46] M. Imran, V. Caligiuri, M. Wang, L. Goldoni, M. Prato, R. Krahne, L. De Trizio, L. Manna, *J. Am. Chem. Soc.* **2018**, *140*, 2656.
[47] F. Zhang, H. Zhong, C. Chen, X.-G. Wu, X. Hu, H. Huang, J. Han, B. Zou, Y. Dong, *ACS Nano* **2015**, *9*, 4533.
[48] S. Sun, D. Yuan, Y. Xu, A. Wang, Z. Deng, *ACS Nano* **2016**, *10*, 3648.
[49] H. Huang, A. S. Susha, S. V. Kershaw, T. F. Hung, A. L. Rogach, *Adv. Sci.* **2015**, *2*, 1500194.
[50] X. Li, Y. Wu, S. Zhang, B. Cai, Y. Gu, J. Song, H. Zeng, *Adv. Funct. Mater.* **2016**, *26*, 2435.
[51] S. Wei, Y. Yang, X. Kang, L. Wang, L. Huang, D. Pan, *Chem. Commun.* **2016**, *52*, 7265.
[52] F. Ambroz, W. D. Xu, S. Gadipelli, D. J. L. Brett, C. T. Lin, C. Contini, M. A. McLachlan, J. R. Durrant, I. P. Parkin, T. J. Macdonald, *Part. Part. Syst. Charact.* **2020**, *37*, 1900391.
[53] H. Huang, F. Zhao, L. Liu, F. Zhang, X.-G. Wu, L. Shi, B. Zou, Q. Pei, H. Zhong, *ACS Appl. Mater. Interfaces* **2015**, *7*, 28128.
[54] D. M. Jang, D. H. Kim, K. Park, J. Park, J. W. Lee, J. K. Song, *J. Mater. Chem. C* **2016**, *4*, 10625.
[55] Y. Tong, E. Bladt, M. F. Aygüler, A. Manzi, K. Z. Milowska, V. A. Hintermayr, P. Docampo, S. Bals, A. S. Urban, L. Polavarapu, J. Feldmann, *Angew. Chem. Int. Ed.* **2016**, *55*, 13887.
[56] Q. Pan, H. Hu, Y. Zou, M. Chen, L. Wu, D. Yang, X. Yuan, J. Fan, B. Sun, Q. Zhang, *J. Mater. Chem. C* **2017**, *5*, 10947.
[57] Z. Long, H. Ren, J. Sun, J. Ouyang, N. Na, *Chem. Commun.* **2017**, *53*, 9914.
[58] H. Liu, Z. Wu, H. Gao, J. Shao, H. Zou, D. Yao, Y. Liu, H. Zhang, B. Yang, *ACS Appl. Mater. Interfaces* **2017**, *9*, 42919.
[59] M. Chen, Y. Zou, L. Wu, Q. Pan, D. Yang, H. Hu, Y. Tan, Q. Zhong, Y. Xu, H. Liu, B. Sun, Q. Zhang, *Adv. Funct. Mater.* **2017**, *27*, 1701121.
[60] Z.-J. Li, E. Hofman, A. H. Davis, A. Khammang, J. T. Wright, B. Dzikovski, R. W. Meulenberg, W. Zheng, *Chem. Mater.* **2018**, *30*, 6400.
[61] A. L. Antaris, H. Chen, K. Cheng, Y. Sun, G. S. Hong, C. R. Qu, S. Diao, Z. X. Deng, X. M. Hu, B. Zhang, X. D. Zhang, O. K. Yaghi, Z. R. Alamparambil, X. C. Hong, Z. Cheng, H. J. Dai, *Nat. Mater.* **2016**, *15*, 235.
[62] D. Q. Chen, G. L. Fang, X. Chen, L. Lei, J. S. Zhong, Q. A. Mao, S. Zhou, J. N. Li, *J. Mater. Chem. C* **2018**, *6*, 8990.
[63] L.-J. Chen, C.-R. Lee, Y.-J. Chuang, Z.-H. Wu, C. Chen, *J. Phys. Chem. Lett.* **2016**, *7*, 5028.
[64] L. J. Chen, J. H. Dai, J. D. Lin, T. S. Mo, H. P. Lin, H. C. Yeh, Y. C. Chuang, S. A. Jiang, C. R. Lee, *ACS Appl. Mater. Interfaces* **2018**, *10*, 33307.
[65] L. J. Chen, *RSC Adv.* **2018**, *8*, 18396.
[66] K. S. Elvira, X. C. I. Solvas, R. C. R. Wootton, A. J. deMello, *Nat. Chem.* **2013**, *5*, 905.
[67] S.-Y. Teh, R. Lin, L.-H. Hung, A. P. Lee, *Lab Chip* **2008**, *8*, 198.
[68] I. Lignos, S. Stavrakis, G. Nedelcu, L. Protesescu, A. J. deMello, M. V. Kovalenko, *Nano Lett.* **2016**, *16*, 1869.
[69] V. Malgras, S. Tominaka, J. W. Ryan, J. Henzie, T. Takei, K. Ohara, Y. Yamauchi, *J. Am. Chem. Soc.* **2016**, *138*, 13874.
[70] S. Demchyshyn, J. M. Roemer, H. Groiß, H. Heilbrunner, C. Ulbricht, D. Apaydin, A. Böhm, U. Rütt, F. Bertram, G. Hesser, M. C. Scharber, N. S. Sariciftci, B. Nickel, S. Bauer, E. D. Głowacki, M. Kaltenbrunner, *Sci. Adv.* **2017**, *3*, e1700738.
[71] B. Wang, C. Y. Zhang, W. L. Zheng, Q. G. Zhang, Z. Q. Bao, L. Kong, L. Li, *Chem. Mater.* **2020**, *32*, 308.
[72] R. Naphade, S. Nagane, G. S. Shanker, R. Fernandes, D. Kothari, Y. Zhou, N. P. Padture, S. Ogale, *ACS Appl. Mater. Interfaces* **2016**, *8*, 854.
[73] L. Protesescu, S. Yakunin, O. Nazarenko, D. N. Dirin, M. V. Kovalenko, *ACS Appl. Nano Mater.* **2018**, *1*, 1300.
[74] Z. P. Zhang, Y. Li, C. Liang, G. N. Yu, J. F. Zhao, S. J. Luo, Y. Huang, C. L. Su, G. C. Xing, *Small* **2020**.
[75] S. T. Ha, X. Liu, Q. Zhang, D. Giovanni, T. C. Sum, Q. Xiong, *Adv. Opt. Mater.* **2014**, *2*, 838.
[76] J. Xing, X. F. Liu, Q. Zhang, S. T. Ha, Y. W. Yuan, C. Shen, T. C. Sum, Q. Xiong, *Nano Lett.* **2015**, *15*, 4571.
[77] K. Park, J. W. Lee, J. D. Kim, N. S. Han, D. M. Jang, S. Jeong, J. Park, J. K. Song, *J. Phys. Chem. Lett.* **2016**, *7*, 3703.
[78] L. Huang, Q. Gao, L.-D. Sun, H. Dong, S. Shi, T. Cai, Q. Liao, C.-H. Yan, *Adv. Mater.* **2018**, *30*, 1800596.
[79] H. Needleman, *Annu. Rev. Med.* **2004**, *55*, 209.
[80] T. C. Jellicoe, J. M. Richter, H. F. J. Glass, M. Tabachnyk, R. Brady, S. E. Dutton, A. Rao, R. H. Friend, D. Credgington, N. C. Greenham, M. L. Böhm, *J. Am. Chem. Soc.* **2016**, *138*, 2941.
[81] M. J. Ashley, M. N. O'Brien, K. R. Hedderick, J. A. Mason, M. B. Ross, C. A. Mirkin, *J. Am. Chem. Soc.* **2016**, *138*, 10096.
[82] A. Wang, X. Yan, M. Zhang, S. Sun, M. Yang, W. Shen, X. Pan, P. Wang, Z. Deng, *Chem. Mater.* **2016**, *28*, 8132.
[83] X. Wu, W. Song, Q. Li, X. Zhao, D. He, Z. Quan, *Chem. Asian J.* **2018**, *13*, 1654.
[84] M. Leng, Z. Chen, Y. Yang, Z. Li, K. Zeng, K. Li, G. Niu, Y. He, Q. Zhou, J. Tang, *Angew. Chem. Int. Ed.* **2016**, *55*, 15012.
[85] M. Leng, Y. Yang, Z. Chen, W. Gao, J. Zhang, G. Niu, D. Li, H. Song, J. Zhang, S. Jin, J. Tang, *Nano Lett.* **2018**, *18*, 6076.
[86] S. E. Creutz, H. B. Liu, M. E. Kaiser, X. S. Li, D. R. Gamelin, *Chem. Mater.* **2019**, *31*, 4685.
[87] J. Pal, S. Manna, A. Mondal, S. Das, K. V. Adarsh, A. Nag, *Angew. Chem. Int. Ed.* **2017**, *56*, 14187.
[88] D. M. Jang, K. Park, D. H. Kim, J. Park, F. Shojaei, H. S. Kang, J. P. Ahn, J. W. Lee, J. K. Song, *Nano Lett.* **2015**, *15*, 5191.
[89] Q. A. Akkerman, V. D'Innocenzo, S. Accornero, A. Scarpellini, A. Petrozza, M. Prato, L. Manna, *J. Am. Chem. Soc.* **2015**, *137*, 10276.
[90] Y.-C. Chen, H.-L. Chou, J.-C. Lin, Y.-C. Lee, C.-W. Pao, J.-L. Chen, C.-C. Chang, R.-Y. Chi, T.-R. Kuo, C.-W. Lu, D.-Y. Wang, *J. Phys. Chem. C* **2019**, *123*, 2353.
[91] W. Lv, X. Tang, L. Li, L. Xu, M. Li, R. Chen, W. Huang, *J. Phys. Chem. C* **2019**, *123*, 24313.
[92] V. M. Goldschmidt, *Naturwissenschaften* **1926**, *14*, 477.
[93] M.-G. Ju, J. Dai, L. Ma, X. C. Zeng, *J. Am. Chem. Soc.* **2017**, *139*, 8038.
[94] R. E. Beal, D. J. Slotcavage, T. Leijtens, A. R. Bowring, R. A. Belisle, W. H. Nguyen, G. F. Burkhard, E. T. Hoke, M. D. McGehee, *J. Phys. Chem. Lett.* **2016**, *7*, 746.
[95] T. Leijtens, E. T. Hoke, G. Grancini, D. J. Slotcavage, G. E. Eperon, J. M. Ball, M. De Bastiani, A. R. Bowring, N. Martino, K. Wojciechowski, M. D. McGehee, H. J. Snaith, A. Petrozza, *Adv. Energy Mater.* **2015**, *5*, 1500962.
[96] S. Z. Wang, Y. Hua, M. K. Wang, F. Y. Liu, L. M. Ding, *Mater. Chem. Front.* **2019**, *3*, 1139.

[97] C. H. Lu, G. V. Biesold, Y. J. Liu, Z. T. Kang, Z. Q. Lin, *Chem. Soc. Rev.* **2020**, *49*, 4953.
[98] A. Amat, E. Mosconi, E. Ronca, C. Quarti, P. Umari, M. K. Nazeeruddin, M. Grätzel, F. De Angelis, *Nano Lett.* **2014**, *14*, 3608.
[99] T. M. Koh, K. Fu, Y. Fang, S. Chen, T. C. Sum, N. Mathews, S. G. Mhaisalkar, P. P. Boix, T. Baikie, *J. Phys. Chem. C* **2014**, *118*, 16458.
[100] B. Xu, W. Wang, X. Zhang, W. Cao, D. Wu, S. Liu, H. Dai, S. Chen, K. Wang, X. Sun, *J. Mater. Chem. C* **2017**, *5*, 6123.
[101] J. J. Gallardo, E. Blanco, A. Sánchez-Coronilla, J. C. Pinero, J. Navas, *Appl. Mater. Today* **2020**, *18*, 100488.
[102] L. Protesescu, S. Yakunin, S. Kumar, J. Bär, F. Bertolotti, N. Masciocchi, A. Guagliardi, M. Grotevent, I. Shorubalko, M. I. Bodnarchuk, C.-J. Shih, M. V. Kovalenko, *ACS Nano* **2017**, *11*, 3119.
[103] C. Wang, Y. Zhang, A. Wang, Q. Wang, H. Tang, W. Shen, Z. Li, Z. Deng, *Chem. Mater.* **2017**, *29*, 2157.
[104] X. Zhang, H. Liu, W. Wang, J. Zhang, B. Xu, K. L. Karen, Y. Zheng, S. Liu, S. Chen, K. Wang, X. W. Sun, *Adv. Mater.* **2017**, *29*, 1606405.
[105] I. Lignos, V. Morad, Y. Shynkarenko, C. Bernasconi, R. M. Maceiczyk, L. Protesescu, F. Bertolotti, S. Kumar, S. T. Ochsenbein, N. Masciocchi, A. Guagliardi, C.-J. Shih, M. I. Bodnarchuk, A. J. deMello, M. V. Kovalenko, *ACS Nano* **2018**, *12*, 5504.
[106] K. Hills-Kimball, Y. Nagaoka, C. Cao, E. Chaykovsky, O. Chen, *J. Mater. Chem. C* **2017**, *5*, 5680.
[107] M. R. Linaburg, E. T. McClure, J. D. Majher, P. M. Woodward, *Chem. Mater.* **2017**, *29*, 3507.
[108] D. Amgar, T. Binyamin, V. Uvarov, L. Etgar, *Nanoscale* **2018**, *10*, 6060.
[109] P. Todorović, D. Ma, B. Chen, R. Quintero-Bermudez, M. I. Saidaminov, Y. Dong, Z.-H. Lu, E. H. Sargent, *Adv. Opt. Mater.* **2019**, *7*, 1901440.
[110] G. Grancini, M. K. Nazeeruddin, *Nat. Rev. Mater.* **2019**, *4*, 4.
[111] C. Wu, Y. Zou, T. Wu, M. Ban, V. Pecunia, Y. Han, Q. Liu, T. Song, S. Duhm, B. Sun, *Adv. Funct. Mater.* **2017**, *27*, 1700338.
[112] A. Swarnkar, A. R. Marshall, E. M. Sanehira, B. D. Chernomordik, D. T. Moore, J. A. Christians, T. Chakrabarti, J. M. Luther, *Science* **2016**, *354*, 92.
[113] Z. W. Ma, Z. Liu, S. Y. Lu, L. R. Wang, X. L. Feng, D. W. Yang, K. Wang, G. J. Xiao, L. J. Zhang, S. A. T. Redfern, B. Zou, *Nat. Commun.* **2018**, *9*, 4506.
[114] L. Zhang, C. M. Liu, L. R. Wang, C. L. Liu, K. Wang, B. Zou, *Angew. Chem. Int. Ed.* **2018**, *57*, 11213.
[115] L. Zhang, K. Wang, Y. Lin, B. Zou, *J. Phys. Chem. Lett.* **2020**, *11*, 4693.
[116] G. Liu, L. P. Kong, W. G. Yang, H. K. Mao, *Mater. Today* **2019**, *27*, 91.
[117] M. L. H. Green, G. Parkin, *J. Chem. Educ.* **2014**, *91*, 807.
[118] M. L. H. Green, *J. Organomet. Chem.* **1995**, *500*, 127.
[119] J. You, Y. Yang, Z. Hong, T.-B. Song, L. Meng, Y. Liu, C. Jiang, H. Zhou, W.-H. Chang, G. Li, Y. Yang, *Appl. Phys. Lett.* **2014**, *105*, 183902.
[120] H. Zhou, Q. Chen, G. Li, S. Luo, T.-B. Song, H.-S. Duan, Z. Hong, J. You, Y. Liu, Y. Yang, *Science* **2014**, *345*, 542.
[121] K. K. Bass, R. E. McAnally, S. Zhou, P. I. Djurovich, M. E. Thompson, B. C. Melot, *Chem. Commun.* **2014**, *50*, 15819.
[122] J. Zhao, B. Cai, Z. Luo, Y. Dong, Y. Zhang, H. Xu, B. Hong, Y. Yang, L. Li, W. Zhang, C. Gao, *Sci. Rep.* **2016**, *6*, 21976.
[123] J. A. Christians, P. A. Miranda Herrera, P. V. Kamat, *J. Am. Chem. Soc.* **2015**, *137*, 1530.
[124] S. N. Habisreutinger, T. Leijtens, G. E. Eperon, S. D. Stranks, R. J. Nicholas, H. J. Snaith, *Nano Lett.* **2014**, *14*, 5561.
[125] S. Huang, Z. Li, B. Wang, N. Zhu, C. Zhang, L. Kong, Q. Zhang, A. Shan, L. Li, *ACS Appl. Mater. Interfaces* **2017**, *9*, 7249.
[126] A. Alberti, I. Deretzis, G. Pellegrino, C. Bongiorno, E. Smecca, G. Mannino, F. Giannazzo, G. G. Condorelli, N. Sakai, T. Miyasaka, C. Spinella, A. La Magna, *ChemPhysChem* **2015**, *16*, 3064.
[127] D. B. Straus, S. Guo, R. J. Cava, *J. Am. Chem. Soc.* **2019**, *141*, 11435.
[128] D. Meggiolaro, E. Mosconi, F. De Angelis, *ACS Energy Lett.* **2017**, *2*, 2794.
[129] N. Aristidou, C. Eames, I. Sanchez-Molina, X. Bu, J. Kosco, M. S. Islam, S. A. Haque, *Nat. Commun.* **2017**, *8*, 15218.
[130] W. Nie, J.-C. Blancon, A. J. Neukirch, K. Appavoo, H. Tsai, M. Chhowalla, M. A. Alam, M. Y. Sfeir, C. Katan, J. Even, S. Tretiak, J. J. Crochet, G. Gupta, A. D. Mohite, *Nat. Commun.* **2016**, *7*, 11574.
[131] Y. Tian, M. Peter, E. Unger, M. Abdellah, K. Zheng, T. Pullerits, A. Yartsev, V. Sundström, I. G. Scheblykin, *Phys. Chem. Chem. Phys.* **2015**, *17*, 24978.
[132] A. Dualeh, P. Gao, S. I. Seok, M. K. Nazeeruddin, M. Grätzel, *Chem. Mater.* **2014**, *26*, 6160.
[133] M. Kulbak, S. Gupta, N. Kedem, I. Levine, T. Bendikov, G. Hodes, D. Cahen, *J. Phys. Chem. Lett.* **2016**, *7*, 167.
[134] B. T. Diroll, G. Nedelcu, M. V. Kovalenko, R. D. Schaller, *Adv. Funct. Mater.* **2017**, *27*, 1606750.
[135] A. C. Balazs, T. Emrick, T. P. Russell, *Science* **2006**, *314*, 1107.
[136] A. Usuki, Y. Kojima, M. Kawasumi, A. Okada, Y. Fukushima, T. Kurauchi, O. Kamigaito, *J. Mater. Res.* **2011**, *8*, 1179.
[137] Y. Kojima, A. Usuki, M. Kawasumi, A. Okada, Y. Fukushima, T. Kurauchi, O. Kamigaito, *J. Mater. Res.* **2011**, *8*, 1185.
[138] Q. Zhou, Z. Bai, W.-G. Lu, Y. Wang, B. Zou, H. Zhong, *Adv. Mater.* **2016**, *28*, 9163.
[139] H. Zhang, X. Wang, Q. Liao, Z. Xu, H. Li, L. Zheng, H. Fu, *Adv. Funct. Mater.* **2017**, *27*, 1604382.
[140] Y. Guo, K. Shoyama, W. Sato, E. Nakamura, *Adv. Energy Mater.* **2016**, *6*, 1502317.
[141] T. Y. Li, X. Z. Xu, C. H. Lin, X. W. Guan, W. H. Hsu, M. L. Tsai, X. S. Fang, T. Wu, J. H. He, *Adv. Sci.* **2020**, 1902439.
[142] D. N. Dirin, L. Protesescu, D. Trummer, I. V. Kochetygov, S. Yakunin, F. Krumeich, N. P. Stadie, M. V. Kovalenko, *Nano Lett.* **2016**, *16*, 5866.
[143] H.-C. Wang, S.-Y. Lin, A.-C. Tang, B. P. Singh, H.-C. Tong, C.-Y. Chen, Y.-C. Lee, T.-L. Tsai, R.-S. Liu, *Angew. Chem. Int. Ed.* **2016**, *55*, 7924.
[144] C. Sun, Y. Zhang, C. Ruan, C. Y. Yin, X. Y. Wang, Y. D. Wang, W. W. Yu, *Adv. Mater.* **2016**, *28*, 10088.
[145] H. Hu, L. Wu, Y. Tan, Q. Zhong, M. Chen, Y. Qiu, D. Yang, B. Sun, Q. Zhang, Y. Yin, *J. Am. Chem. Soc.* **2018**, *140*, 406.
[146] Q. Zhong, M. Cao, H. Hu, D. Yang, M. Chen, P. Li, L. Wu, Q. Zhang, *ACS Nano* **2018**, *12*, 8579.
[147] G. Yang, Q. Fan, B. Chen, Q. Zhou, H. Zhong, *J. Mater. Chem. C* **2016**, *4*, 11387.
[148] S. Yuan, D. Chen, X. Li, J. Zhong, X. Xu, *ACS Appl. Mater. Interfaces* **2018**, *10*, 18918.
[149] Z. F. Zhao, Z. H. Wu, J. Cheng, L. Jing, Y. F. Hou, *J. Phys. Chem. C* **2018**, *122*, 16887.
[150] Y. Wang, D. Yu, Z. Wang, X. Li, X. Chen, V. Nalla, H. Zeng, H. Sun, *Small* **2017**, *13*, 1701587.
[151] X. M. Chen, F. Zhang, Y. Ge, L. F. Shi, S. Huang, J. L. Tang, Z. Lv, L. Zhang, B. S. Zou, H. Z. Zhong, *Adv. Funct. Mater.* **2018**, *28*, 1706567.
[152] Q. Liao, X. Jin, H. B. Fu, *Adv. Opt. Mater.* **2019**, *7*, 25.
[153] Q. Wei, X. J. Li, C. Liang, Z. P. Zhang, J. Guo, G. Hong, G. C. Xing, W. Huang, *Adv. Opt. Mater.* **2019**, *7*, 1900080.
[154] P. Rastogi, A. Chu, C. Greboval, J. L. Qu, U. N. Noumbe, S. S. Chee, M. Goyal, A. Khalili, X. Z. Xu, H. Cruguel, S. Ithurria, B. Gallas, J. F. Dayen, L. Dudy, M. G. Silly, G. Patriarche, A. Degiron, G. Vincent, E. Lhuillier, *Nano Lett.* **2020**, *20*, 3999.

[155] M. G. Gong, R. Sakidja, R. Goul, D. Ewing, M. Casper, A. Stramel, A. Elliot, J. Z. Wu, *ACS Nano* **2019**, *13*, 1772.
[156] E. A. Gaulding, J. Hao, H. S. Kang, E. M. Miller, S. N. Habisreutinger, Q. Zhao, A. Hazarika, P. C. Sercel, J. M. Luther, J. L. Blackburn, *Adv. Mater.* **2019**, *31*, 1902250.
[157] Y. Wang, Z. Y. Lv, Q. F. Liao, H. Q. Shan, J. R. Chen, Y. Zhou, L. Zhou, X. L. Chen, V. A. L. Roy, Z. P. Wang, Z. X. Xu, Y. J. Zeng, S. T. Han, *Adv. Mater.* **2018**, *30*, 1800327.
[158] M. A. Green, E. D. Dunlop, J. Hohl-Ebinger, M. Yoshita, N. Kopidakis, X. Hao, *Prog Photovolt* **2020**, *28*, 629.
[159] E. M. Sanehira, A. R. Marshall, J. A. Christians, S. P. Harvey, P. N. Ciesielski, L. M. Wheeler, P. Schulz, L. Y. Lin, M. C. Beard, J. M. Luther, *Sci. Adv.* **2017**, *3*, eaao4204.
[160] L. M. Wheeler, E. M. Sanehira, A. R. Marshall, P. Schulz, M. Suri, N. C. Anderson, J. A. Christians, D. Nordlund, D. Sokaras, T. Kroll, S. P. Harvey, J. J. Berry, L. Y. Lin, J. M. Luther, *J. Am. Chem. Soc.* **2018**, *140*, 10504.
[161] Q. Wang, Z. Jin, D. Chen, D. Bai, H. Bian, J. Sun, G. Zhu, G. Wang, S. Liu, *Adv. Energy Mater.* **2018**, *8*, 1800007.
[162] J. Xue, J.-W. Lee, Z. Dai, R. Wang, S. Nuryyeva, M. E. Liao, S.-Y. Chang, L. Meng, D. Meng, P. Sun, O. Lin, M. S. Goorsky, Y. Yang, *Joule* **2018**, *2*, 1866.
[163] J. Xue, R. Wang, L. Chen, S. Nuryyeva, T.-H. Han, T. Huang, S. Tan, J. Zhu, M. Wang, Z.-K. Wang, C. Zhang, J.-W. Lee, Y. Yang, *Adv. Mater.* **2019**, *31*, 1900111.
[164] A. Hazarika, Q. Zhao, E. A. Gaulding, J. A. Christians, B. J. Dou, A. R. Marshall, T. Moot, J. J. Berry, J. C. Johnson, J. M. Luther, *ACS Nano* **2018**, *12*, 10327.
[165] S. Christodoulou, F. Di Stasio, S. Pradhan, A. Stavrinadis, G. Konstantatos, *J. Phys. Chem. C* **2018**, *122*, 7621.
[166] Q. Zhao, A. Hazarika, X. Chen, S. P. Harvey, B. W. Larson, G. R. Teeter, J. Liu, T. Song, C. Xiao, L. Shaw, M. Zhang, G. Li, M. C. Beard, J. M. Luther, *Nat. Commun.* **2019**, *10*, 2842.
[167] M. Hao, Y. Bai, S. Zeiske, L. Ren, J. Liu, Y. Yuan, N. Zarrabi, N. Cheng, M. Ghasemi, P. Chen, M. Lyu, D. He, J.-H. Yun, Y. Du, Y. Wang, S. Ding, A. Armin, P. Meredith, G. Liu, H.-M. Cheng, L. Wang, *Nat. Energy* **2020**, *5*, 79.
[168] S. Panigrahi, S. Jana, T. Calmeiro, D. Nunes, R. Martins, E. Fortunato, *ACS Nano* **2017**, *11*, 10214.
[169] F. Liu, Y. Zhang, C. Ding, T. Toyoda, Y. Ogomi, T. S. Ripolles, S. Hayase, T. Minemoto, K. Yoshino, S. Dai, Q. Shen, *J. Phys. Chem. Lett.* **2018**, *9*, 294.
[170] F. Liu, C. Ding, Y. H. Zhang, T. S. Ripolles, T. Kamisaka, T. Toyoda, S. Hayase, T. Minemoto, K. Yoshino, S. Y. Dai, M. Yanagida, H. Noguchi, Q. Shen, *J. Am. Chem. Soc.* **2017**, *139*, 16708.
[171] Y. X. Yao, P. J. Hang, P. Wang, L. B. Xu, C. Cui, J. S. Xie, K. Xiao, G. Li, P. Lin, S. Liu, D. Y. Xie, S. Y. Che, D. R. Yang, X. G. Yu, *Nanotechnology* **2020**, *31*, 085401.
[172] X. Zhang, Z. Jin, J. Zhang, D. Bai, H. Bian, K. Wang, J. Sun, Q. Wang, S. F. Liu, *ACS Appl. Mater. Interfaces* **2018**, *10*, 7145.
[173] R. Singh, S. R. Suranagi, S. J. Yang, K. Cho, *Nano Energy* **2018**, *51*, 192.
[174] J. B. Hoffman, G. Zaiats, I. Wappes, P. V. Kamat, *Chem. Mater.* **2017**, *29*, 9767.
[175] Q. Zeng, X. Zhang, X. Feng, S. Lu, Z. Chen, X. Yong, S. A. T. Redfern, H. Wei, H. Wang, H. Shen, W. Zhang, W. Zheng, H. Zhang, J. S. Tse, B. Yang, *Adv. Mater.* **2018**, *30*, 1705393.
[176] M. Cha, P. Da, J. Wang, W. Wang, Z. Chen, F. Xiu, G. Zheng, Z.-S. Wang, *J. Am. Chem. Soc.* **2016**, *138*, 8581.
[177] J. Zhang, D. Bai, Z. Jin, H. Bian, K. Wang, J. Sun, Q. Wang, S. Liu, *Adv. Energy Mater.* **2018**, *8*, 1703246.
[178] J. Zhang, Z. Jin, L. Liang, H. Wang, D. Bai, H. Bian, K. Wang, Q. Wang, N. Yuan, J. Ding, S. Liu, *Adv. Sci.* **2018**, *5*, 1801123.
[179] Y. Shirasaki, G. J. Supran, M. G. Bawendi, V. Bulovic, *Nat. Photonics* **2013**, *7*, 13.
[180] M. Era, S. Morimoto, T. Tsutsui, S. Saito, *Appl. Phys. Lett.* **1994**, *65*, 676.
[181] T. Hattori, T. Taira, M. Era, T. Tsutsui, S. Saito, *Chem. Phys. Lett* **1996**, *254*, 103.
[182] J. Song, J. Li, X. Li, L. Xu, Y. Dong, H. Zeng, *Adv. Mater.* **2015**, *27*, 7162.
[183] J. Pan, L. N. Quan, Y. Zhao, W. Peng, B. Murali, S. P. Sarmah, M. Yuan, L. Sinatra, N. M. Alyami, J. Liu, E. Yassitepe, Z. Yang, O. Voznyy, R. Comin, M. N. Hedhili, O. F. Mohammed, Z. H. Lu, D. H. Kim, E. H. Sargent, O. M. Bakr, *Adv. Mater.* **2016**, *28*, 8718.
[184] J. Li, L. Xu, T. Wang, J. Song, J. Chen, J. Xue, Y. Dong, B. Cai, Q. Shan, B. Han, H. Zeng, *Adv. Mater.* **2017**, *29*, 1603885.
[185] X. Z. Xu, X. J. Zhang, W. Deng, J. S. Jie, X. H. Zhang, *Small Methods* **2018**, *2*, 1700340.
[186] D. Yang, M. Cao, Q. Zhong, P. Li, X. Zhang, Q. Zhang, *J. Mater. Chem. C* **2019**, *7*, 757.
[187] S. Cai, X. Xu, W. Yang, J. Chen, X. Fang, *Adv. Mater.* **2019**, *31*, 1808138.
[188] D. Q. Chen, X. Chen, *J. Mater. Chem. C* **2019**, *7*, 1413.
[189] X. Zhang, S. Chen, X. Wang, A. Pan, *Small Methods* **2019**, *3*, 1800294.
[190] L. Gao, K. Zeng, J. Guo, C. Ge, J. Du, Y. Zhao, C. Chen, H. Deng, Y. He, H. Song, G. Niu, J. Tang, *Nano Lett.* **2016**, *16*, 7446.
[191] P. Ramasamy, D.-H. Lim, B. Kim, S.-H. Lee, M.-S. Lee, J.-S. Lee, *Chem. Commun.* **2016**, *52*, 2067.
[192] J. Song, L. Xu, J. Li, J. Xue, Y. Dong, X. Li, H. Zeng, *Adv. Mater.* **2016**, *28*, 4861.
[193] L. Niu, Q. Zeng, J. Shi, C. Cong, C. Wu, F. Liu, J. Zhou, W. Fu, Q. Fu, C. Jin, T. Yu, X. Liu, Z. Liu, *Adv. Funct. Mater.* **2016**, *26*, 5263.
[194] X. Li, D. Yu, F. Cao, Y. Gu, Y. Wei, Y. Wu, J. Song, H. Zeng, *Adv. Funct. Mater.* **2016**, *26*, 5903.
[195] X.-G. Zhao, J.-H. Yang, Y. Fu, D. Yang, Q. Xu, L. Yu, S.-H. Wei, L. Zhang, *J. Am. Chem. Soc.* **2017**, *139*, 2630.
[196] A. O. El-Ballouli, O. M. Bakr, O. F. Mohammeed, *Chem. Mater.* **2019**, *31*, 6387.
[197] J. Yuan, X. Ling, D. Yang, F. Li, S. Zhou, J. Shi, Y. Qian, J. Hu, Y. Sun, Y. Yang, X. Gao, S. Duhm, Q. Zhang, W. Ma, *Joule* **2018**, *2*, 2450.
[198] K. Chen, Q. Zhong, W. Chen, B. Sang, Y. Wang, T. Yang, Y. Liu, Y. Zhang, H. Zhang, *Adv. Funct. Mater.* **2019**, *29*, 1900991.
[199] X. Ling, S. Zhou, J. Yuan, J. Shi, Y. Qian, B. W. Larson, Q. Zhao, C. Qin, F. Li, G. Shi, C. Stewart, J. Hu, X. Zhang, J. M. Luther, S. Duhm, W. Ma, *Adv. Energy Mater.* **2019**, *9*, 1900721.
[200] J. W. Shi, F. C. Li, J. Y. Yuan, X. F. Ling, S. J. Zhou, Y. L. Qian, W. L. Ma, *J. Mater. Chem. A* **2019**, *7*, 20936.
[201] F. Liu, C. Ding, Y. H. Zhang, T. Karnisaka, Q. Zhao, J. M. Luther, T. Toyoda, S. Hayase, T. Minemoto, K. Yoshino, B. Zhang, S. Dai, J. K. Jiang, S. X. Tao, Q. Shen, *Chem. Mater.* **2019**, *31*, 798.
[202] Z. Zolfaghari, E. Hassanabadi, D. Pitarch-Tena, S. J. Yoon, Z. Shariatinia, J. van de Lagemaat, J. M. Luther, I. Mora-Sero, *ACS Energy Lett.* **2019**, *4*, 251.
[203] J. Yuan, C. Bi, S. Wang, R. Guo, T. Shen, L. Zhang, J. Tian, *Adv. Funct. Mater.* **2019**, *29*, 1906615.
[204] M. M. Tavakoli, M. Nasilowski, J. Zhao, M. G. Bawendi, J. Kong, *Small Methods* **2019**, *3*, 1900449.
[205] J. Kim, B. Koo, W. H. Kim, J. Choi, C. Choi, S. J. Lim, J.-S. Lee, D.-H. Kim, M. J. Ko, Y. Kim, *Nano Energy* **2019**, *66*, 104130.
[206] K. Q. Chen, W. Jin, Y. P. Zhang, T. Q. Yang, P. Reiss, Q. H. Zhong, U. Bach, Q. T. Li, Y. W. Wang, H. Zhang, Q. L. Bao, Y. L. Liu, *J. Am. Chem. Soc.* **2020**, *142*, 3775.

[207] S. B. Shivarudraiah, M. Ng, C. H. A. Li, J. E. Halpert, *ACS Appl. Energy Mater.* **2020**, *3*, 5620.
[208] C. M. Liu, Q. S. Zeng, Y. Zhao, Y. Yu, M. X. Yang, H. Gao, H. T. Wei, B. Yang, *Solar Rrl* **2020**, *4*, 2000102.
[209] Q. A. Akkerman, M. Gandini, F. Di Stasio, P. Rastogi, F. Palazon, G. Bertoni, J. M. Ball, M. Prato, A. Petrozza, L. Manna, *Nat. Energy* **2016**, *2*, 16194.
[210] D. Ghosh, M. Y. Ali, D. K. Chaudhary, S. Bhattacharyya, *Sol. Energy Mater. Sol. Cells* **2018**, *185*, 28.
[211] F. C. Li, S. J. Zhou, J. Y. Yuan, C. C. Qin, Y. G. Yang, J. W. Shi, X. F. Ling, Y. Y. Li, W. L. Ma, *ACS Energy Lett.* **2019**, *4*, 2571.
[212] M. F. Aygüler, M. D. Weber, B. M. D. Puscher, D. D. Medina, P. Docampo, R. D. Costa, *J. Phys. Chem. C* **2015**, *119*, 12047.
[213] H. Cho, S.-H. Jeong, M.-H. Park, Y.-H. Kim, C. Wolf, C.-L. Lee, J. H. Heo, A. Sadhanala, N. Myoung, S. Yoo, S. H. Im, R. H. Friend, T.-W. Lee, *Science* **2015**, *350*, 1222.
[214] A. B. Wong, M. Lai, S. W. Eaton, Y. Yu, E. Lin, L. Dou, A. Fu, P. Yang, *Nano Lett.* **2015**, *15*, 5519.
[215] S. Kumar, J. Jagielski, S. Yakunin, P. Rice, Y.-C. Chiu, M. Wang, G. Nedelcu, Y. Kim, S. Lin, E. J. G. Santos, M. V. Kovalenko, C.-J. Shih, *ACS Nano* **2016**, *10*, 9720.
[216] W. Deng, X. Xu, X. Zhang, Y. Zhang, X. Jin, L. Wang, S.-T. Lee, J. Jie, *Adv. Funct. Mater.* **2016**, *26*, 4797.
[217] X. Zhang, H. Lin, H. Huang, C. Reckmeier, Y. Zhang, W. C. H. Choy, A. L. Rogach, *Nano Lett.* **2016**, *16*, 1415.
[218] X. Zhang, B. Xu, J. Zhang, Y. Gao, Y. Zheng, K. Wang, X. W. Sun, *Adv. Funct. Mater.* **2016**, *26*, 4595.
[219] X. Zhang, C. Sun, Y. Zhang, H. Wu, C. Ji, Y. Chuai, P. Wang, S. Wen, C. Zhang, W. W. Yu, *J. Phys. Chem. Lett.* **2016**, *7*, 4602.
[220] G. Li, F. W. R. Rivarola, N. J. L. K. Davis, S. Bai, T. C. Jellicoe, F. de la Peña, S. Hou, C. Ducati, F. Gao, R. H. Friend, N. C. Greenham, Z.-K. Tan, *Adv. Mater.* **2016**, *28*, 3528.
[221] X. Zhang, W. Cao, W. Wang, B. Xu, S. Liu, H. Dai, S. Chen, K. Wang, X. W. Sun, *Nano Energy* **2016**, *30*, 511.
[222] E. Yassitepe, Z. Yang, O. Voznyy, Y. Kim, G. Walters, J. A. Castañeda, P. Kanjanaboos, M. Yuan, X. Gong, F. Fan, J. Pan, S. Hoogland, R. Comin, O. M. Bakr, L. A. Padilha, A. F. Nogueira, E. H. Sargent, *Adv. Funct. Mater.* **2016**, *26*, 8757.
[223] Q. Van Le, M. Park, W. Sohn, H. W. Jang, S. Y. Kim, *Adv. Electron. Mater.* **2017**, *3*, 1600448.
[224] X. Zhang, B. Xu, W. Wang, S. Liu, Y. Zheng, S. Chen, K. Wang, X. W. Sun, *ACS Appl. Mater. Interfaces* **2017**, *9*, 4926.
[225] X. Du, G. Wu, J. Cheng, H. Dang, K. Ma, Y.-W. Zhang, P.-F. Tan, S. Chen, *RSC Adv.* **2017**, *7*, 10391.
[226] Q. Shan, J. Li, J. Song, Y. Zou, L. Xu, J. Xue, Y. Dong, C. Huo, J. Chen, B. Han, H. Zeng, *J. Mater. Chem. C* **2017**, *5*, 4565.
[227] J. C. Yu, A.-Y. Lee, D. B. Kim, E. D. Jung, D. W. Kim, M. H. Song, *Advanced Materials Technologies* **2017**, *2*, 1700003.
[228] T. Chiba, K. Hoshi, Y.-J. Pu, Y. Takeda, Y. Hayashi, S. Ohisa, S. Kawata, J. Kido, *ACS Appl. Mater. Interfaces* **2017**, *9*, 18054.
[229] P. Liu, W. Chen, W. Wang, B. Xu, D. Wu, J. Hao, W. Cao, F. Fang, Y. Li, Y. Zeng, R. Pan, S. Chen, W. Cao, X. W. Sun, K. Wang, *Chem. Mater.* **2017**, *29*, 5168.
[230] S. Zou, Y. Liu, J. Li, C. Liu, R. Feng, F. Jiang, Y. Li, J. Song, H. Zeng, M. Hong, X. Chen, *J. Am. Chem. Soc.* **2017**, *139*, 11443.
[231] H. Wu, Y. Zhang, X. Zhang, M. Lu, C. Sun, T. Zhang, W. W. Yu, *Adv. Opt. Mater.* **2017**, *5*, 1700377.
[232] J. Shamsi, P. Rastogi, V. Caligiuri, A. L. Abdelhady, D. Spirito, L. Manna, R. Krahne, *ACS Nano* **2017**, *11*, 10206.
[233] H. C. Wang, W. G. Wang, A. C. Tang, H. Y. Tsai, Z. Bao, T. Ihara, N. Yarita, H. Tahara, Y. Kanemitsu, S. M. Chen, R. S. Liu, *Angew. Chem. Int. Ed.* **2017**, *56*, 13650.
[234] S. Q. Lou, T. T. Xuan, C. Y. Yu, M. M. Cao, C. Xia, J. Wang, H. L. Li, *J. Mater. Chem. C* **2017**, *5*, 7431.
[235] C. Zou, C. Y. Huang, E. M. Sanehira, J. M. Luther, L. Y. Lin, *Nanotechnology* **2017**, *28*, 455201.
[236] C. Qin, T. Matsushima, A. S. D. Sandanayaka, Y. Tsuchiya, C. Adachi, *J. Phys. Chem. Lett.* **2017**, *8*, 5415.
[237] J. Pan, Y. Shang, J. Yin, M. De Bastiani, W. Peng, I. Dursun, L. Sinatra, A. M. El-Zohry, M. N. Hedhili, A.-H. Emwas, O. F. Mohammed, Z. Ning, O. M. Bakr, *J. Am. Chem. Soc.* **2018**, *140*, 562.
[238] Y. Tan, Y. Zou, L. Wu, Q. Huang, D. Yang, M. Chen, M. Ban, C. Wu, T. Wu, S. Bai, T. Song, Q. Zhang, B. Sun, *ACS Appl. Mater. Interfaces* **2018**, *10*, 3784.
[239] Z. Shi, S. Li, Y. Li, H. Ji, X. Li, D. Wu, T. Xu, Y. Chen, Y. Tian, Y. Zhang, C. Shan, G. Du, *ACS Nano* **2018**, *12*, 1462.
[240] J.-S. Yao, J. Ge, B.-N. Han, K.-H. Wang, H.-B. Yao, H.-L. Yu, J.-H. Li, B.-S. Zhu, J.-Z. Song, C. Chen, Q. Zhang, H.-B. Zeng, Y. Luo, S.-H. Yu, *J. Am. Chem. Soc.* **2018**, *140*, 3626.
[241] X. Zhang, X. Bai, H. Wu, X. Zhang, C. Sun, Y. Zhang, W. Zhang, W. Zheng, W. W. Yu, A. L. Rogach, *Angew. Chem. Int. Ed.* **2018**, *57*, 3337.
[242] S. Yuan, Z.-K. Wang, M.-P. Zhuo, Q.-S. Tian, Y. Jin, L.-S. Liao, *ACS Nano* **2018**, *12*, 9541.
[243] A. Subramanian, Z. Pan, Z. Zhang, I. Ahmad, J. Chen, M. Liu, S. Cheng, Y. Xu, J. Wu, W. Lei, Q. Khan, Y. Zhang, *ACS Appl. Mater. Interfaces* **2018**, *10*, 13236.
[244] J. Song, J. Li, L. Xu, J. Li, F. Zhang, B. Han, Q. Shan, H. Zeng, *Adv. Mater.* **2018**, *30*, 1800764.
[245] X. Y. Chin, A. Perumal, A. Bruno, N. Yantara, S. A. Veldhuis, L. Martínez-Sarti, B. Chandran, V. Chirvony, A. S.-Z. Lo, J. So, C. Soci, M. Grätzel, H. J. Bolink, N. Mathews, S. G. Mhaisalkar, *Energy Environ. Sci.* **2018**, *11*, 1770.
[246] T. Chiba, Y. Hayashi, H. Ebe, K. Hoshi, J. Sato, S. Sato, Y.-J. Pu, S. Ohisa, J. Kido, *Nat. Photonics* **2018**, *12*, 681.
[247] Y. Liu, J. Cui, K. Du, H. Tian, Z. He, Q. Zhou, Z. Yang, Y. Deng, D. Chen, X. Zuo, Y. Ren, L. Wang, H. Zhu, B. Zhao, D. Di, J. Wang, R. H. Friend, Y. Jin, *Nat. Photonics* **2019**, *13*, 760.
[248] W. Deng, X. Jin, Y. Lv, X. Zhang, X. Zhang, J. Jie, *Adv. Funct. Mater.* **2019**, *29*, 1903861.
[249] F. H. Ye, H. J. Zhang, P. Wang, J. L. Cai, L. Wang, D. Liu, T. Wang, *Chem. Mater.* **2020**, *32*, 3211.
[250] J. Liu, Y. Xue, Z. Wang, Z.-Q. Xu, C. Zheng, B. Weber, J. Song, Y. Wang, Y. Lu, Y. Zhang, Q. Bao, *ACS Nano* **2016**, *10*, 3536.
[251] P. Zhu, S. Gu, X. Shen, N. Xu, Y. Tan, S. Zhuang, Y. Deng, Z. Lu, Z. Wang, J. Zhu, *Nano Lett.* **2016**, *16*, 871.
[252] X. S. Tang, Z. Q. Zu, H. B. Shao, W. Hu, M. Zhou, M. Deng, W. W. Chen, Z. G. Zang, T. Zhu, J. M. Xue, *Nanoscale* **2016**, *8*, 15158.
[253] X. Li, D. Yu, J. Chen, Y. Wang, F. Cao, Y. Wei, Y. Wu, L. Wang, Y. Zhu, Z. Sun, J. Ji, Y. Shen, H. Sun, H. Zeng, *ACS Nano* **2017**, *11*, 2015.
[254] X. Xu, X. Zhang, W. Deng, L. Huang, W. Wang, J. Jie, X. Zhang, *ACS Appl. Mater. Interfaces* **2018**, *10*, 10287.
[255] H. Wu, H. Si, Z. Zhang, Z. Kang, P. Wu, L. Zhou, S. Zhang, Z. Zhang, Q. Liao, Y. Zhang, *Adv. Sci.* **2018**, *5*, 1801219.

Shizhe Wang is currently a Ph.D. candidate in the Department of Chemistry, University of Munich (LMU). He received his master degree from National Center for Nanoscience and Technology (NCNST), Chinese Academy of Sciences (2019). His current research focuses on the development of lead-free perovskite materials.

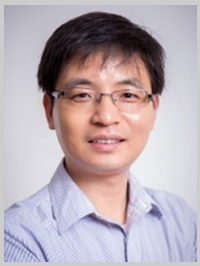

Qiao Zhang is a professor in Institute of Functional Nano and Soft Materials (FUNSOM), Soochow University, China. He received his Ph.D. degree from University of California Riverside (2012). After being a postdoctoral fellow in the Department of Chemistry, University of California Berkeley (2012–2014), he joined Soochow University, in 2014. His main research field is molecular level studies of surface and heterogeneous catalysis, controllable synthesis of all-inorganic perovskite with tunable optical properties and their applications.

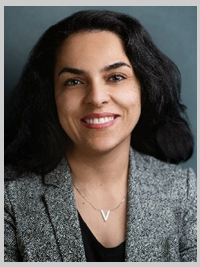

Tayebeh Ameri is a senior lecturer in the Institute for Materials and Processes, Chemical Engineering discipline at the University of Edinburgh. She received her PhD degree in Engineering Sciences from the Johannes Kepler University Linz, in 2010. Afterwards, she conducted her postdoctoral and Habilitation research in the Department of Material Science and Engineering at the University of Erlangen-Nürnberg (FAU). From 2018 till 2020, she was a team leader and lecturer in the Department of Physical Chemistry at the University of Munich (LMU). Her main research interests include investigation and development of printed optoelectronic devices with a focus on energy and detection applications.